NTNU

Norwegian University of
Science and Technology

Master Slag Production for the Recovery of Rare Earth Elements

Fredrik André Elgvin Rodahl

Materials Technology
Submission date: July 2017
Supervisor: Ragnhild Aune, IMA
Co-supervisor: Mark Kennedy, IMT

Norwegian University of Science and Technology
Department of Materials Science and Engineering

Declaration

I hereby declare that except for references cited and duly acknowledged, the views expressed here are the product of my own research.

Fredrik André Elgvin Rodahl

Trondheim, Norway

Acknowledgement

This master's thesis, done spring 2017, is a part of the Masters degree at NTNU, Trondheim, in Materials Science and Engineering, with a specialization in Process Metallurgy.

First, I want to thank Professor Ragnhild Elizabeth Aune for accepting me as her student, as well as being an academic mentor without comparison. She has encouraged working with individual responsibility and taught me how to really solve problems by applying the scientific method.

I also want to grant a huge thanks to Tianming Sun, who has been my lab partner throughout this project, and Mark William Kennedy for being a source of great insight. I would also like to thank Dmitry Slizovskiy, Jonas Einan Gjøvik and Ivar Andre Ødegaard at Department of Material Science and Engineering, for all the help with equipment and furnaces at NTNU.

A thanks to Fei Wang for the help at KU Leuven, Kai Tang at Sintef for thermodynamic modeling, Severin Lierhagen for ICP-MS analysis, Magnus Rotan for XRD guidance and Johannes Ofstad for HSE concerns.

I would like to acknowledge the REEcover project, as a source of funding and for making this project possible.

Finally I want to give a huge thanks to my partner Hanne Kalvøy Betten, for all the emotional and nutritional support during this thesis. My friends deserve a thanks for the years at NTNU we made unforgettable. I also want to thank my family for providing support, even when I didn't specifically request it. My parents raised a child with a critical mind, and I'm ultimately indebted to them for anything I have the possibility to do with my life.

Fredrik André Elgvin Rodahl

Trondheim, Norway

Abstract

The Rare Earth Elements (REEs) is a term describing a group of 17 elements which are critical components in many technological applications due to their magnetic or optical properties. In contrast to the name, these elements are relatively abundant, but distributed in low concentration throughout the Earth's crust. Recovery of these elements is currently focused mainly in China, but the strategic importance of these elements within the EU motivates innovation in local resource extraction.

The development of a pyrometallurgical approach for the recovery of REEs from iron mine tailings containing apatite has been the main focus of the present work. This was realized through the production of a Master Slag, *i.e.* a slag of uniform relative composition of $Nd_2O_3-SiO_2-CaO$ made from an Apatite Concentrate produced by LKAB in Kiruna, Sweden, which is a Swedish iron mining company. An experimental investigation into the $Nd_2O_3-SiO_2-B_2O_3$ phase diagram was also performed for the intention of developing fundamental thermodynamic data for the Nd-Fe-B system – commercially known as the system used in permanent magnets.

The developed thermal process of producing the Master Slag includes two main steps, *i.e.* (1) removal of phosphorus, which was achieved with a 99.7% reduction, and (2) melting of the remaining material at 1873 K for 60 min in an induction furnace; followed by rapid cooling. Scanning Electron Microscope - Energy Dispersive X-ray Spectrometry (SEM-EDS), X-Ray Diffraction (XRD) and Inductively Coupled Plasma - Mass Spectrometry (ICP-MS) were used for the chemical analysis of the obtained material. The produced Master Slag proved to consist of three phase regions, these differed mainly by their neodymium concentration. The Nd-rich phase contained the compounds $Ca_2Nd_3(SiO_4)_3F$ and variations of $Ca_2Nd_3(SiO_4)_2(PO_4)O$ with an overall Nd-concentration of 20-48% by weight. However, sampling at a lower temperature seems to indicate a higher Nd-concentration in the Nd-rich phase.

The evaluation of the $Nd_2O_3-SiO_2-B_2O_3$ phase diagram proved to offer several critical issues. A method for equilibriation of samples at high temperature (1673 K) without vaporization of B, as well as the optimization of the equilibriation time to secure reproducible results were the focus in the present work.

Sammendrag

De Sjeldne Jordartene (REEs) er et begrep som beskriver en gruppe av 17 grunnstoffer, som er kritiske komponenter i mange teknologiske applikasjoner, på grunn av deres unike magnetiske eller optiske egenskaper. I motsetning til hva navnet skulle tilsi er disse grunnstoffene relativt rikelig fordelt i jordskorpen, dog i lave konsentrasjoner. Utvinning av grunnstoffene skjer hovedsaklig i Kina, men den strategiske viktigheten de innehar for EU motiverer til innovasjon med nye lokale utvinningsmetoder.

Utviklingen av en pyrometallurgisk tilnærming for å utvinne REEs fra apatittholdig gruveavfall fra jerngruver, har vært hovedmålet for denne oppgaven. Dette har blitt gjennomført gjennom for produksjonen av en Hovedslagg, definert i dette arbeidet som en slagg med uniform relativ konsentrasjon av $Nd_2O_3{-}SiO_2{-}CaO$, laget av et Apatittkonsentrat produsert av LKAB som er et svensk jerngruveselskap fra Kiruna, Sverige. En eksperimentell utforskning av fasediagrammet til $Nd_2O_3{-}SiO_2{-}B_2O_3$ ble gjennomført med intensjon om å utvikle grunnleggende termodynamisk data for Nd-Fe-B systemet – kommersielt kjent som systemet brukt i permanente magneter.

Den utviklede termiske prosessen for produksjon av Hovedslagg er en todelt prosess, *dvs.* (1) fjerning av fosfor, som ble oppnådd med 99.7% reduksjon, og (2) smelting ved 1873 K i 60 min i en induksjonsovn med påfølgende hurtig avkjøling. Sveipeelektronmikroskop - Energidispersiv Røntgenspektroskopi (SEM-EDS), Røntgendiffraksjon (XRD) og Induktivt Koblet Plasma - Massespektrometri (ICP-MS) ble brukt for kjemisk analyse av the produserte materialet. Hovedslaggen viste seg å bestå av tre faseregioner, skilt hovedsaklig av deres konsentrasjonsforskjell av neodym. Den Nd-rike fasen inneholder forbindelsen $Ca_2Nd_3(SiO_4)_3F$ og variasjoner av $Ca_2Nd_3(SiO_4)_2(PO_4)O$, med totalt sett 20-48% vektfraksjon Nd. Det ble observert indikasjoner på at lavere temperatur ga høyere Nd-konsentrasjon i den Nd-rike fasen.

Evalueringen av fasediagrammet til $Nd_2O_3{-}SiO_2{-}B_2O_3$ viste seg å gi flere vanskelige problemstillinger. Fokuset i dette arbeidet en metode for å oppnå likevekt i prøvene ved høy temperatur (1673 K) uten å fordampe B, samt å optimalisere tiden for oppnåelse av likevekt.

Contents

List of Figures

List of Tables

Abbreviations

CALPHAD	CALculation of PHAse Diagrams
CIS	Commonwealth of Independent States
CRT	Cathode Ray Tube
CNF	Calcium Neodymium Fluoride
CNSF	Calcium Neodymium Fluoride Silicate
CNSO	Calcium Neodymium Oxide Silicate
CNSP	Calcium Neodymium Oxide Phosphate Silicate
CRT	Cathode Ray Tube
CSF	Cuspidine
CSO	Calcium Silicate
EDS	Energy-Dispersive X-ray Spectroscopy
EPMA	Electron Probe Micro Analysis
EC	European Commision
EOL	End-Of-Life
EU	European Union
FCC	Fluid Catalytic Cracking
FP7	Seventh Framework Programme
HREE	Heavy Rare Earth Element
HSE	Health, Safety and Environment
ICP-MS	Inductively Conducting Plasma - Mass Spectroscopy
ICDD	The International Centre for Diffraction Data
KTH	Royal Institute of Technology
KU Leuven	Catholic University of Leuven
LED	Light Emitting Diode
LKAB	Luossavaara-Kiirunavaara Aktiebolag
LREE	Light Rare Earth Element
MCS	Mineral Commodity Summary
MRI	Magnetic Resonance Imaging
NTNU	orwegian University of Science and Technology
REE	Rare Earth Element
REEcover	Recovery of Rare Earth Elements from Magnetic Waste in the WEEE Recycling Industry and Tailings from the Iron Ore Industry
REO	Rare Earth Oxide
SEM	Scanning Electron Microscopy
USGS	United States Geological Survey
WEEE	Waste Electric and Electronic Equipment
XRD	X-Ray Diffraction
YHTMC	Shaanxi Yuheng Tungsten & Molybdenum Co.Ltd

Chapter 1

Introduction

Rare Earth Elements (REEs) are a group of 17 elements that are essential to the technological foundation of modern life. A good example is Nd (neodymium) in neodymium-iron-boron magnets ($Nd_2Fe_{14}B$), which are the strongest permanent magnets presently available. The inherent strength of Nd-magnets makes them critical for a large amount of important technologies that includes smartphones, hybrid and electric vehicles, as well as windmills, hard drives, audio equipment among other things. Their properties help bring down size and weight of magnetic components, which is crucial to be competitive in the technological market. Applications such as lasers, protective glass and dielectric equipment are also products where Nd is an important addition, mostly because of its magnetic or optical properties [1]. Most of the REEs have important impacts on different technologies. Table 2.1 shows some applications where individual REEs are used, presenting the possibilities and potential of REEs.

The criticality of REEs, as defined in the report for the European Union (EU) entitled "Report on Critical Raw Materials for the EU (2014)" [2], is summed up by supply risk and economic importance, as presented in Figure 1.1. The supply risk includes the unstable market price for REEs which have been an important feature during the last couple of years. Based on the recently announced Chinese plans of increasing their production of electric vehicles, global REE prices are "poised to skyrocket" [3]. A secured and stable supply of REEs to the EU is one of the main motivations behind many of the European project financed by the European Commission (EC) over the years.

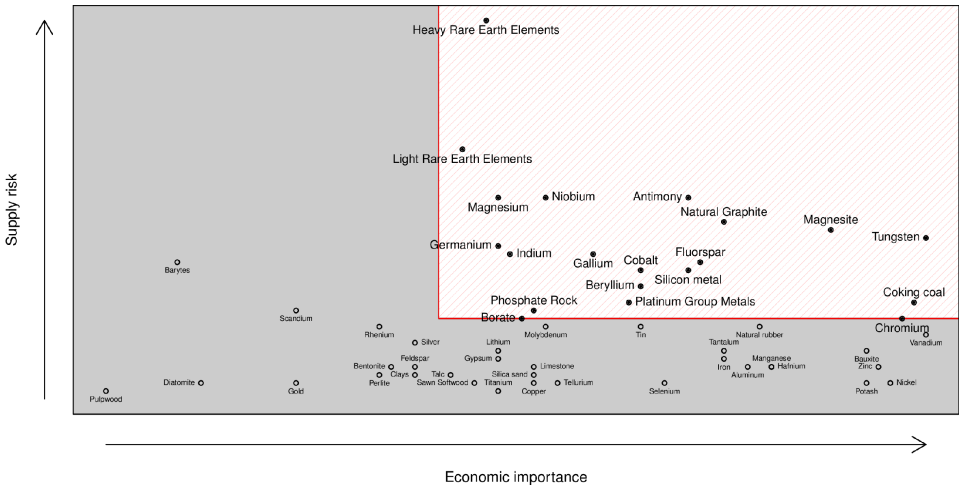

Figure 1.1 – Criticality of raw materials in the EU[2].

The impact that the production of REEs have had on the environment have become a targeted concern over the years by multiple parties [2, 4, 5, 6]. It is a clear consensus that REE production can have severe consequences for local environment without serious regulation which prompts research into cleaner production and fuels consideration of alternative sources. For the EU, the reliance on import of these critical elements creates a motivation for local sources of REEs. The REEcover project (Recovery of Rare Earth Elements from Magnetic Waste in the WEEE Recycling Industry and Tailings from the Iron Ore Industry) is a project funded by the EC under the Seventh Framework Programme (FP7), which aims to research new and sustainable ways to recover REEs. The project consists of two directions of REE-recovery, *i.e.* one from WEEE (Waste Electric and Electronic Equipment) from the electronics industry, and the other from tailings from the mining industry. The present work is part of the second direction and the focus is on the raw material source from mine tailings with very low concentrations of REEs [7].

An Apatite Concentrate is created from iron ore tailings supplied from LKAB (Luossavaara-Kiirunavaara Aktiebolag) in Kiruna, Sweden is the raw material studied in this thesis. Analysis and characterization of the REEs in the Apatite Concentrate have previously been shown to be complicated

[8, 9]. However, there is a need to develop a fundamental understanding of the chemical behavior of the REEs in apatite for the continued technological development of the process routes for the ultimate recovery of REEs. The main goal of the present work is to produce a Master Slag, which is defined as a slag created from the iron mine tailings, and to recover REEs from this slag. Nd has been chosen as the representative element for the REEs present in the raw material, and the chemical behavior of this element after pyrometallurgical treatment have been studied. Since the Apatite Concentrate is a raw waste material that is not represented by a uniform composition, the effect of contaminating species on the chemistry of the slag, aswell as on the Nd is also of interest as well. The identification of phases with higher concentrations of Nd than the raw material will make it possible to consider routes of separating this phase in future endeavors, with the ultimate goal of completely recovering REEs from this unused source of mining waste.The present work is a continuation of the work summarized in the report "Procedure for Master Slag Production Based on the Synthetic System of Nd_2O_3, SiO_2 and CaO" [9] by the present author.

Experimental work on the thermodynamic system of $Nd_2O_3-SiO_2-B_2O_3$ have also been performed. This is a collaboration project between NTNU (Norwegian University of Science and Technology), KU Leuven (Catholic University of Leuven) and SINTEF Materials and Chemistry. The purpose of studying this system is to tie the metallurgical work on the Master Slag, to the presence of B (boron) in Nd permanent magnets. Nd-magnets is a potential source of Nd which could be used to dope the Apatite Concentrate to obtain the Master Slag. A recycling process could therefore potentially utilize both WEEE and industrial mining waste, combining two of the most unused sources of REEs. Such an approach has the potential to improve both the respective REE-recovery rates. By understanding the thermodynamics of the system $Nd_2O_3-SiO_2-B_2O_3$ it is believed that an increased the understanding of the behavior of Nd in the proposed Master Slag is also obtained. Preparation and thermal treatment of $Nd_2O_3-SiO_2-B_2O_3$ samples with different chemical composition has in this regard been prepared, thermally treated and the results discussed.

Chapter 2

Background

The importance of the REEs for modern life can hardly be exaggerated. An overview of the REEs and some of their useful applications are presented in Table 2.1, which can give a useful perspective of the prevalence of the REEs. They exist everywhere in the earth's crust, with varying concentrations, but they are not extracted equally over the globe. This chapter presents information of how, where and why the REE sources are exploited, as well as presenting the motivations for the extraction of these resources where it is currently not being done.

2.1 Rare Earth Elements

As a group, the REEs are fairly abundant, in respect to other elements regarded as rare or critical. The individual REEs differ greatly in their abundance between the elements in the group. The most common REE is Ce (cerium) being approximately as abundant as Cu (Copper), while Pm (promethium) doesn't appear naturally at all [10]. Figure 2.1 show the abundance of selected elements relative to the presence of Si (silicon) in the crust. The elements are none the less rare in the fact that they seldom appear in local high concentrations, and never in any type of pure ore, as some precious metals do. The form they mostly appear in is as oxides as part of minerals. The minerals containing the most REEs are bastnäsite, monazite and xenotime, with the individual REEs appearing in different minerals in varying quantities [10, 11]. They are spread around in the earth's crust, although with some areas containing higher than normal amounts of these REE-bearing minerals. These areas are viewed as either REE "deposits" or

"reserves", respectively defined by the USGS (United States Geological Survey) as total resources available and total resources suitable for industrial recovery [12].

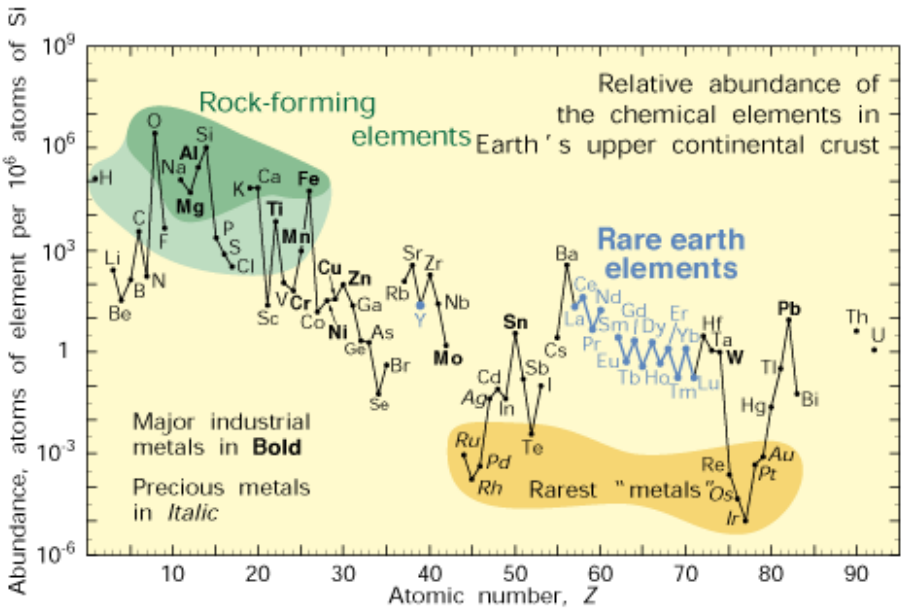

Figure 2.1 – Relative abundance of the chemical elements in the Earth's upper continental crust. REEs marked in blue color. Abundance in number of atoms per 10^6 atoms of Si [10].

2.2 Rare Earth Element Reserves

USGS has published MCSs (Mineral Commodity Summaries) regarding rare earths since 1996, depicting among other things the total REO (Rare Earth Oxide) reserves in the world [12]. The amount of reserves reported by the summaries gives an indication for how much REEs could possibly be extracted from various countries in the world, but it can not guarantee that these deposits exist in a fashion where it is economically feasible to extract REEs today. Figures 2.2 and 2.3 show the world reserves summarized by the USGS in 1996 and 2017 respectively. These two summaries display the

Table 2.1 – Overview of the REEs with their symbols and applications, from the work of Dutta *et. al.* [11].

Element	Symbol	At.#	Application
Scandium	Sc	21	Aerospace framework, high-intensity street lamps, bicycle frames, baseball bats
Yttrium	Y	39	Television and computer screens, LED (Light Emitting Diode) lights, cancer treatment drugs, alloys, catalyst
Lanthanum	La	57	Camera lenses, carbon lighting applications such as studio lighting and projector lights, battery electrodes
Cerium	Ce	58	Catalytic converters in cars, colored glass, steel production, refining crude oils
Praseodymium	Pr	59	Strong magnets, welding goggles, lasers, aircraft engines
Neodymium	Nd	60	Powerful magnets used in hard drives, microphones, wind turbines and hybrid cars, lasers
Promethium	Pm	61	Not usually found in nature
Samarium	Sm	62	Cancer treatment, nuclear reactor control rods, X-ray lasers
Europium	Eu	63	Color television screens, computer screens, fluorescent glass, genetic screening tests, nuclear reactor control rods
Gadolinium	Gd	64	X-ray and MRI (Magnetic Resonance Imaging) scanning systems, shielding in nuclear reactors, alloys, green phosphors
Terbium	Tb	65	Television and computer screens, fuel cells, solar systems
Dysprosium	Dy	66	Commercial lighting, hard disk devices, transducers
Holmium	Ho	67	Lasers, glass coloring, high-strength magnets
Erbium	Er	68	Glass colorant, signal amplification in fiber optic cables, metallurgical uses
Thulium	Tm	69	High-efficiency lasers, portable X-ray machines, high temperature superconductors
Ytterbium	Yb	70	Improves stainless steel, lasers, ground monitoring devices, industrial catalysts
Lutetium	Lu	71	Cracking hydrocarbons in oil refineries

degree reported reserves can change depending on the definition the country is willing to use. The numbers will also always be subject to uncertainty for what kind of information the respective countries are willing to report. The largest changes between the reported reserves are as follows.

- The reported United States reserves were updated from 13 Mt to 1.4 Mt in 2015.
- "Former Soviet Union" was separated into "Russia" and "CIS" (Commonwealth of Independent States) in 2004.
- "CIS" was moved into "Other countries" in 2013.
- Brazilian reserves were updated from ~0 Mt to 22 Mt in 2014.
- Vietnamese reserves were added in 2017, with 22 Mt.
- India's reserves were updated twice, from 1,3 Mt to 3,1 Mt in 2011 and from 3,1 Mt to 6,9 Mt in 2017.
- China's reserves were updated twice, from 43 Mt to 55 Mt in 2011 and from 55 Mt to 44 Mt in 2017.
- Many additional minor changes in reported reserves from 1996 to 2017.

The total reported reserves have as a result fluctuated from 100 Mt to 150 Mt, according to these summaries. In the same interval between 1995 and 2016, total production of REOs have increased from 70 kt in 1995 to 126 kt in 2016, with a height of 130 kt in 2011. At these points, China's marked share of production changed from <50% in 1995 through ~100% in 2011, to 86% in 2016. Table 2.2 shows these selectively chosen values. One important thing to keep in mind about these numbers is that they come from a single source, so their values should not be asserted as absolute truth, but they give a reasonable perspective into an important aspect concerning REEs as a resource. Three main points can be extracted from the information gathered:

- The difficulty and inaccuracy in reporting raw material reserves and deposits.
- The low correlation between reported reserves and current production.
- China's historically dominating market share.

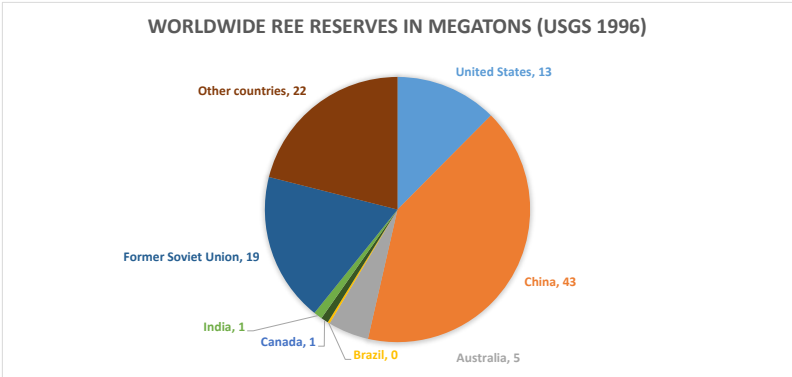

Figure 2.2 – 1996 estimate of global REE reserves in megatons by USGS.

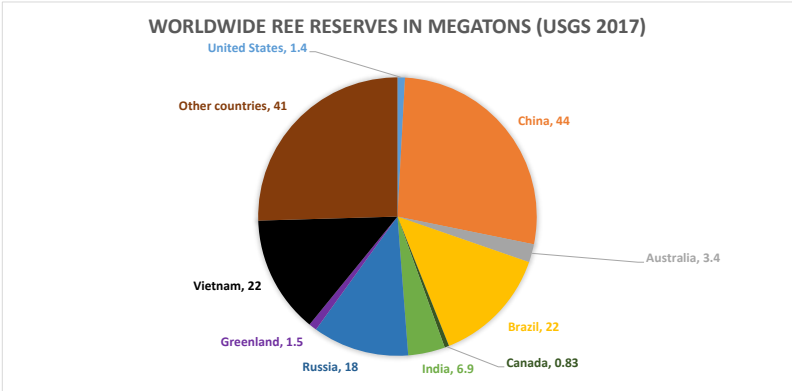

Figure 2.3 – 2017 estimate of global REE reserves in megatons by USGS.

China's market share increased in the 1990s, often recognized as a consequence of their increased exports which undercut the global market in such a way that most non-Chinese operations had to close, *e.g.* Molycorps Mountain Pass mine [13]. There were reports that illegal mining operations in China were starting to be curbed around 2010. Around 2011 global demand of REEs suddenly far exceeded the production and prices increased exponentially over a short time for some of the REEs, like Dy, Eu and Tb [13, 14, 15]. This meant that the price for Dy increased by approximately 450% in just 2011 alone, before going down to a price still above pre-2011 prices [15]. The volatility in combination with the large power imbalance favoring China over this market implicate the importance of research into production and recycling of REEs. In Figure 2.4, the price of four selected REEs (Pr, Nd, Dy, Tb) is plotted over the time period 2005–2015, which shows the huge price increase for the less available elements.

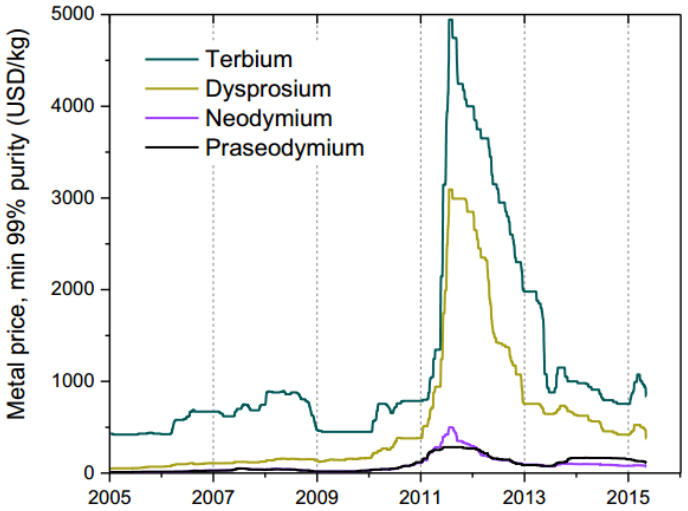

Figure 2.4 – Price variation of Nd, Pr, Dy and Tb, 2005–2015. Presented by Pavel *et.al* (2017), with data from Asian Metal (2015). [16, 17]

It is reasonable to assume that more measures will be taken worldwide to determine the potential REE reserves, which means the data will improve in the coming years. As an example, even Norwegian industry recognize the potential of REE extraction and call for a geological survey of the "Fensfeltet", which is scheduled to be done in 2018 [18].

Table 2.2 – Estimates of worldwide production of REEs, and corresponding Chinese market share, compiled by USGS between 1996 and 2017. [12]

Year	Total Worldwide Production [kt]	Chinese Market Share [%]
1995	70	42
2011	130	100
2016	126	86

2.3 Rare Earth Mining and Processing

REEs are mined in either open or underground pits, using standard procedures such as drilling, blasting, loading, and dragging to the mill procedures [19]. The specifics of mineral mining will not be emphasized in any way in the present study, but the important aspect of REE-extraction is that it involves mining and processing of huge volumes of rock and minerals. A summarized process flow can be described by REE mining from ore deposits, grinding, cracking the minerals to produce mixed REO concentrates, separation, purification of oxides, and refining to produce industrial grade REEs [11]. Two of the largest mines in the world are open pit mines in Bayan Obo, China and Mountain Pass in the United States. The process will include a lot of both acidic and alkaline chemicals, while also including radioactive elements and heavy metals from the ore itself. In combination with the huge volume of ore processed, the tailings produced can be of large environmental concern, as seen with the Bayan Obo mine. Its tailings pond is one of the largest in the world and posing large risk to surrounding water, soil and air quality, as well as neighboring communities [6]. In addition to dedicated mines, REEs can also be extracted as a by-product in supplement to a main product.

The Balance Problem

There is an important phenomenon which must be seen in relation with price fluctuations. While in a "normal" market, a high demand would result in higher supply to meet that demand. However, things are not so simple in the REE market. A single rare earth, like Dy, can have a higher demand than *e.g.* Ce, but Dy is only found as a minor constituent in the same ore you find Ce. The conflict here is that trying to meet the Dy demand will heavily influence the supply of Ce and possibly crash that price. The industrial interests in

REE will mostly extract a whole range of REOs, meaning they will have to be careful which demands they meet to not overly destroy the profit margins on the remaining elements. Binnemans (2013) goes into more detail of this problem, but the one important thing to conclude is that the REE situation as a global resource is quite unique in the way it behaves [20]. Binnemans suggested three possible mitigations to this problem dubbed "The Balance Problem" by P. Falconnet in 1985 [21, 20]. The three suggestions were:

- Discover applications utilizing the REEs that are produced in excess.
- Make REE producers diversify the types of rare earth ores extracted, while also focusing on less common ores containing REEs such as loparite and eudialyte.
- Stimulate recycling of REEs.

Recycling can focus on recovering the specific elements needed, which will exist in vastly different combinations than natural ores, leading to diversification of REE supply. Binnemans claims that the current market is driven by Nd and Dy prices, motivated by the need for strong permanent magnets, which makes these elements a natural point of focus for recycling. The market for REEs is an extremely important factor when considering routes for recycling, especially for the viability of a potential industrial recycling process.

2.4 Rare Earth Element Recycling

Even though the present study is considering raw material in the form of natural minerals product very heterogeneous composition, which is similar to other recycling sources. A wide variety of contaminating species is present in mine tailings, which requires a process capable of handling the chemical variance. Even the REEs will be expected to appear in varying composition, both as groups with the LREEs (Light Rare Earth Elements) and the HREEs (Heavy Rare Earth Elements), but also in the form of individual element concentration. The recycling procedure and its methods need to consider this when designing different steps in the process. In combination with varying composition, the low concentrations of REEs make recycling of these an extremely complicated process. A thorough recycling procedure can not be completed in a single thesis, and the present study is focused specifically on continuing the development of the creation of a Master Slag from the mentioned Apatite Concentrate, stemming from iron mines in Kiruna,

Sweden. None the less, some relevant background information about recycling or recovery of REEs will be covered in this section, both to provide some further motivation and to give a brief introduction to the research done into this topic.

Recycling of rare earths is increasing popularity within academic research these days, as it has continuously the last 15 years. Figure 2.5 shows the growing popularity of publishing within this topic over the years. Using the ScienceDirect database, the search term "recycling AND (rare earth OR REE)" was applied to journals from the years 1960 to 2017. It must be emphasized that the numbers in no way assert the specific number of articles written about rare earth recycling in total, but only the number of hits on the search term. The data is still relevant to show the growing popularity of related articles within a single specific database. The growth observed here could be described as very close to exponential. The modern interest of recycling methods of REEs can not be denied, and could be considered natural consequence of the circumstances.

As the demand for REEs is rocketing, propelled by the green energy sector, sustainable recovery is brought forth as a natural response to the rare earth mining business which is often seen as a rather "dirty" business which have dangerous and toxic waste as byproduct [2, 4, 5, 6]. Recycling activities are not only being performed in laboratory scale in development projects, however. Several companies have reported that they are developing their own recycling methods of electronic scrap for the purpose of recovering REEs and other critical elements. Two examples of this is a technology developed by the U.S. Department of Energy's Critical Materials Institute, licensed to U.S. Rare Earths Inc., and a robot called "Liam" made by Apple Inc. for dismantling and recycling their iPhones [22, 23]. Although efforts are being made and demands for REEs are growing, increasing the incentives for recycling practices, recycling is still a very small part of REE-sources. In the landmark review by K. Binnemans *et.al.* (2013) "Recycling of Rare Earths: A Critical Review", they conclude that up to 2011 less than 1% of REEs were actually recycled [24].

Binnemans *et.al's.* review studies several methods of recycling for a range of REE sources, including magnets, rejected magnets, phosphors, batteries and others. It mentions landfilled REE containing residues, which Apatite Concentrate from iron mine tailings would be considered, but they chose not to include that REE-stream in their review. The review is still very

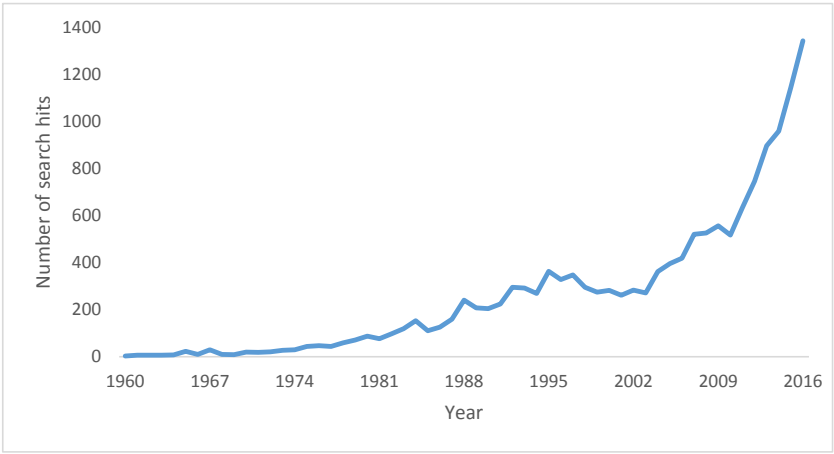

Figure 2.5 – Academic interest in recycling of REEs. Results from a search in the ScienceDirect database with the search term "recycling AND (rare earth OR REE)" within journals in the time period 1960–2016.

interesting and provides insights into motivations for recycling, as well as important issues facing the field. A part of the motivation for increased recycling of rare earths is mentioned in the section on "The Balance Problem". Recycling can target specific critical elements, or combinations that will be of great benefit. Knowing the combinations of REEs in different products gives a good view of how to recover the most scarce elements. Table 2.3 lists the rare earth usage in %, as average consumption distribution by some important REE-containing applications. It gives the founding information for which applications should be in focus for each element in a recycling procedure. For example, magnets are desired to be recycled for the elements Nd, Pr and Dy which are in very high demand, while things like auto catalysts would have less incentives as Ce is the most abundant anyway. Excluding CRT (Cathode Ray Tube) televisions, most of the REE-streams considered

in the review have an increasing or stable contribution of REEs, which is important for the longevity of potential recycling operations.

Table 2.3 – Rare earth usage in %, as average consumption distribution by application. Adapted from Curtis *et.al.* (2010) [25].

Application	La	Ce	Pr	Nd	Sm	Eu	Tb	Dy	Y	Other
Magnets	0	0	23.4	69.4	0	0	0.2	5	0	2
Battery Alloy	50	33.4	3.3	10	3.3	0	0	0	0	0
Metallurgy	26	52	5.5	16.5	0	0	0	0	0	0
Auto Catalysts	5	90	2	3	0	0	0	0	0	0
FCC	90	10	0	0	0	0	0	0	0	0
Polishing Powder	31.5	65	3.5	0	0	0	0	0	0	0
Glass Additives	24	66	1	3	0	0	0	0	2	4
Phosphors	8.5	11	0	0	0	4.9	4.6	0	69.2	1.8
Ceramics	17	12	6	12	0	0	0	0	53	0
Others	19	39	4	15	2	0	0	0	19	1

Methods of Recycling

While examples of industrial recycling of REEs exist, they can still be characterized as kind of fringe and not the norm. There are still huge issues facing the total field of REE recovery that must be addressed for this to truly take off. Three big issues are mentioned in the Binnemans *et.al.* (2013) review, namely [24]

- Inefficient collection.
- Technological problems.
- Lack of incentives.

Inefficient collection is caused by several factors, such as wide variety of applications containing REEs, little public knowledge and education on what REEs are and no centralized collection. All three issues are actually also connected, as there exist no universal solution for collecting and handling the huge variety of electronic waste, phosphors or other REE-containing applications. This also makes the potential technological solutions expensive or inefficient, which again does not promote more or wider collection. The solution is creating closed and fully integrated recycling routes built on the

many processes developed for different REE sources, but optimizing and developing this route is no simple feat. Creating more efficient procedures for the different processes mentioned in the reviews of Binnemans *et.al.* (2013) and Kumar *et.al.* (2017) would be a good place to begin such a recycling route [24, 26]. There are different methods that can be applied on different raw materials, both in primary production and in recycling. A careful consideration of the composition of the material is needed to determine a good route for recycling. Some of the most common methods are:

- Hydrometallurgical method.
- Pyrometallurgical method.
- Gas phase extraction.
- Reprocessing or reapplication.

Hydrometallurgical Method

Hydrometallurgical processing is by far the most common route for recovery of REEs from EOL (End-of-Life) products, as it is easily applied to a wide range of materials. The process has similar processing steps as primary production of REE containing ores [24]. In general the process contains many steps to obtained pure elements or compositions useful for new applications. The leaching processes utilized a large volume of chemicals, many of which might be dangerous for environment, equipment and people.

An example process is the leaching of valuable elements from $SmCo_5$ and $Sm_2(Co,Fe,Cu,Zr)_{17}$ swarf uses a hydrometallurgical process involving sulfuric, nitric, hydrochloric and perchloric acids. Further separation can be acquired in this process by using oxalate acid or ammonia, depending on preferred separation [27, 24]. Lyman and Palmer (U.S. Bureau of Mines) developed a hydrometallurgical process for the separation of REEs from bulk $Nd_2Fe_{14}B$ magnet scrap [28]. This process shows the large amounts of chemical that might be needed in a hydrometallurgical process. To dissolve 1 kg of $Nd_2Fe_{14}B$ scrap, 10 L of 2 M H_2SO_4 solution is needed. This is to keep the pH low enough to keep $Fe(OH)_3$ from precipitating. To achieve this a base is added, such as NaOH, KOH or NH_4OH at which a neodymium alkali metal or ammonium sulfate double salt $Nd_2(SO_4)_3{\cdot}(Na,K,NH_4)_2SO_4{\cdot}6\,H_2O$ is formed [28, 24]. This can be further leached with HF, creating NdF_3, which can be reduced to metal form by calciothermic reduction with calcium metal.

Pyrometallurgical Method

In comparison to hydrometallurgical routes, the pyrometallurgical route consumes less chemicals and have been developed as an alternative to the former processes. A favorable point for a pyrometallurgical route as recycling process is it can operate with both metals and oxides without problem. For a hydrometallurgical route these metals would have to be converted to oxides before separation, a step which can be considered quite wasteful in a process aiming to create metals again. A pyrometallurgical route can consist of one of these three different methods, which are separately applicable depending on the source material.

- Direct remelting.
- Liquid metal extraction.
- Slag refining.

Direct remelting is best for the purest alloys, where the same alloy can be reused, but any oxygen content makes this process problematic as rare earths heavily prefer the oxide phase. Liquid metal extraction utilizes the different solution coefficients in two immiscible liquid metal phases. This method was developed to be able to handle a large compositional variety of source material, but can be hampered by the inability to separate some transition metals from the preferred phases [24]. One version of the slag refining method that has been applied is a glass slag method used on $Nd_2Fe_{14}B$ scrap. Using BO_3, Saito *et.al* (2003) extracted neodymium from $Nd_2Fe_{14}B$-alloys by super-cooling the slag to a glass slag phase. This process left behind alpha$-$Fe and FeB_2 phases with extremely low Nd-content [29].

The pyrometallurgical method is the one utilized in the present study. Through slag refining, the current process intend to enrich the REE content of mine tailing based slag, while at the same time removing problematic or volatile species. As the tailings themselves contain a too low concentration of REEs for hydrometallurgical separation, doping with REEs from *e.g.* Nd magnets could enrich the slag into a product where REEs can easily be separated. This could present a source of REEs previously considered to be unobtainable.

Gas Phase Extraction

Gas phase extraction utilizes reactivity between solid phase REE-containing materials with a gas phase compound. One such method is to react solid

RE-chlorides with aluminum chloride gas to create gas phase complexes [30]. These chloride gases can then be separated from other metal chlorides which are created, by using their different volatility [24]. This process can be used on chlorinated $Nd_2Fe_{14}B$-magnets, recovered from chlorinating magnet scrap with ammonia chloride [31].

Reprocessing or reapplication

The reprocessing or reapplication method will only be suitable for big units or sources of recyclable material with a similar composition both in source material and in end product, *e.g.* large magnets from windmills, magnets from hard drives or for single phosphors [24]. This method is very favorable where applicable as the procedures are very simple and no chemical processing is required. It can be considered a niche method for some specific applications and products.

2.5 Previous Work

The present study follows the work detailed in the project called "Procedure of Master Slag Production Based on the Synthetic System of Nd_2O_3, SiO_2 and CaO" written as part of the coursework for master's degree in material science and engineering at NTNU (Norwegian University of Technology and Science) for Department of Material Science and Engineering. This work is done as part of a collaboration project between NTNU and KTH (Royal Institute of Technology) in Stockholm, Sweden. The work is done under the REEcover project which is elaborated in the next section as well as in the introduction.

The project started with the characterization of Apatite Concentrate, as presented in the article "Apatite Concentrate, a Potential New Source of Rare Earth Elements" by Sun *et. al.* (2015) [8]. The Apatite Concentrate was studied to determine composition and distribution of REEs. Melting and wetting properties were studied to determine melting temperature range and the behavior with different substrates to determine suitable crucible materials. The compositional analysis indicated the possibility of phases containing relatively high concentrations of REEs, mostly in appearing in the mineral monazite. However, the low total concentration of REEs meant it was difficult to get good enough results to make a solid conclusions. A doped high REE concentration material was suggested to avoid the problem of detection difficulties. The experiments also revealed that the melting temperature was

too high for the induction furnace to melt the material properly, even when reaching temperatures of over 2273K. A potential source of the high melting point was suggested to be the high phosphorus content present in the Apatite Concentrate. A process was then developed to remove phosphorus from the material [32]. This low phosphorus containing apatite is the current basis for this study, which also details the procedure of producing the low phosphorus material.

The goal of the project "Procedure of Master Slag Production Based on the Synthetic System of Nd_2O_3, SiO_2 and CaO" was to create a possible procedure for creating a Master Slag-like material of homogeneous composition of the synthetic system mentioned. The important conclusions reached was that a melting temperature of at least 1873 K for 60 minutes was needed for complete melting. This step was to be repeated 2 times with crushing and milling of the slag in between, to reach a suitable homogeneity. The preliminary tests with synthetic slag confirmed the suspicions that the phosphate-free material was suitable for melting. The preliminary step of removal of phosphate from the Master Slag was therefore recommended before trying to create the Master Slag from the Apatite Concentrate.

2.6 REEcover

REEcover is a project funded by the EC under FP7 to search for potential new sources of REEs. It is separated into two paths, both with the goal of recovering REEs. These two are recycling of REEs from WEEE, and recovery of REEs from iron mine tailings. This project focuses on the latter, and considers iron mine tailings from the LKAB mine in Kiruna, Sweden. A simple distinction for the processing procedures is that WEEE consists of low volume, high REE concentration materials, while the mine tailings consist of high volume, low REE-concentration materials. This project is trying to develop a process for upgrading the REE-content in an Apatite Concentrate. This upgraded material is defined here as a Master Slag, and the goal is to create a Master Slag that can be the basis for further REE separation and recovery.

The project has potential benefits for a range of different industries. Investigating the possibility of extracting REEs from low-concentration sources could also interest other parties, and benefit many industries that rely on REEs. The present study contains the experimental work for only a small part of this vision, but the small strokes still paint the big picture.

Chapter 3

Theory

Modern energy production, high efficiency applications and advanced technologies are in critical need of REEs to be able to compete with existing technology. Alternative sources or process routes for recovery of REEs is highly sought after. This section will provide the theoretical foundation for the production and processing of the Master Slag, as well as the potential for REE recovery.

3.1 Chemistry

The Rare Earth Elements

The REEs are a group of 17 elements, consisting of the lanthanides, Y and Sc [1]. The elements are grouped because of their similar chemical properties, and especially so for the elements close to each other in the periodic table. It took a long time for scientists to discover how to separate the different elements. The first ones were discovered in Ytterby in Sweden in the late 1700s, a city which gave name to several of the elements, such as Y. The last one to be discovered was Pm, the only element without stable isotopes, which where created and discovered in the 1940s. A key property of the REEs is that they do not exist as pure rare earth compounds. They exist in various mixtures, scattered in low concentrations in the earth's crust [1]. This means that it is hard to find sources where the concentration is high enough for economically feasible extraction, as well as requiring advanced separation methods to recover the elements. This is possibly a reason for

the naming of these elements, as several of them are more abundant than elements such as copper [1].

A key property of the REEs is their ionic size which decreases with increasing atomic number of the lanthanides. Almost all the elements are most stable in their trivalent condition, and the size differences of these trivalent ions can be visualized with a trend seen in relation to their atomic number. When moving from La going right in the lanthanide group, the ionic radii become smaller and smaller, ending at the smallest, Lu [1]. This trend can be seen in Figure 3.1, where the alternative valency situations are also shown. Other valencies such as Ce_4^+ and Sm_2^+ exist, but the trivalent state is the most common. For practical reasons, the REEs are often separated into to subgroups. These groups are called the Light Rare Earth Elements (LREE) and the Heavy Rare Earth Elements (HREE). The distinction between these two can vary mildly depending on area of use. Gupta [1] refers to the report from Jackson and Christiansen from 1993 [33], and groups La to Gd into the LREEs, and Tb to Lu, including Y, as the HREEs [1, 33]. Henderson [34] refers to La to Sm as the LREEs, and Gd to Lu, including Y, as the HREEs [34]. Henderson also mentions the occasionally used third subgroup Middle Rare Earth Elements (MREEs), including the elements from Pm to Hm [34].

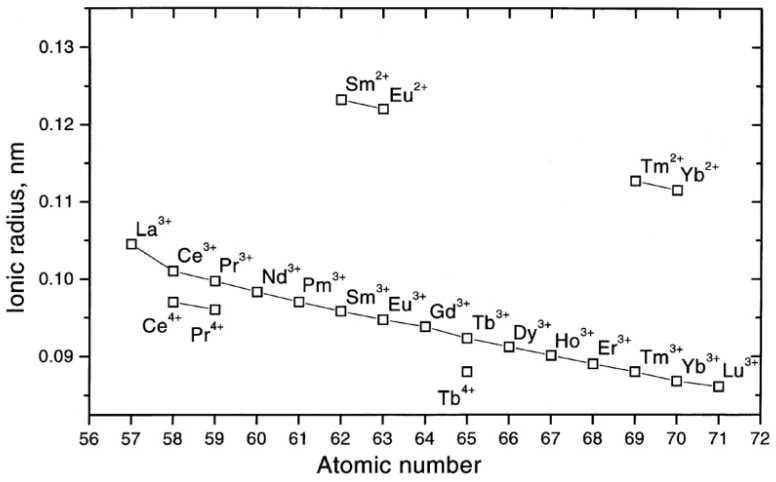

Figure 3.1 – The Lanthanide contraction [1].

The reason for the contraction in size as the atomic number increases, can

be explained by the increased effective nuclear charge, that affects the additional electrons. The f-orbitals have a very directional geometry, and the lower electron states will therefore not shield very well for the higher electron states. Shielding can be explained as an electron's ability to decrease the nuclear charge experienced by another electron in a higher energy state. This means that for every "next" proton, the corresponding additional electron will experience a higher effective nuclear charge and will be "pulled" harder towards the nucleus, which results in the size decrease of the entire 4f shell [1]. The size of Y corresponds more with the HREEs, and will more often be found in minerals where they are present [1]. Sc is quite different in size and does not really behave in similar ways as the other REEs, and is not generally found in rare earth minerals [1]. Y and Sc do not have f-orbitals, but have valence electrons in 4d and 3d orbitals, respectively. The 4f electrons are also the cause of the unique magnetic properties of the REEs, which is maybe the most important difference from other elements, and is what created a demand for their use. The chemical similarity due to the similar size of some of the REEs is the reason why *i.e.* Nd is used to study the behavior of all the LREEs, not just Nd itself.

Apatite Concentrate

Apatite Concentrate is a name given to the material obtained as the apatite ($Ca_5(PO_4)_3$ (OH,F,Cl)) containing part of tailings from the iron mine industry in Kiruna. Studies done on the Apatite Concentrate confirms the presence of REEs, with a dominance of LREEs. The REEs exist in the apatite, as well as in inclusions or particles of monazite ($(Ce,La,Nd,Th)PO_4$) and allanite ($Ca(R,Ca)Al_2(Fe^{+2},Fe^{+3})(SiO_4)(Si_2O_7)O(OH)$) [7], where R is a REE. According to Sun *et. al.* [8], who did most of the work on Apatite Concentrate at NTNU prior to the present study, the content of REEs in Apatite Concentrate in question was estimated to 3517 $mg\,kg^{-1}$ [8]. Out of these REEs, it was estimated that the content of Nd was in the range of 800 $mg\,kg^{-1}$ [35]. Considering that apatite itself is only a small part of the iron ore tailings, the real concentration of REEs in this raw material is very low. However, the sheer volume of mine tailings makes this a considerable REE source, despite its low concentrations. The three most common REEs in Apatite Concentrate is Ce, La and Nd [7, 8].

Phosphorus Removal

The Apatite Concentrate in this study is the raw sample from LKAB, and contains a large amount of P_2O_5. Its content was measured to be ~32 wt.% P_2O_5 [8]. As a part of the present study, the removal of phosphorus is included as a experimental step, as it is crucial to the actual process of creating a Master Slag. The experiment itself requires extreme caution and safety procedures, as the compounds white phosphorus (P_4) and phosphine gas (PH_3) are produced. The procedure and safety measures are described in Chapter 4.2.

In conventional production of white phosphorus, called the Wöhler process, fluorapatite reacts with carbon and silica to form P_2 gas according to Equation (3.1) [36]. Due to the low amount of silica in the Apatite Concentrate, this reaction will probably contribute only a small part. The main reaction for phosphorus production will come from reduction of apatites as described in Equation (3.2a). The P_2 gas ultimately condenses into P_4 below 1100 K, as in Equation (3.2b) [32, 37]. When dry air comes in contact with the condensed P_4, P_4O_{10}, also known as P_2O_5, is spontaneously formed as shown in Equation (3.2c).

$$2\,Ca_5(PO_4)_3F + 15\,C + 9\,SiO_2 \longrightarrow 3\,P_2(g) + 9\,CaSiO_3 + CaF_2 + 15\,CO(g) \tag{3.1}$$

$$2\,Ca_5(PO_4)_3F + 15\,C \longrightarrow 3\,P_2(g) + 9\,CaO + CaF_2 + 15\,CO(g) \tag{3.2a}$$

$$2\,P_2(g) \longrightarrow P_4(l) \tag{3.2b}$$

$$P_4(l) + 5\,O_2(g) \longrightarrow P_4O_{10}(s) \tag{3.2c}$$

Not all phosphorus will react to P_2O_5 this way, and can be present as *e.g.* AlP. The addition of water will react with this according to Equation (3.3) [32].

$$AlP + 3\,H_2O \longrightarrow Al(OH)_3 + PH_3 \tag{3.3}$$

At temperatures above 2073 K, the formation of CaC_2 will greatly increase [38], which will also proportionally increase the production of P_2 gas. This is explained by the consumption of CaO in the reaction for CaC_2 production,

shown in Equation (3.4), which by Le Châtelier's Principle [39] will increase the reaction rate of Equation (3.2a).

$$CaO + 3\,C \longrightarrow CaC_2 + CO \tag{3.4}$$

When CaC_2 is present when water is added, it will spontaneously react and form acetylene gas and $Ca(OH)_2$ [35], as shown in Equation (3.5). $Ca(OH)_2$ will decompose into CaO during heating, and release water vapor.

$$CaC_2 + 2\,H_2O \longrightarrow C_2H_2(g) + Ca(OH)_2 \tag{3.5}$$

Master Slag

The Master Slag is the term determined for the slag created by the melting of a low-phosphorus Apatite Concentrate. The purpose of the slag is to create a single composition material from an Apatite Concentrate, containing up-concentrated phases of REEs. The purpose of the Master Slag is to be the basis material for separation of REEs from iron mine tailings. To do this, a consistent composition is important for establishing such a procedure. Currently, the Master Slag created with the relative composition of Nd_2O_3, SiO_2 and CaO at 10%, 42.5% and 47.5% respectively. This composition is kept to have the same conditions for analysis, as this project is still in the characterization stage. With the additional knowledge of the behavior of Nd in this slag at this composition, it will be possible to do experiments with varying compositions of Nd to discover the optimal concentrations of REEs in the Master Slag to balance process difficulty and economics. The lower amount of REEs that needs to be added to a Master Slag will increase the economic potential for the process.

In the present study, preliminary experiments are performed to understand the fundamental behavior of a Master Slag, and compare the compositional results with theoretical behavior of Nd according to thermodynamic estimates. Getting an understanding of the properties of Nd in this slag system will be crucial for any future pyrometallurgical routes in REE recovery. A natural source of Nd-doping of the iron mine tailings would be from electronic waste, in the form of neodymium-iron-boron ($Nd_2Fe_{14}B$) magnet scrap. In the present study there will be featured experiments for the purpose of creating the Nd_2O_3-SiO_2-B_2O_3 phase diagram. This will provide background into the thermodynamic fundamentals of Nd-B containing systems and be relevant for the future of this project. As the overall focus

is recycling purposes, both the experimental work experience and the thermodynamic data gathered can be important for the development of similar recycling process routes.

3.2 Thermodynamics

According to Callen [40], "thermodynamics is the study of the restrictions on the possible properties of matter that follow from the symmetry properties of the fundamental laws of physics", and according to Atkins [41], "Thermodynamics, the study of the transformations of energy". These explanations assert the fundamental importance of thermodynamics in all aspects regarding matter and energy. As materials scientists, the knowledge of how materials behave in a given system comes from their thermodynamic properties. All systems change towards the equilibrium state, and knowledge of which properties affect this equilibrium enables the manipulation of materials to their suited properties. With this in mind, the thermodynamic background of the Nd_2O_3-SiO_2-CaO ternary system, of which the Master Slag is based on, is presented in this section. In addition, the thermodynamic background of the Nd_2O_3-SiO_2-B_2O_3 ternary system is also presented. This system contains information on how B affects the chemistry of Nd in silica-based slags, as well as providing crucial information for any effort into recycling Nd-magnets, where B is a central element.

Binary Systems

The different binaries as well as a short summary of their history is presented here. Applicable information about some phases and transitions are added where relevant. The binaries in question are:

- i) $CaO-SiO_2$
- ii) $Nd_2O_3-SiO_2$
- iii) Nd_2O_3-CaO
- iv) $Nd_2O_3-B_2O_3$
- v) $B_2O_3-SiO_2$

i) $CaO-SiO_2$
This system is very common in metallurgical slags, and has been investigated and optimized thoroughly [42]. This system forms the basis of the Master

Slag which is and is an integral part of the present study. The binary phase diagram is presented in Figure 3.2.

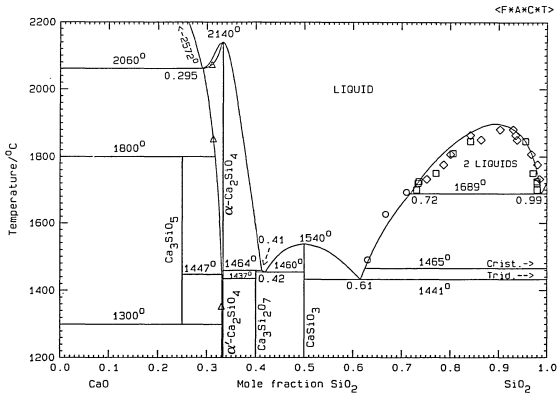

Figure 3.2 – SiO_2−CaO binary phase diagram. As optimized by Eriksson *et.al.* (1994) [42].

ii) Nd_2O_3−SiO_2

This binary system was first researched in the 1960s, independently by Toropov (1965) and Miller (1964), without significant differences [43, 44]. The stable compounds in this binary system are Nd_2SiO_5, $Nd_2Si_2O_7$ and $Nd_{14}Si_9O_{39}$, excluding the pure oxides [45]. The binary phase diagram is presented in Figure 3.3.

iii) Nd_2O_3−CaO

Previous assessments of the ternary system Nd_2O_3-SiO_2-CaO by Le *et. al.* could not determine the thermodynamic properties of this binary [45]. Instead an assumption of ideal solution for the liquid phase, and no solution of the solid phase was made. The binary phase diagram is presented in Figure 3.4.

iv) Nd_2O_3−B_2O_3

This binary system was optimized by Jakobsson *et. al.* (2017) [46], by comparing thermodynamic data obtained by different researchers [47, 48] with calculations of Gibbs energies for the system. The measurements have reported the stable solid phases $NdBO_3$, NdB_3O_6 and $Nd_4B_2O_9$. The binary phase diagram is presented in Figure 3.5.

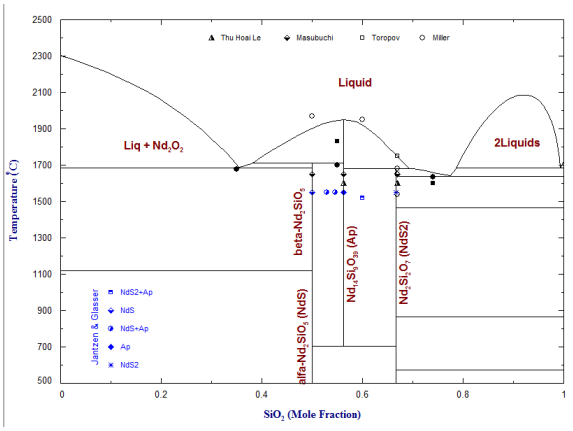

Figure 3.3 – Nd_2O_3–SiO_2 binary phase diagram. As optimized by Le *et.al.* (2016) [45].

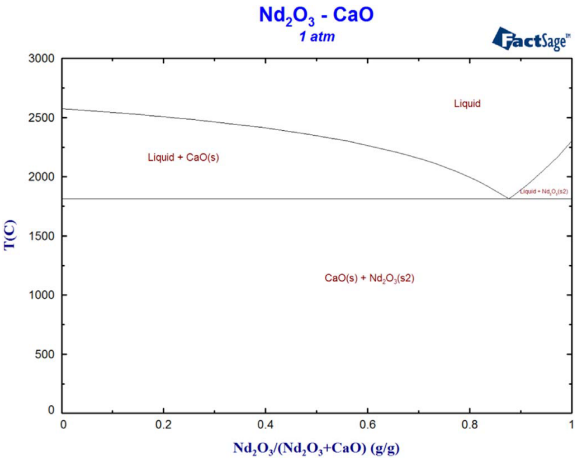

Figure 3.4 – Nd_2O_3–CaO binary phase diagram. As estimated by Le *et.al.* (2016) [45].

v) B_2O_3–SiO_2

The optimization of this system were done by Decterov, Swamy and Jung [49, 50]. The thermodynamic data is directly available in the FactSage FTOxid database. Decterov *et. al* reviewed several different researcher's approach to experimenting on this system, and discussed the differences and complexities arising from different research techniques. The existence of a metastable phase was reported, but not included in the optimization as Decterov *et. al.* could not find supporting evidence for this conclusion [49].

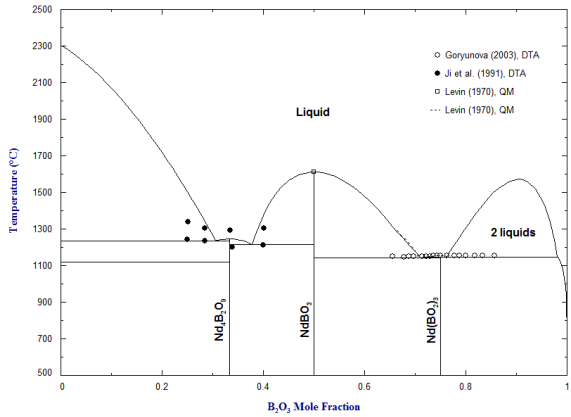

Figure 3.5 – Nd_2O_3–B_2O_3 binary phase diagram. As optimized by Jakobsson *et. al.* (2017) [46].

The binary phase diagram is presented in Figure 3.6.

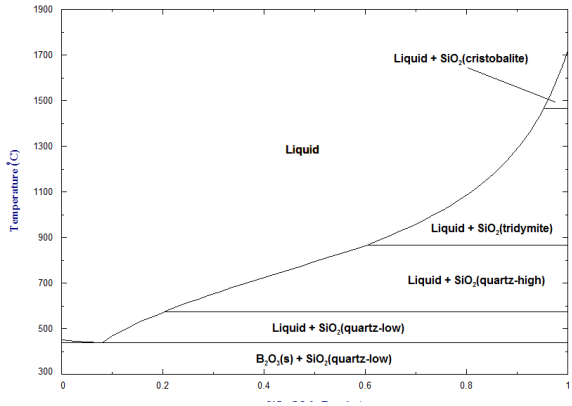

Figure 3.6 – B_2O_3–SiO_2 binary phase diagram. Made by Sun *et. al.* [35] based on data from Swamy *et. al.* (2009) [50].

Ternary Systems

The binary systems presented in the previous section compose the ternary systems presented here. As all species included are oxides, it could be useful to consider these systems as pseudo-quaternary, but for all intents and

purposes, oxygen can be neglected as a separate species, as it will always be present as oxide.

- i) Nd_2O_3–SiO_2–CaO
- ii) Nd_2O_3–SiO_2–B_2O_3

i) Nd_2O_3–SiO_2–CaO

A thermodynamic description of this system was made by Le *et. al.* (2016) using the CALPHAD approach, utilizing the Modified Quasichemical Model (MQM). This model is briefly explained in 3.2. The optimization included experimental data from previous researchers on phase equilibrium in this system [51, 52]. The phase equilibria for the compositions Ca_2SiO_4–$Nd_4Si_3O_{12}$ and Ca_3SiO_5–Nd_2SiO_5 were studied by Jantzen and Glasser [52], who used the data to propose an isothermal section of the system at 1673K (1400°C). Based on the radial similarity of Ca^{2+} and Nd^{3+} ions, as well as the affinity for silicates, Le *et. al.* proposed different ternary solid solutions in the system. They are $(Ca,Nd)_2SiO_4$, $(Ca,Nd)_3SiO_5$ and $Ca_{2+x}Nd_{8-x}(SiO_4)_6O_{2-0.5x}$. The third compound was studied by Fahey *et. al.*, and at 1773 K and 1873 K, x was found to be in the range 0-0.8 and 0-0.7 respectively [53]. Isothermal sections of the ternary system was proposed for 1873 K (1600°C), and is presented in Figure 3.7.

ii) Nd_2O_3–SiO_2–B_2O_3

There exists no phase diagram presently for the Nd_2O_3–SiO_2–B_2O_3 system, but it is in the process of being developed in a collaboration between KU Leuven, KTH, NTNU and SINTEF [35]. In the present study, experimental work with the purpose of optimizing this phase diagram has been done, as described in Chapter 4.2. Figure 3.8 show the modeled isothermal section at 1873 K of the Nd_2O_3–SiO_2–B_2O_3 ternary phase diagram, with points marked for experimental verification conducted during the present study.

The CALPHAD Approach

The CALPHAD (CALculation of PHAse Diagrams) approach is a method where calculated thermodynamic values are used to estimate the properties of a system. Lukas [54] explains it as "The Calphad technique [...] is now a powerful method in a wide field of applications where modeled Gibbs energies and derivatives thereof are used to calculate properties and simulate transformations of real multicomponent materials." Where thermodynamics describe the equilibrium of a system, CT (Computational Thermodynamics)

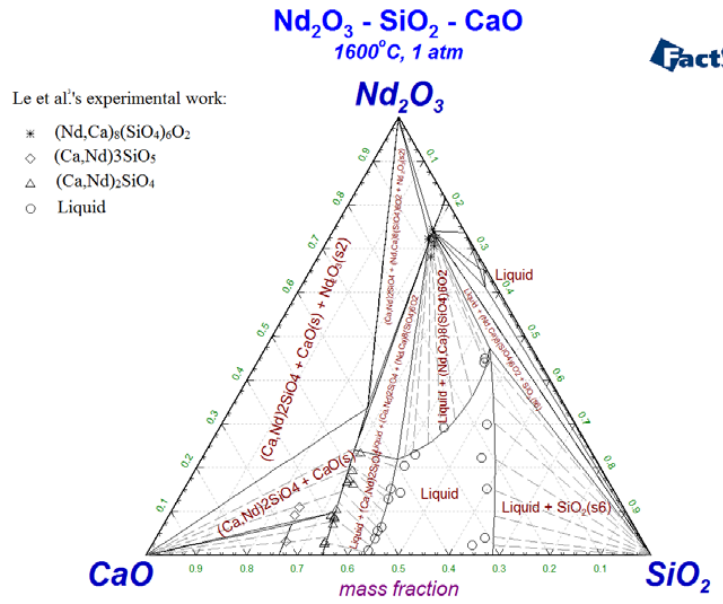

Figure 3.7 – Isothermal section of the Nd_2O_3–SiO_2–CaO phase diagram at 1873 K (1600°C), by Le *et. al.* [45].

describe the equilibrium state using thermodynamic functions that depend on temperature, pressure and composition [54].

Modified Quasichemical Method

The MQM (Modified Quasichemical Model) [55] is a suitable model for describing liquid oxide phase. It considers short-range ordering of the second-nearest neighbors of cations with O^{2-} as a common anion in the oxide melt. In the present study, CT was not specifically applied, but experimental work in the process of optimizing the Nd_2O_3–SiO_2–B_2O_3 phase diagram was conducted as detailed in Chapter 4.2. The description of the CALPHAD approach and MQM here is present to aid to understanding of how a phase diagram is constructed, and to see how experimental data can aid this process. A brief description of this model is given below. In molten Nd_2O_3–SiO_2–B_2O_3, the Gibbs energies of the second-nearest-neighbor pair

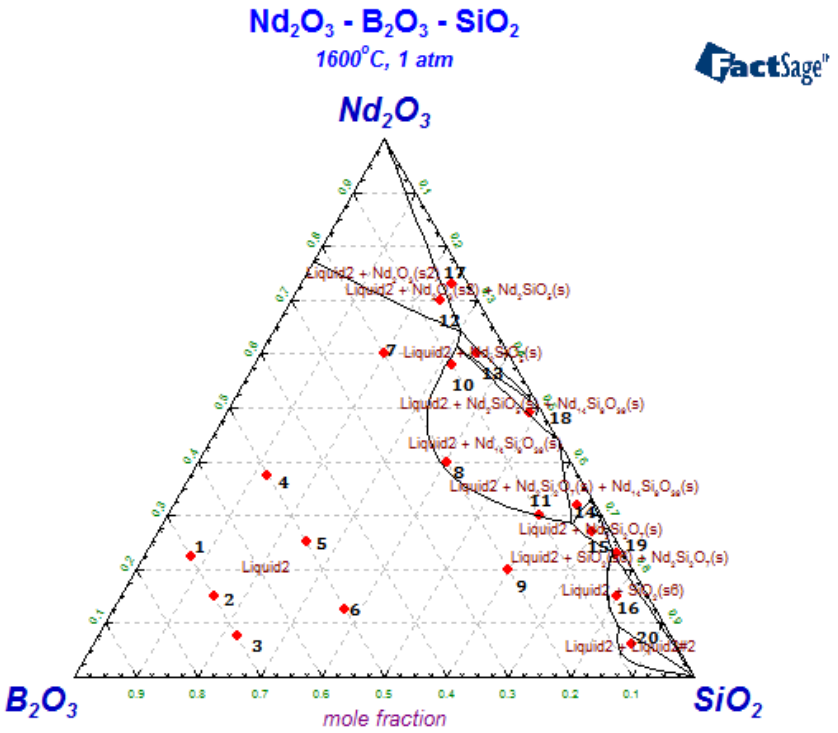

Figure 3.8 – The compositions of the samples for the phase diagram experiment, marked on the modeled Nd_2O_3–SiO_2–B_2O_3 phase diagram. Data listed in Table A1.

exchange reactions are,

$$(Nd - Nd) + (Si - Si) = 2(Nd - Si) \qquad \Delta g_{NdSi} \tag{3.6a}$$

$$(Nd - Nd) + (B - B) = 2(Nd - B) \qquad \Delta g_{NdB} \tag{3.6b}$$

$$(Si - Si) + (B - B) = 2(Si - B) \qquad \Delta g_{SiB} \tag{3.6c}$$

Where (A - B) indicate the second-nearest neighbor pair and Δg_{AB} is the Gibbs energy change of the exchange reaction. With these approximations of Gibbs energies, the phase diagram can be computationally modeled.

Chapter 4

Experimental

This chapter contains the experimental work as well as describing the technical equipment used during the study. All pyrometallurgical experiments were conducted in a vacuum induction furnace at Department of Material Science, NTNU, except for the phase diagram experiment conducted at KU Leuven, which is described in Chapter 4.2. The analysis where done with help from technical staff at Department of Material Science at NTNU, as acknowledged. Figure 4.1 show a simplified version of the REE-recovery process through the production of Master Slag. The scope of this thesis include the steps from Apatite Concentrate trough Master Slag production.

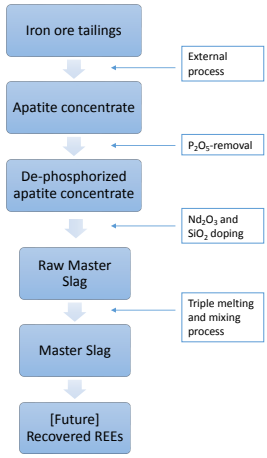

Figure 4.1 – Process flow sheet for the recovery of REEs from the production of Master Slag.

4.1 Equipment and Materials

A full list of equipment and chemicals with relevant specifications are supplied in Appendix A. The vacuum induction furnace is shown in Figure 4.2.

Figure 4.2 – Vacuum induction furnace, produced by Elatec Technology corp.

Induction Furnace Setup

Before setting up the experiments the inside of the furnace and the coil was thoroughly cleaned. A large piece of graphite wool was fitted around the outer crucible, so that the height of the wool was a bit higher than the crucible. A piece of mica was placed on the outside of the wool before being placed inside the induction coil. A tight fit was obtained between the insulation and the coil.

Setup Variations

The different experiments conducted with the induction furnace used basically the same standard setup, with variations depending on the specific needs of the experiment. Below are listed the biggest variations on the setup used in with the induction furnace. Schematic diagrams of the cross sections of these set-ups are presented in Figure 4.3, 4.4 and 4.5 for the respective experiment variations.

Phosphorus removal:

- No inner crucible was used.
- Deeper outside graphite crucible was used.

- Thermocouple placed in graphite tube.

Melting experiments:

- Both graphite and molybdenum inner crucible were used during melting experiments. See discussion in Chapter 6.2.
- Molybdenum wires were hooked over the crucibles, holding the inner crucible contained as a safety measure.

Sampling experiments:

- Molybdenum inner crucible.
- No casting.
- Copper rod with handle used to take samples.

4.2 Experimental Methods

The procedures described here are all heavily based on the procedure described in "Procedure for Master Slag Production Based on the Synthetic System of Nd_2O_3, SiO_2 and CaO" [9]. In this thesis, the creation and characterization of Master Slag consist of three main procedures: Phosphorus removal, slag melting and slag sampling. The phosphorus removal and the sampling technique were not done in the previously mentioned project, but the same procedure were used as a basis with modifications according to each experiment type.

In addition to the production of the Master Slag, experimental work was conducted for the creation of the Nd_2O_3–SiO_2–B_2O_3 phase diagram. While not directly related to the Master Slag production, the B_2O_3-containing system is of interest for the future of upgrading slag content from B containing, Nd-based materials.

Phosphorus Removal from Apatite Concentrate Procedure

Apatite Concentrate contains around 32% P_2O_5 by weight, which is required to be removed to achieve a material that can melt at the relevant temperature [8]. To remove this phosphorus, a pyrometallurgical procedure was developed previously at NTNU [32]. The reactions during the procedure

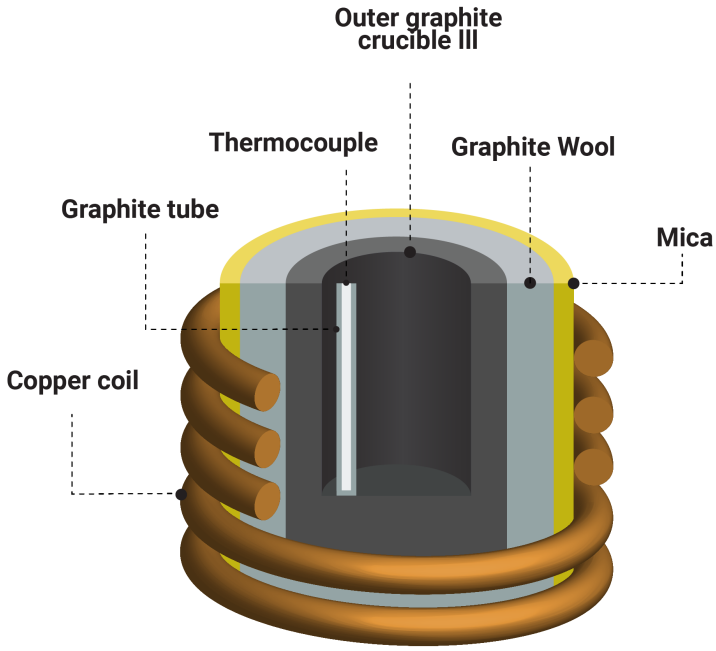

Figure 4.3 – Schematic diagram of the experimental setup inside the furnace for the phosphorus removal experiment. Samples are placed inside "Outer graphite crucible III". [56]

create very dangerous chemicals, and serious safety precautions and preparation were taken.

The raw Apatite Concentrate was placed in a large graphite crucible, which in turn was placed inside the induction coil inside the vacuum induction furnace following the description in Chapter 4.1. This setup is schematically depicted in Figure 4.3. At approximately atmospheric pressure, the furnace chamber was constantly purged with inert gas (argon 5.0) at ~9.4 $\mathrm{L\,min^{-1}}$ (20 SCFH). The temperature was gradually increased to ~2123 K. During the temperature increase, close observation to development of smoke and small particles from the crucible were made, as well as any pressure increase. After approximately 60 minutes at temperature above 2073 K, and until smoke development became minimal, the furnace was shut down and sample

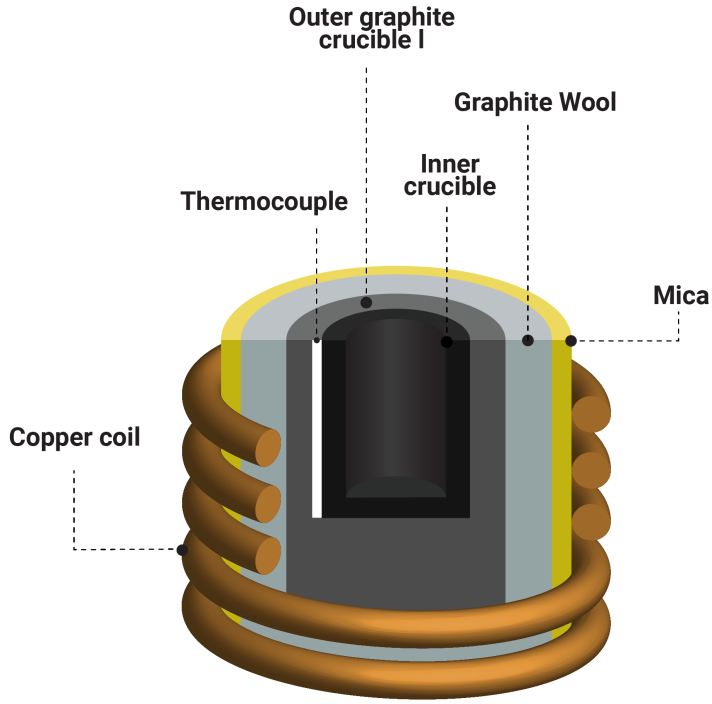

Figure 4.4 – Schematic diagram of the experimental setup inside the furnace for the melting experiment. Samples are placed inside "Graphite inner crucible". [56]

left to cool, still under inert gas purge. When the temperature in the crucible was measured to become below 973 K, dry air was pumped into the chamber, as a large amount of white smoke developed. Air flow was maintained for 12 h for safety reasons and diffusion time, while the sample cooled down to room temperature. A 3M 7000-series mask with 3M 6057 filters were equipped by all operators in the room before the furnace door was opened. With extreme caution, the crucible with sample was moved to fume hood and placed inside an open desiccator. Distilled water was poured into the crucible until it was ~80% full and the fume hood door was closed, as gas development and bubbles were observed. After 2-3 hours, the sample was stirred and left in the fume hood over night to completely react with the water to produce phosphine gas. No fume hoods connected to the same ventilation system were operated during the time phosphine gas were produced in this process.

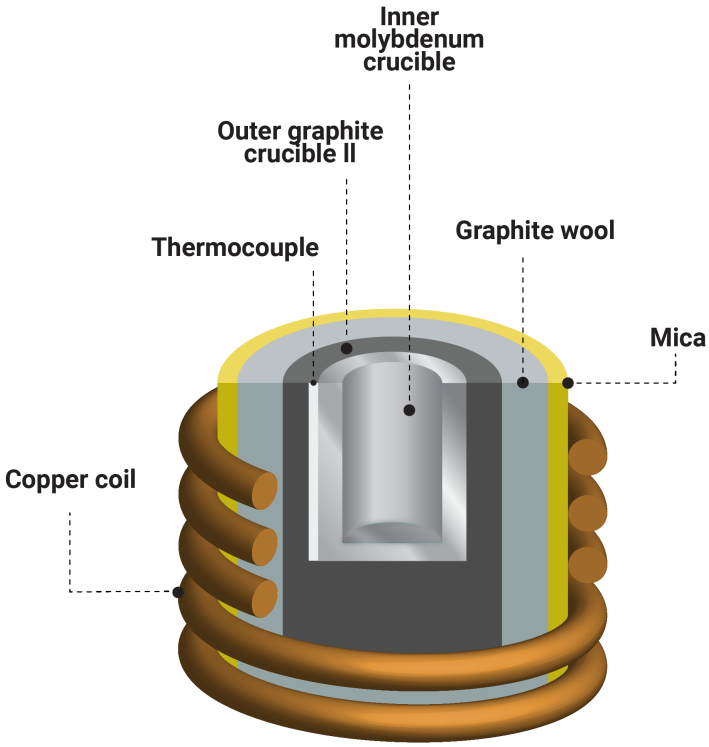

Figure 4.5 – Schematic diagram of the experimental setup inside the furnace for the melting experiment. Samples are placed inside "Molybdenum inner crucible". [56]

After total evaporation of phosphine, the sample was completely dried with a Büchner funnel vacuum filtration setup. Phosphine gas concentrations were continuously monitored during and after the experiment, using "Phosphine 0.1/c" Dräger tubes, in the room, in the furnace (when possible) and in the fume hood.

Master Slag Melting Procedure

The procedure described here was developed in the previously referenced work [9]. The setup was assembled as depicted in Figure 4.4 or 4.5, and the sample placed inside the inner crucible. This setup was first assembled with graphite inner crucible for synthetic samples, but later only molybdenum

inner crucible was used, see Chapter 6 for discussion around this. The synthetic system was treated as it was, and to the raw Master Slag (dephosphorized Apatite Concentrate), Nd_2O_3 and SiO_2 were added so that the relative composition of the elements Nd_2O_3, SiO_2 and CaO were respectively 10%, 42.5% and 47.5% based on weight. The temperature was gradually increased to ~1873 K, and held there for 60 minutes. The material were then cast in a copper mold in an inert atmosphere by tilting the copper coil with the crucibles inside. The cool slag was then crushed in a ring mill at 800 rpm for 15 seconds. This procedure was repeated until the sampling procedure was applied.

Master Slag Sampling Procedure

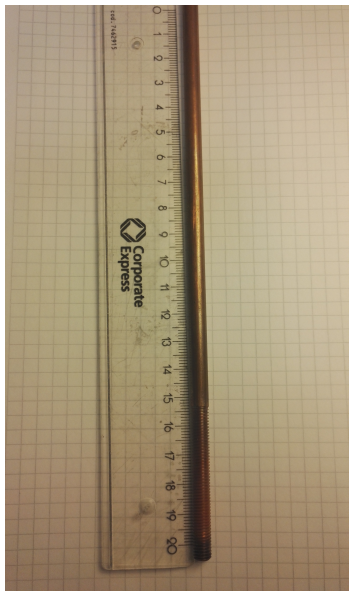

Figure 4.6 – Copper rod used for sampling. Total rod length is 35cm.

Figure 4.7 – Tube chamber for sampling. Red arrow indicates the insertion chamber.

The procedure follows the same structure as in Chapter 6.2 up until the casting, where in-situ sampling with a copper rod was applied instead. A copper rod was inserted through a tube directly down into the crucible from the top. The temperature was set to 1873 K and three samples were taken at each of the set temperature, before it was lowered to 1853 K, 1823 K, 1803

K, 1773 K and 1723 K. Three samples at each temperature were attempted at 0, 10, and 20 minutes holding time after target temperature was reached. The first sample at 1873 K was taken after 1 hour holding time, which is the required time for melting after the procedure [9]. The dip into the crucible required a quick and smooth movement. A piece of slag solidified on the top of the rod which was then withdrawn from the furnace. The tube-chamber in which the rod was inserted contained a vacuum chamber that was purged with inert gas (Argon 5.0) three times before being connected to the furnace atmosphere. The tube-chamber can be seen in Figure 4.7. When removed, the rod with the piece of slag was cooled down in a bucket of water, before the samples were dried and stored. The setup was identical to the melting setup, which is depicted in Figure 4.5. In addition to this setup, a copper rod with a steel handle was used for sampling through a tube chamber in the induction furnace, shown in Figures 4.6 and 4.7, respectively.

Nd_2O_3–SiO_2–B_2O_3-Phase Diagram Procedure

This experiment were conducted at KU Leuven, and the equilibrium melting was done in a Al_2O_3 tube furnace.

Two mixtures of Nd_2O_3, SiO_2 and B_2O_3 were pressed into pellets and sintered in a muffle furnace at 1073 K for 10 hours. These pellets were then crushed. 18 other samples where mixed from the sintered samples, with different amounts of Nd_2O_3 and SiO_2 into the compositions listed in Table A1, using a weight with 0.01 mg precision. Sample "PD1" and "PD2" were the sintered mixtures. All the 20 samples were then carefully mixed in a mortar, being thoroughly cleaned between samples. The samples were then filled into separate envelops of Pt-20%Rh foil, and marked. The envelopes were then placed in a supporting Al_2O_3 crucible. Then the supporting crucible was hung by a Pt-20%Rh wire in a hot zone of a Al_2O_3 tube furnace and heated up to the desired temperature 1873 K for 24 hours. The crucible was then dropped into a bucket of cold water for quenching. The envelopes were then dried and prepared for analysis. For discussion around the experiment temperature, see Chapter 6.4.

Analysis

Analysis were conducted with equipment at NTNU. ICP-MS, SEM-EDS and XRD were used for the characterization of the Master Slag samples. This section provides specific information about the equipment used.

ICP-MS
ICP-MS analysis were done in accordance to International Organization for Standardization (ISO) number 14869-2 "Soil quality - Dissolution for the determination of total element content - — Part 2: Dissolution by alkaline fusion" [57]. The process principle is described:

> "To avoid reduction of metallic oxides to metals, the dried and ground sample is first ignited at and afterwards fused with a mixture of dilithium tetraborate (one part) and lithium metaborate (four parts). While still liquid, the melt is poured quantitatively into dilute nitric acid. The suspension is then stirred until the solid phase dissolves completely."

The entire procedure is detailed in the referenced standard [57]. This method was chosen as it was capable of dissolving both Nd and Si, providing the possible analysis for the samples used.

SEM-EDS
SEM-EDS analysis were done by a LVFESEM Zeiss Supra 55 VP. Pictures were taken with the following specifications:

- EHT: 15.00 kV.
- AsB detector for BSE.
- SE2 detector for SE.
- WD: 9-13.5 mm.
- Magnification up to 2000X.

Where EHT (Extra High Tension) is the accelerating voltage, WD is the working distance, BSE is back-scattered electrons and SE is secondary electrons. BSE are electrons "knocked" out from the sample volume below the electron beam. The excitation of these electrons release characteristic x-rays for each band gap of each element. EDS (Electron Dispersive X-Ray Spectroscopy) detects these characteristic x-rays and estimate the relative composition in the volume scanned.

XRD
XRD was recorded on a Bruker D8 Advance fitted with a Lynxeye XE detector, operating with Cu Kα radiation accelerated at 40 kV and 40 mA. The data were recorded from 15° 2Θ to 75° 2Θ using a step size of 0.013°

and a counting time of 0.38 s per step. A variable divergence slit opening was used exposing 6 mm of the sample through the recordings. The characterization were done with the PDF-4+ database, licensed from ICDD (The International Centre for Diffraction Data).

Chapter 5

Results

This chapter will present the relevant results of the experimental procedures described in Chapter 4.1. In Chapter 6, these results are explained and supplied with relevant information. To reiterate, the presented results will fall into these categories:

- Phosphorus Removal
- Master Slag Melting
- Master Slag Sampling
- Nd_2O_3–SiO_2–B_2O_3 Phase Diagram

5.1 Phosphorus Removal

The phosphorus removal experiment was in the big picture an intermediate experiment to prepare the Apatite Concentrate for further use. The main objective is to document the the relative content of phosphorus before and after the procedure. The suggested reactions by which this happens is also proposed in Chapter 6. Continuous improvements to the experiment procedure were done as new information were obtained. During one of the parallels, there was an issue due to operator error causing the holding temperature to be too low. Figure 5.1 shows the temperature and pressure profile of this experiment where temperature reached a max of 1935K, while Figure 5.2 shows the profiles for one experiment where the max temperature reached 2100K, which was a more preferable procedure. Table 5.1 shows the

ICP-MS analysis result of the Apatite Concentrate, as well as the resulting composition of the de-phosphorized samples. The difference between the start and end phosphorus content is between ~12-14% of starting weight. The experiments with max temperatures around ~2100 K all ended with a phosphorus concentrations of less than 1000ppm, from a starting concentration of ~14%. Due to the nature of the raw material there will be a varying starting composition, but this process has shown the ability of removing practically all the phosphorus present, with the capability of removing up to 99.7% of the phosphorus. The phosphorus contents is highlighted in bold in Table 5.1. The temperature and pressure plots of all phosphorus removal experiments conducted during the present study can be found in Appendix C and the raw temperature data is presented in Table A2.

Table 5.1 – Results from ICP-MS analysis of Apatite Concentrate and the de-phosphorized products after the phosphorus removal experiment.

Element	Apatite [ppm]	De-P#2 [ppm]	De-P#3 [ppm]	De-P#4 [ppm]
Nd	671	1622	1164	2012
Y	528	990	1029	1083
Dy	83.9	189.3	85	81
Tb	16.3	32.9	<150	<150
Ce	1510	3442	X	X
La	703	1537	1526	1649
Pr	163	408	<150	<150
Sm	110	252	<70	<70
Gd	120	276	<150	<150
Si	56238	X	8896	16519
Al	1067	2039	1610	1714
Ca	325050	723845	635737	655491
P	**141671**	**882**	**20177**	**436**
Fe	7376	2371	15239	2179
Mg	7095	6692	9792	4043
Ti	515	1359	X	X
K	205	X	<200	<200
Na	767	X	<200	<200
Mn	1349	533	1594	625

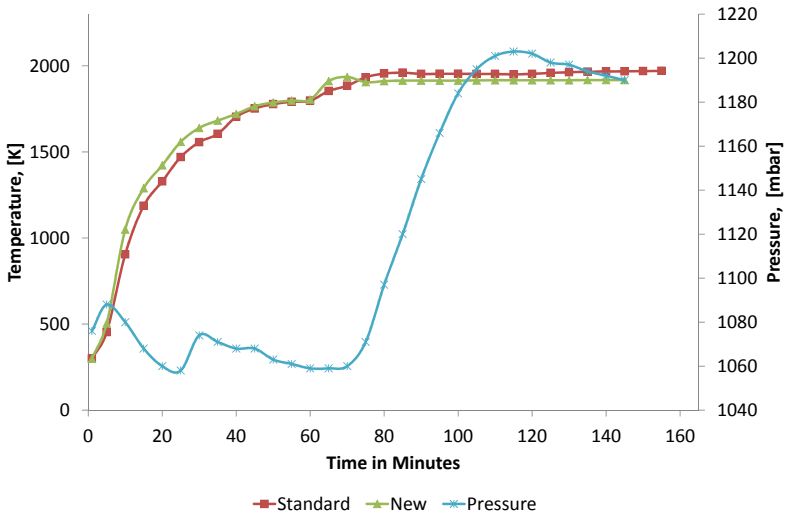

Figure 5.1 – Temperature and pressure plot of phosphorus removal experiment #1.

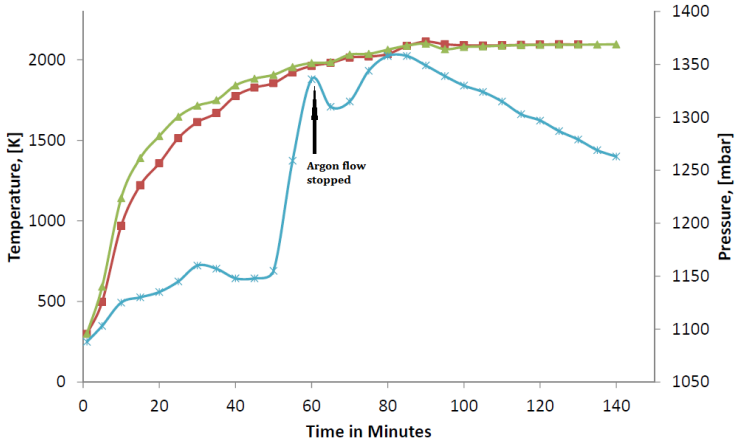

Figure 5.2 – Temperature and pressure plot of phosphorus removal experiment #2.

5.2 Master Slag Melting

The melting of Master Slag follows the procedure developed on the synthetic Nd_2O_3–SiO_2–CaO-system [9]. The synthetic system referenced was also smelted with different concentrations of Nd_2O_3, with the purpose of gathering more information of the system in practice when Nd-content varied. In addition, the synthetic system was perfect for optimizing the Sampling procedure detailed in Chapter 4.2.

Synthetic System

It was decided that the developed procedure would be applied to samples with different compositions of Nd_2O_3–SiO_2–CaO, following the liquidus line of the relevant phase diagram presented in Figure 3.7. It was decided to attempt a high Nd-concentration sample of 20% Nd_2O_3 by weight and a low Nd-concentration sample of 5% Nd_2O_3 by weight, in addition to the previously tested 10% Nd composition. Their respective compositions were 20%-39%-41%, 5%-41%-54%, and 10%-42.5%-47.5% of Nd_2O_3–SiO_2–CaO by weight. Both the 5%-Nd and the 20%-Nd samples did not successfully melt during the melting procedure, and was not possible to cast. This was after one and two melting repetitions, respectively. The temperature and pressure data can be seen in Table A3 and the plots are presented in Figures C.5, C.6 and C.7.

The 10% Nd samples were run following the Master Slag Melting procedure until it was time for the Sampling procedure. The temperature and pressure plots can be seen in Figures C.8-C.12. The temperature data is presented in Table A4.

Master Slag

Two complete samples of Master Slag ("MS1" and "MS2") were prepared, before they were mixed in preparation of the Sampling procedure. Two separately smelted samples of Master Slag were needed for one Sampling experiment, due to the nature of taking samples in-situ with a copper rod to be able to reach down into the slag. Samples of the Master Slags were taken for analysis with SEM-EDS. The compositional result of EDS can be seen in Tables 5.2 and 5.3. The EDS spots are shown in Figure 5.4, from the area shown in Figure 5.3.

Pictures of the Master Slag sample "MS1" is seen in Figures 5.6, 5.7 and 5.8. Figure 5.6 show that the color in normal lighting is a dark, onyx-like black. Figure 5.7 show the sample in bright light, with a deep blue-violet color, being slightly transparent with a "swirl" of crystalline phase within the glass. Figure 5.8 show the cross-section of the sample, displaying the two phases.

Table 5.2 – EDS results of Sample "MS1" and "MS2", given in mass%. Sample spots can be seen in Figure 5.4. Regions consist of phases as described in Table 5.7.

Sample	Spot	Mass% Nd	Si	Ca	O	F	Region*
MS1	1	8.52	18.52	32.45	33.22	2.30	**B**
	2	8.14	18.7	32.97	32.95	1.84	**B**
	3	7.56	18.23	34.32	32.26	2.76	**B**
	4	8.08	18.18	34.66	31.1	3.02	**B**
MS2	1	31.12	14.06	21.2	25.63	3.03	**A**
	2	36.20	12.39	18.94	24.67	3.33	**A**
	3	5.79	21.25	32.67	35.66	-	**C**

* Region marked according the specifications in Table 5.8, and highlighted for visibility.

Table 5.3 – EDS results of Sample "MS1" and "MS2", given in atom%. Sample spots can be seen in Figure 5.4. Regions consist of phases as described in Table 5.7.

Sample	Spot	Atom% Nd	Si	Ca	O	F	Region*
MS1	1	1.43	15.92	19.55	50.13	2.93	**B**
	2	1.36	16.04	19.82	49.63	2.33	**B**
	3	1.27	15.74	20.76	48.88	3.53	**B**
	4	1.37	15.85	21.17	47.6	3.9	**B**
MS2	1	6.31	14.64	15.47	46.84	4.67	**A**
	2	7.71	13.56	14.52	47.37	5.39	**A**
	3	0.95	17.97	19.35	52.92	-	**C**

* Region marked according the specifications in Table 5.8, and highlighted for visibility.

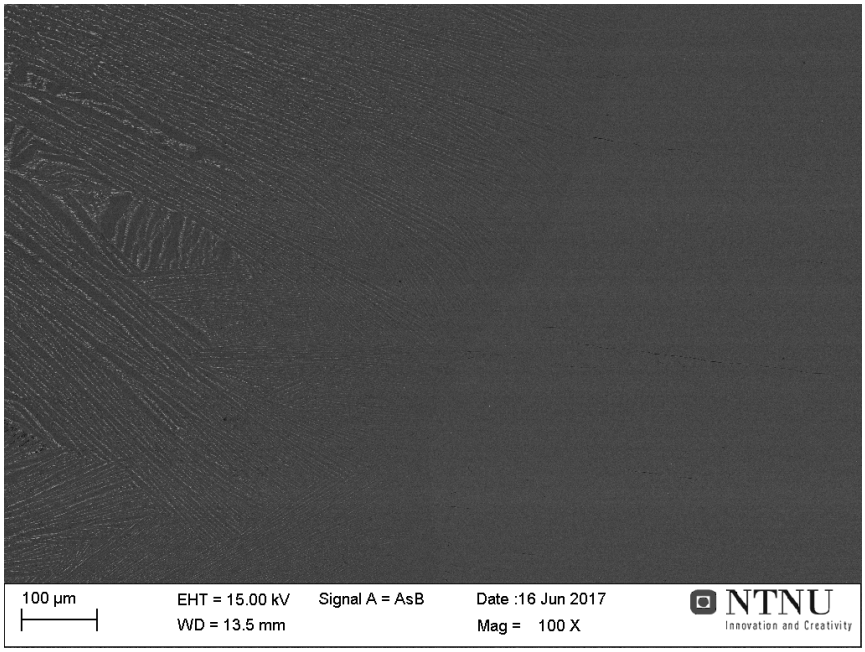

Figure 5.3 – SEM image of sample "MS1", recorded with AsB detector for BSE. Specifications detailed on image.

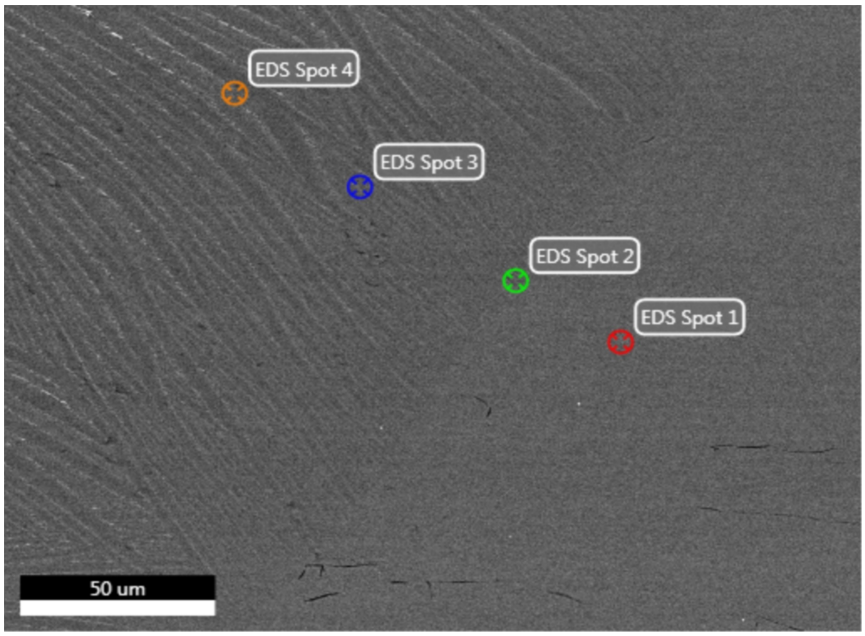

Figure 5.4 – Sample "MS1", recorded with AsB detector for BSE at 1500X magnification with EDS spots marked. The same area is pictured in Figure 5.3 at 100X magnification, and the data from EDS analysis are in Tables 5.2 and 5.3.

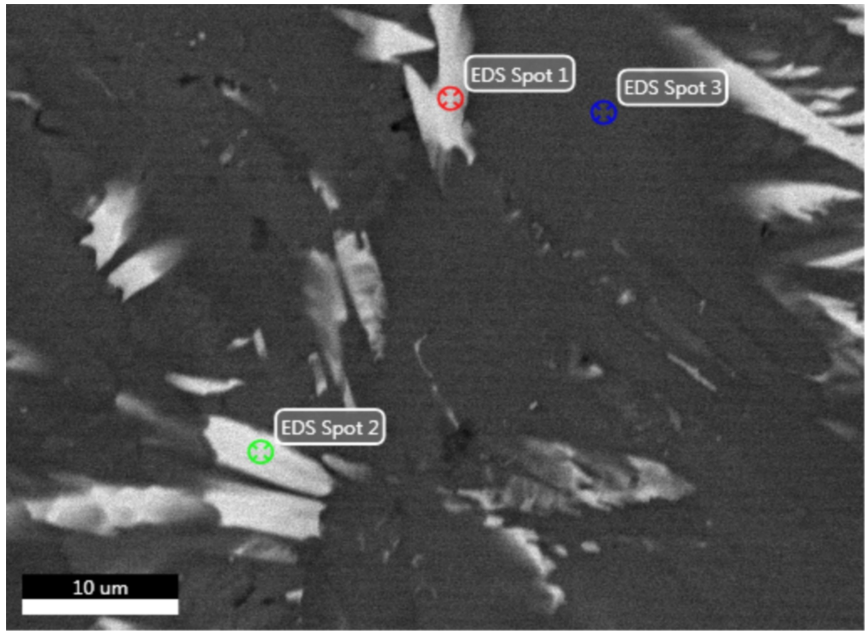

Figure 5.5 – Sample "MS2", recorded with AsB detector for BSE at 1500X magnification with EDS spots marked. The data from EDS analysis are in Tables 5.2 and 5.3.

Figure 5.6 – Sample "MS1" with the glassy phase towards the camera.

Figure 5.7 – Sample "MS1" with light showing the purple color.

Figure 5.8 – Cross section of sample "MS1", showing the two phases.

5.3 Master Slag Sampling

Samples "MS1" and "MS2" described in the previous section were mixed into a single sample ("MS3") after being crushed in a ring mill. To this sample the Sampling Procedure described in Chapter 4.2 was applied. Using the copper rod, it was attempted to extract three samples per temperature, but due to the nature of the experiment, it was not always guaranteed a sufficient sample. 11 successful samples were extracted and their temperature, holding time and mass data are presented in Table 5.4. These samples were taken for analysis by ICP-MS, SEM and XRD. The difficulty of accurately dipping the copper rod into the slag and retrieving a sample should be noted, which resulted in the large variety of sample mass recovered. The "Time" noted in Table 5.4 refers to the holding time at the relevant temperature after the sampling procedure was begun, *i.e.* "Sample 1" was taken with a holding time of 60 minutes as the procedure detailed, and used thereafter as the new reference point in time.

Table 5.4 – Overview of in-situ samples taken, with temperature, holding time and total weight of sample recovered.

Sample	Temperature [K]	Time [min]	Sample Mass [mg]
Sample 1	1873	0	560
Sample 2	1873	10	200
Sample 3	1873	20	264
Sample 4	1853	0	261
Sample 5	1853	10	649
Sample 6	1823	0	430
Sample 7	1823	10	935
Sample 8	1803	0	242
Sample 9	1803	10	981
Sample 10	1773	0	491
Sample 11	1723	0	1889

Analysis of the samples taken were done with SEM-EDS and XRD, and sent for ICP-MS. Due to a conflict with deadline and employee vacations, ICP-MS results were not recorded, and will be presented in future published articles. Tables 5.5 and 5.6 shows the recorded composition as analyzed by EDS of "Sample 11", with the phase region as interpreted in comparison

Table 5.5 – EDS results of "Sample 11", given in mass%. Sample spots can be seen in Figure 5.10. Regions consist of phases as described in Table 5.7, determined in combination with XRD results.

Sample	Spot	Mass%						Region*
		Nd	Si	Ca	O	P	F	
11	1	43.93	11.82	17.53	23.67	0.84	2.21	**A**
	2	41.49	12.17	19.52	23.87	0.94	2.01	**A**
	3	7.92	14.09	41.68	28.47	-	7.84	**B**
	4	9.03	14.07	41.05	28.48	-	7.38	**B**
	5	2.76	23.12	36.73	37.39	-	-	**C**
	6	2.88	23.07	36.57	37.47	-	-	**C**

* Region marked according the specifications in Table 5.8, and highlighted for visibility.

Table 5.6 – EDS results of "Sample 11", given in atom%. Sample spots can be seen in Figure 5.10. Regions consist of phases as described in Table 5.7, determined in combination with XRD results.

Sample	Spot	Atom%						Region
		Nd	Si	Ca	O	P	F	
11	1	10.93	15.1	15.7	53.11	0.97	4.18	**A**
	2	10.14	15.28	17.17	52.6	1.07	3.73	**A**
	3	1.45	13.24	27.45	46.97	-	10.89	**B**
	4	1.67	13.33	27.27	47.4	-	10.34	**B**
	5	0.47	20.10	22.38	57.06	-	-	**C**
	6	0.49	20.05	22.28	57.18	-	-	**C**

* Region marked according the specifications in Table 5.8, and highlighted for visibility.

with XRD results. The EDS spots can be seen at 1500X magnification in Figure 5.10 and this area can be seen at 100X magnification in Figure 5.9. The XRD pattern of "Sample 11" is presented in Figure 5.11, along with the compounds matching the characteristic signals. These compounds are described in further detail in Table 5.7. The compositional data of "Sample 2" to "Sample 10" can be seen in Tables 5.9 and 5.10, and their respective EDS images in Figures C.16-C.32. Discussion of these results can be found in Chapter 6.3.

Table 5.7 – Suggested phases and phase compositions in the Master Slag, as detected by XRD.

Phase	Name	Composition	PDF #
CSO	Calcium Silicate	$CaSiO_3$	00-001-0720
CNSF	Calcium Neodymium Fluoride Silicate	$Ca_2Nd_3(SiO_4)_3F$	04-006-0312
CNSP	Calcium Neodymium Oxide Phosphate Silicate	$Ca_2Nd_3(SiO_4)_2(PO_4)O$, $Ca_2Nd_7(PO_4)(SiO_4)_5O_2$	04-001-9516 00-029-0352
CSF	Cuspidine	$Ca_4Si_2O_7F_2$	00-011-0075
CNSO	Calcium Neodymium Oxide Silicate	$Ca_2Nd_3(SiO_4)_3O_{0.5}$	04-018-2088
CNF	Calcium Neodymium Fluoride	$Ca_xNd_yF_z$	

Table 5.8 – Suggestion for the phase regions in the Master Slag and their Nd content.

Nd-content	Weight%	SEM color	Possible phase(s)	**Region**
High	20-48	White	CNSF+CNSP	**A**
Medium	6-9	Light grey	CSF, CNSO, CNF	**B**
Low	0.5-3	Dark grey	CSO	**C**

Table 5.9 – EDS results of "Sample 10" through "Sample 2", given in mass%. Figures C.16 through C.32 show the SEM picture with spots for the respective samples. Phase determined in combination with XRD results.

Sample	Spot	Mass%							Region*
		Nd	Si	Ca	O	P	F	Al	
10	1	46.68	11.79	15.93	22.57	0.93	2.1	-	**A**
	2	48.07	11.46	15.13	22.14	0.88	2.34	-	**A**
	3	3.85	23.24	36.01	36.55	-	-	0.35	**B**
	4	4.11	23.02	35.62	36.86	-	-	0.39	**B**
	5	-	23.36	38.21	38.43	-	-	-	**C**
	6	0.64	23.39	37.72	37.93	-	-	0.32	**C**
9	1	33.68	15.25	21.32	26.88	1.05	1.82	-	**A**
	2	33.46	14.08	21.09	27.38	1.18	2.04	0.77	**A**
	3	2.9	23.31	36.89	36.9	-	-	-	**C**
	4	2.79	22.84	36.1	38.27	-	-	-	**C**
	5	6.56	14.1	43.79	27.78	-	7.77	-	**B**
	6	9.17	14.16	42.28	27.3	-	7.09	-	**B**
8	1	21.66	13.72	25.89	33	0.73	4.35	0.64	**A**
	2	20.44	14.41	27.18	32.66	0.61	4.09	0.61	**A**
	3	-	22.46	35.95	33.22	-	-	-	**C**
	4	3	23.27	36.74	36.99	-	-	-	**B**
7	1	47.1	11.65	15.75	22.39	0.89	2.23	-	**A**
	2	46.86	11.68	15.51	22.95	0.73	2.27	-	**A**
	3	1.54	23.34	37.54	37.58	-	-	-	**C**
	4	1.62	23.71	37.69	36.97	-	-	-	**C**
	5	7.93	14.04	42.78	27.92	-	7.34	-	**B**
	6	7.96	13.85	42.96	27.73	-	7.5	-	**B**
6	1	36.17	12.78	21.36	26.2	0.92	2.56	-	**A**
5	1	5.22	23.16	34.94	36.29	-	-	0.39	**B**
4	1	34.75	13.56	20.83	26.92	1.17	2.19	0.58	**A**
3	1	31.14	14.19	21.91	29.29	1.16	2.30	-	**A**
2	1	24.98	15.87	25.3	30.76	0.91	2.18	-	**A**

* Region marked according the specifications in Table 5.8. Highlighted for visibility.

Table 5.10 – EDS results of "Sample 10" through Sample 2", given in atom%. Figures C.16 through C.32 show the SEM picture with spots for the respective samples. Phase determined in combination with XRD results.

Sample	Spot	Atom%							Region*
		Nd	Si	Ca	O	P	F	Al	
10	1	12.02	15.59	14.77	52.4	1.12	4.11	-	**A**
	2	12.56	15.38	14.22	52.14	1.07	4.63	-	**A**
	3	0.66	20.43	22.18	56.41	-	-	0.32	**B**
	4	0.7	20.21	21.92	56.81	-	-	0.35	**B**
	5		19.86	22.77	57.36	-	-	-	**C**
	6	0.11	20.01	22.62	56.97	-	-	0.29	**C**
9	1	7.49	17.42	17.06	53.88	1.09	3.07	-	**A**
	2	7.38	15.94	16.74	54.41	1.21	3.42	0.9	**A**
	3	0.49	20.36	22.58	56.57	-	-	-	**C**
	4	0.47	19.71	21.83	57.99	-	-	-	**C**
	5	1.2	13.26	28.86	45.87	-	10.81	-	**B**
	6	1.72	13.61	28.5	46.09	-	10.08	-	**B**
8	1	4.14	13.48	17.82	56.92	0.65	6.32	0.65	**A**
	2	3.9	14.12	18.68	56.2	0.54	5.92	0.63	**A**
	3	-	17.89	20.06	46.45		-	-	**C**
	4	0.51	20.31	22.48	56.7		-	-	**B**
7	1	12.18	15.48	14.66	52.22	1.07	4.37	-	**A**
	2	12.01	15.37	14.31	53.02	0.88	4.41	-	**A**
	3	0.26	20.14	22.7	56.91	-	-	-	**C**
	4	0.27	20.56	22.9	56.27	-	-	-	**C**
	5	1.46	13.32	28.44	46.49	-	10.29	-	**B**
	6	1.47	13.16	28.6	46.24	-	10.53	-	**B**
6	1	8.25	14.97	17.53	53.85	0.98	4.43	-	**A**
5	1	0.9	20.53	21.71	56.49	-	-	0.36	**B**
4	1	7.77	15.57	16.76	54.27	1.22	3.72	0.69	**A**
3	1	6.63	15.5	16.78	56.21	1.15	3.72	-	**A**
2	1	5.04	16.44	18.37	55.96	0.86	3.33	-	**A**

* Region marked according the specifications in Table 5.8, and highlighted for visibility.

5.4 Nd_2O_3–SiO_2–B_2O_3 Phase Diagram

The experiments for the Nd_2O_3–SiO_2–B_2O_3 phase diagram were conducted at KU Leuven, Belgium. The composition for the 20 samples for the experiment is presented in Table A1, and these compositions can be seen represented in the isothermal section of the Nd_2O_3–SiO_2–B_2O_3 phase diagram at 1873 K in Figure 3.8.

Due to the time restraints, it was not possible to evaluate the results before the deadline. However, these experiments were part of a bigger research project, and the results will be published later in the article "Phase Relations and Crystallization Behavior of the Nd_2O_3–SiO_2–B_2O_3 System" with main author Tianming Sun from KTH. Chapter 6.4 discusses the experimental work done, as well as some observations and what kind of results could be expected.

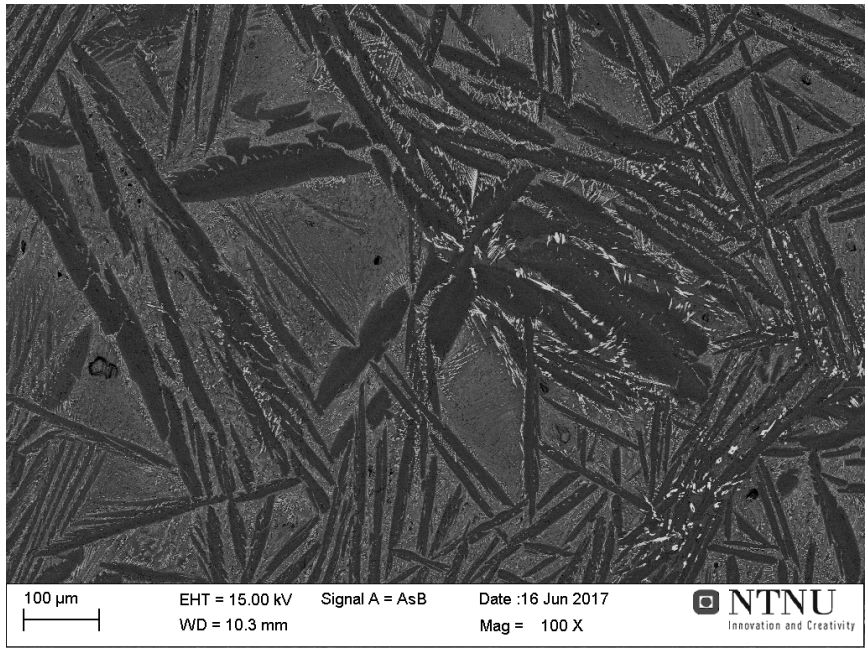

Figure 5.9 – SEM image of "Sample 11", recorded with AsB detector for BSE. Specifications detailed on image.

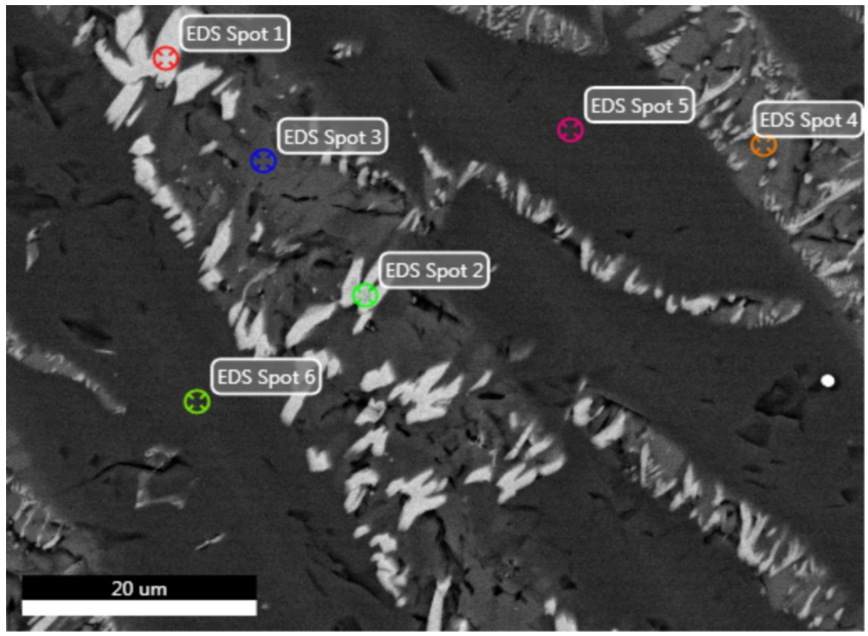

Figure 5.10 – "Sample 11", recorded with AsB detector for BSE at 1500X magnification with EDS spots marked. The same area is pictured in Figure 5.9 at 100X magnification, and the data from EDS analysis are in Tables 5.5 and 5.6.

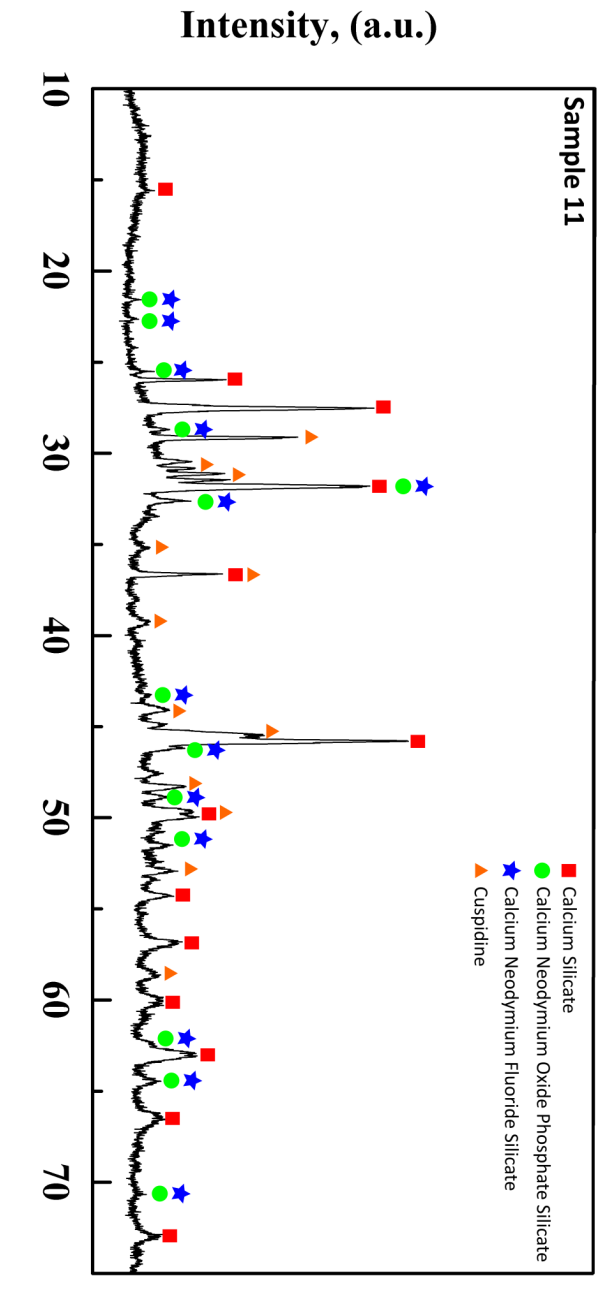

Figure 5.11 – XRD pattern of "Sample 11". The other samples showed identical pattern, with different peak heights.

Chapter 6

Discussion

There is an important note that has to be made about the experimental work done in the present study. While the procedure developed in "Procedure for Master Slag Production Based on the Synthetic System of Nd_2O_3, SiO_2 and CaO" served as a basis, adjustments have been made continuously. This is due to the experimental nature of this work, where even something that can seem very simple, *e.g.* melting a sample, could be demanding with the conditions and equipment available. In the original procedure development, for example, it was observed that while a lid helped the retention of heat and lowered experiment duration and power usage, performing casting with the lid proved to be difficult in the current vacuum induction furnace. In the present work, using the cheaper and easier replaceable graphite inner crucibles was determined to be unreliable for the results with the synthetic slag and a cause of possible contamination of the samples. The use of the more expensive molybdenum crucible was decided for all future experiments. Changes like that are presented chronologically in the discussion of the relevant experiments and results.

This chapter will discuss the experimental work as described in Chapter 4.1 separately, providing explanations and descriptions of events in each type of experiment. To clarify, the experiments under discussion will fall into these categories:

- Phosphorus Removal
- Master Slag Melting

- Master Slag Sampling
- $Nd_2O_3-SiO_2-B_2O_3$ Phase Diagram
- General Experimental Discussion

6.1 Phosphorus Removal

For the present study, the phosphorus removal experiment is a preparation step of the Apatite Concentrate before it can be doped to become the Master Slag. While considering a complete recycling process, there is a possibility to extract both P_2O_5 and CaC_2 as byproducts. Having several potential products is a good way both to diversify the risks, and increasing the economic potential. This will require a more serious study into these markets, when further development on the procedure has been done.

The removal of P_2O_5 was determined to be crucial to lower the temperature of operation [8]. The process of the phosphorus removal was developed previously and is presented in Chapter 4.2. The process involves production of very dangerous chemicals, especially phosphine gas (PH_3) as well as white phosphorus (P_4). A separate risk assessment was conducted by the operators, supervisors and HSE (Health, Safety and Environment) responsible employees at NTNU before the experiments were conducted. One of the precautions was to only allow production and exposure of phosphine gas in a fume hood after work hours, to prevent any unintended exposure of phosphine gas through the fume hood ventilation system in case of power failure. In addition, excellent ventilation, gas sampling apparatus, and appropriate respirators for PH_3 gas were used during the experimental work.

4 parallels were conducted during the present study, to create 4 additional batches of de-phosphorized Apatite Concentrate. Due to operator error on the first experiment, 3 batches were finished successfully in total. The procedure in itself seems very simple, but there were still difficulties experienced with all the experiments. The largest single complicating factor was the pressure increase during the experiments. The experiments were ran at atmospheric pressure and purged with argon gas through an outlet tube connected to the ventilation system as described in the procedure. The furnace is also equipped with a pressure release valve at 1.5 bar. As the release valve would eject the furnace chamber atmosphere straight into the laboratory, the pressure were to be kept reasonably lower than 1.5 bar, to prevent any chance of the toxic chemicals to be released in the open. The downside

of this is if the pressure increase became too large due to the production of the free P, the inert gas purging would have to be stopped and the pressure data would not give any meaningful information after that point.

In the second experiment, after 60 minutes and at 1980 K, the pressure was increasing rapidly towards 1400 mbar, and the inlet gas valve was closed. There was a lot of gas being produced, which only increased with increasing temperature. The pressure dropped immediately after closing the inlet valve, but kept increasing after a little while with the large amount of gas being produced in the crucible. This was puzzling as it was expected that the outlet gas valve would equalize the over-pressure, even through continued gas production. A cloggage of the outlet valve was suspected at this point, which was confirmed after the experiment was completed, in a careful check-up of the furnace. The outlet valve contained a 15 micron 316 stainless steel filter. When removed it began to smoke as it came into contact with air. A conclusion was made that white phosphorus particles clogged the filter and stopped the gas from going through, keeping the pressure from equalizing. The filter was removed and placed in water inside a fume hood, and the outlet valve was connected without a filter for the duration of these later experiments. Figure 6.1 gives an indication for the immense gas production at 2123 K during one of these experiments.

Due to the melting temperature of the Apatite Concentrate at ~1886 K [8], the production of P_2 was expected to greatly increase when melting occurred, as the liquid slag would come into contact with the graphite crucible at a much larger rate. The large increase in pressure that can be seen in all the plots in Figures C.1-C.4 at around 1900 K, agrees with this assumption. The production of P_2 gas is assumed starting at this temperature. The purging gas was still flowing at this point for all experiments, so the pressure data should be reasonable.

The relative compositions of the raw Apatite Concentrate and the dephosphorized material are a crucial results for this experiment. As seen in Table 5.1, the reduction of phosphorus content in the products was substantial in all successful experiments, although "De-P#3" contained notably more than "De-P#2" and "De-P#4". Still, the procedure shows the possibility of removing up to 99.7% phosphorus in these results, which is promising.

The safety measures taken by the operators and the department was in itself a success and a worthy point of discussion. White phosphorus is very

Figure 6.1 – Picture of phosphorus gas production at 2123 K from the viewing hole in the furnace door.

dangerous at contact, but quite easy to avoid if the furnace is sufficiently purged with dry air, and specific procedure is followed when the furnace door is open. The production of phosphine gas, even in contact with the moisture in the air requires constant use of proper gas mask and filters at all times after the furnace had been opened. In the furnace after removal of the crucible, the phosphine levels were measured to ~0.1-3ppm, and similar levels above the crucible inside the fume hood. After being filled with water, reactions were clearly observed with intense bubbling from the production of acetylene and phosphine gas, as described in Equations (3.3) and (3.5). The phosphine levels were measured to be far beyond the detection limits of the 0.1/c Dräger tubes (4ppm), and was estimated to 20-40ppm from the speed of which the tube turned purple.

6.2 Master Slag Melting

Both the synthetic system and the Master Slag followed the same procedure developed at this point. After both the synthetic samples with 5% and 20%

Nd failed, it was determined to only use molybdenum crucibles as the inner crucible. Silicon carbide production was considered as a potential problem, as HSC Chemistry - 7.1 [58] thermodynamic software show that $\Delta_f G_{SiC} = 0$ at ~1783 K, according to the reaction presented in Equation (6.1). There was no substantial gas production at this temperature, though, which makes it undetermined still. Nonetheless, the molybdenum crucible should be almost completely inert, with the largest downside being expensive.

$$\mathrm{SiO_2(l) + 3\,C(s) \rightarrow SiC(s) + 2\,CO(g)} \qquad \mathrm{\Delta_f G_{SiC}} \tag{6.1}$$

Synthetic System

There was nothing abnormal about the experiments with 5% and 20% Nd to suggest what might have happened, and the cause of the failure was not determined. According to the phase diagram in Figure 3.7, both the compositions should be liquid at above 1873 K. The max temperatures of the experiments were 1911 K and 1889 K, which might have been close enough to the liquidus line to struggle with casting. In both the failed attempts, it could be observed that a layer of slag had solidified in a "lid" above the rest of the slag, with a pocket of air in between. It is not possible to determine if this happened before or during casting, but the slag might have been close to the liquidus or partly liquid, causing a disturbance in the heating to immediately solidify the sample. The presence of this "lid" can be seen in Figure 6.2, which is from sample "Synth-5-1", and a similar result was seen with sample "Synth-20-2".

The 10% Nd samples were smelted in the molybdenum crucible and there were no noticeable problems or divergence from the procedure. The graphite crucibles also had a problem with sample being left over in the crucible, but with the molybdenum crucible practically all of the sample was removed during the casting. The samples were crushed in a ring mill and remelted until the Sampling procedure was used. The Sampling procedure was used on the second melting of the second synthetic sample, "Synth-10-2-2". The goal of this experiment was mostly to test the Sampling procedure after the failed sample "Synth-10-1-3", in preparation for the real Master Slag.

Master Slag

Two samples of Master Slag were smelted as it was determined that the amount of slag formed from one sample was too little for the copper rod to reach down during the Sampling procedure. Even though the molybdenum

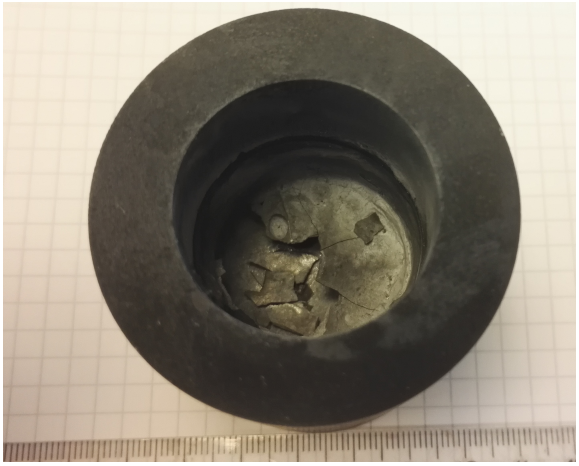

Figure 6.2 – Sample "Synth-5-1", showing the solidified "lid" (here broken) covering the rest of the slag.

crucible was ~80% full of raw master slag before melting, the densification of the material during the pyrometallurigcal treatment reduced the volume by ~30-50% which made it possible to mix samples "MS1" and "MS2" to a single sample, "MS3", before the Sampling procedure. Because of time restraints, only one melting experiment per sample was possible before the Sampling procedure had to be attempted for the Master Slag, while at least two had been preferred to achieve better homogeneity as described in the procedure.

The composition of the Master Slag samples "MS1" and "MS2" as analyzed by EDS, are presented in Table 5.2 and 5.3. The spots analysed for MS1 are shown in Figure 5.4, while the spots for "MS2" are shown in Figure 5.5. Figure 5.3 show the area where the "MS1" spots were analysed at 100X magnification. It was suspected that this region was the phase boundary between the liquid and crystalline phases in the Master Slag, as can be seen by the lines fading into an amorphous phase. While the Nd-content was suspected to increase when entering the crystalline phase, it is seen that the composition is relatively stable across all four points. In combination with the results from the "MS2" analysis it can be concluded that the Nd content is really high in a specific crystalline phase, while generally even in the rest of the phases present. Spot 1 and Spot 2 from "MS2" show a white crystal, indicating a heavier element present, which must be Nd. These crystals show a Nd content of upwards to 36% Nd by weight. There still seems to be a fair

amount of Nd left over outside the crystalline phase, which is not optimal. It is suspected that several remelting experiments will slightly increase the homogenization of the Master Slag, but the consequence of not remelting twice before sampling should only have a small effect.

6.3 Master Slag Sampling

Before the samples recorded in Table 5.4 were even attempted, several experiments were conducted on the synthetic samples to optimize the Sampling procedure. The first attempt was on sample "Synth-10-1-3". The copper rod was dipped into the hot slag, and it was discovered it melted. It was a notable struggle to keep the long rod from vibrating and avoiding contact with the crucible. The result of this was that the copper rod melted, and copper content entered the slag, which was confirmed when the crucible was removed from the furnace. Figure 6.3 shows the molybdenum crucible with synthetic slag contaminated by copper, as seen by the reddish brown color. The speed of the dipping action into the slag was concluded to be of utmost importance, to avoid overheating, and melting, of the rod. It was necessary to machine the rod and the handle completely straight, as the tiny bend which was present was enough to hinder a smooth withdrawal. Another synthetic experiment was planned because of this, as at the operators did not feel confident that a success could be guaranteed the next time.

The second Sampling experiment was conducted on sample "Synth-10-2-2". This experiment was done to rehearse the procedure and discover any potential complications, so that preparations could be made for the Sampling of the Master Slag. During this experiment, the rod did not melt like the first experiment, as the dipping action went way smoother and faster. It was discovered, though, that a larger amount of slag was necessary for the rod to reach down and recover any sample. It was decided that two Master Slag samples were needed for one Sampling procedure. Due to time restraint and equipment schedule it was necessary to complete this in three experiments, so only a single premelting of each sample was possible before the Sampling of the Master Slag.

The samples taken, the temperature, holding time and mass is presented in Table 5.4. Samples were taken from 1873 K to 1723 K, although only a simple sample were successfully extracted at 1773 K and 1723 K. At 1723 K the top of the slag solidified in the crucible before the second attempt. The lower the temperature this process can be conducted at is better for

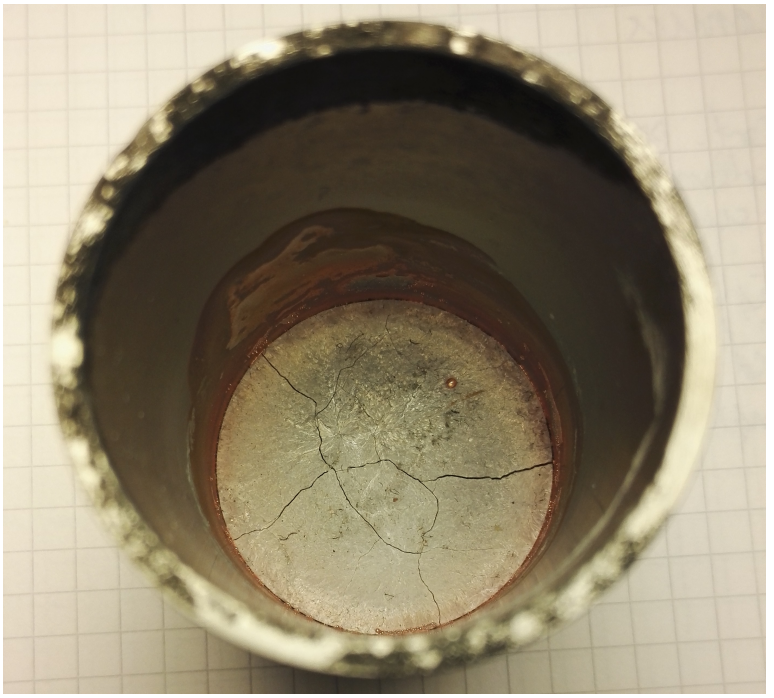

Figure 6.3 – Synthetic sample "Synth-10-1-3" after the copper rod melted during the Sampling procedure.

the energy consumption perspective. The result is also highly dependent on the presence of high Nd-containing phases, as well as how much of the Nd is present in these phases.

From Table 5.5 and 5.9 in combination with the SEM images it can be concluded the presence of three main phase regions. These can be seen in "Sample 11" in Figure 5.10 as spot 1,2 for high Nd-content, 3,4 for medium Nd content, and 5,6 for low Nd content. In this sample it is recorded that high Nd content is ~40% by weight, medium Nd content is ~8% by weight and low Nd content is ~3% by weight. While some of the images are of slightly poor quality, a preliminary range of Nd content in the different phase regions is suggested in Table 5.8. It is to be noted that some of the samples are of poor quality, and the spots does not seem to encompass a single region. "Sample 2" to "Sample 6" including "Sample 8" was of such small amount that only powder sample could be used for SEM, and those results were significantly worse than "Sample 7" and "Sample 9" - "Sample 11". It is necessary for future work into this project to account for this

sample mass problem, and work to recover enough samples to cover the inaccuracies from such a small sample size. The use of EPMA (Electron Probe Micro Analysis) is also highly recommended for a more accurate analysis, for further research into phase characterization.

An interesting phenomenon is the presence of F (fluorine) in all the high-Nd and medium-Nd regions, of around 2% and 7% F by weight, respectively. The presence of F could be expected, however, due to the apatite source. XRD analysis were done on the samples, and matched with the EDS results. The XRD spectrum can be seen in Figure 5.11, along with the compounds matching the characteristic signals. The patterns of "Sample 2" - "Sample 11" all matched each other identically, with slightly different peak heights, or showed up as amorphous. It is likely that the smallest samples have a higher probability of only appearing as amorphous glass, due to the rapid cooling they experience due to their mass. In Table 5.7 the different phases detected by XRD is presented, and these compounds are grouped into phase regions presented in Table 5.8, according to which phase it is likely that they appear according to the EDS results. Due to the reported stoichiometry of the samples reported from the EDS analysis, it is currently considered that the different phase regions consist of a combination of multiple compounds. The inaccuracy of EDS and the noisy result of XRD, due to the highly complicated composition, make accurate determination of phases problematic. Considering the stoichiometry reported, it is also possible that there are other compounds present. It is also important to remember that the EDS uses BSE, which receives diffracted electrons from a volume beneath the spot it scans. If there are different phases present in this volume than on the surface, the reported composition at the spot might differ from the expectations due to the surface chemistry. Therefore it is strongly recommended that additional characterization with larger data size is conducted to determine composition specifically.

In Table 5.8, the high, medium and low Nd regions are presented with suggested phases present, and marked with a **Region** marker **A**, **B**, **C**, which is used in Tables 5.2, 5.3, 5.5, 5.6, 5.9 and 5.10 to identify the phase region of the EDS spot. It is possible that other phases are present in the regions, *e.g.* NdOF, SiO_2 and $Nd_2Si_2O_7$, but the divergence from the XRD pattern were slightly too large for these to include in the results, however their presence is not impossible. It is an assumption made that the phases reported in Table 5.7 are the ones present, as according to the results detected by XRD and EDS in combination. The characteristic x-rays suggest that both F and P

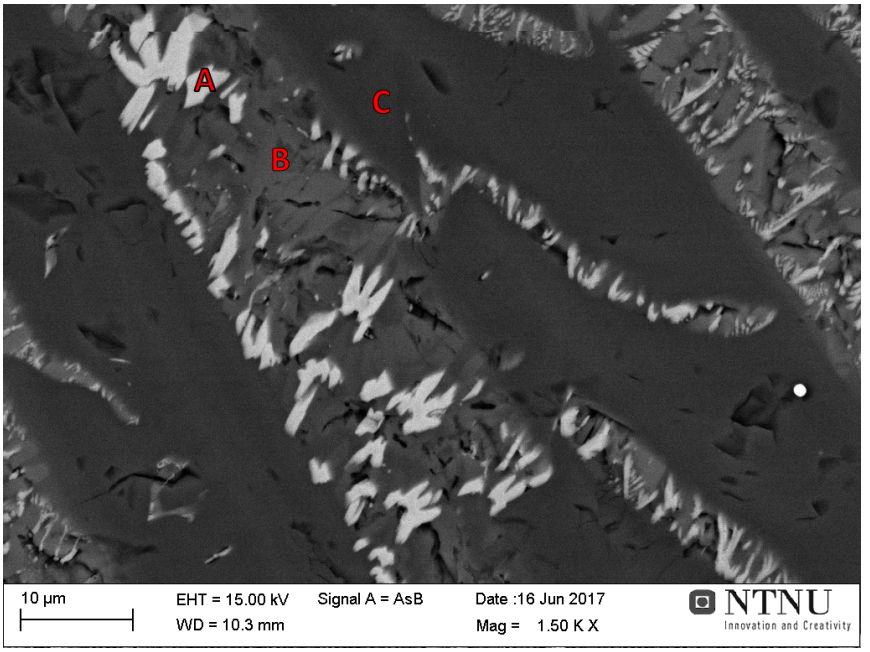

Figure 6.4 – "Sample 11", recorded with AsB detector for BSE at 1500X magnification with suggested phase regions marked in red letters, according to Table 5.8. This image can be seen with EDS spots in Figure 5.10.

is a part of the Nd-rich compounds, but it can not be determined if this increase or decrease the relevant Nd concentration in the phase overall. A visualization of the phase regions **A**, **B** and **C** is seen in Figure 6.4, which is the SEM image from Figure 5.10, with red letters on the respective phase region.

As presented in Table 5.8, the **A** regions, which are the white crystals in the SEM images and here named the high-Nd regions, have the suggested phases CNSF and CNSP. It is possible that there are CSF or CNF present as well, but it is impossible to determine. It can be seen that the relative content of Nd, Si, Ca, O, P and F is very similar over all the samples, indicating the possibility of a single phase or similar phase mix. Sample 8 is a slight outlier here, which is likely from the spot possibly covering phase boundaries. This region is the most interesting for recycling purposes, as it contains the most Nd. Determining the composition, and possibly how to consistently enrich it even more with Nd could be a goal for a future project. The determination

that there at least is one Nd-, and therefore LREE-, rich phase in the Master Slag, means that the possibility for recovery is still present.

The **B** regions are here named the medium-Nd regions, and probably contain a mix of different phases. It is suggested that CSF and CNSO is present, as well as CNF due to the high Ca, Nd, and F content compared to Si. It is also likely that the region contains some CSO. These phases were all present on the XRD analysis. It should be investigated whether F is a problem with enriching this phase with Nd, reducing the possible Nd content in the high-Nd region. If NdF_3 is present as well, while not detected here, it could pose a problem due to the low solubility of REE-fluorides [1].

The **C** regions are here named the low-Nd regions and fairly certainly consists of a $CaSiO_3$ matrix with small amounts of Nd-containing phases mixed in. As can be seen in Figure 5.3, this dark grey region increases over the phase boundary from crystalline to amorphous. It can be deducted that an amorphous $CaSiO_3$, possibly with amorphous SiO_2, dominates the glassy part, but this cannot be detected in XRD. $CaSiO_3$ also forms the matrix surrounding regions **A** and **B** in the crystalline phase.

It was assumed that Al (aluminium) was present in the samples as AlP, but while EDS detected Al, XRD did not indicate the compound in any specific phase. It could not be determined what phase it was present in. While mostly appearing in region **B**, it is not exclusively so.

6.4 Nd_2O_3–SiO_2–B_2O_3 Phase Diagram

When the samples were made, two large batches of sample "PD1" and "PD2" were made with the intention of making all the 18 other samples from these two, mixed with various amounts of Nd_2O_3 and SiO_2. These batches were sintered as a precaution to make it less likely for the volatile B_2O_3 to evaporate during the experiment at 1873 K [59]. Using the calculated phase diagram, the 20 samples were carefully chosen to give the most information for optimization of the phase diagram. The phase diagram with the chosen compositions can be seen in Figure 3.8. The most interesting part of the phase diagram is the low B region, and is also where the most samples were taken. The compositions shown in Figure 3.8 is presented as both mole ratio and weight% in Table A1.

The experiment had to be conducted at KU Leuven in Belgium, as they had the equipment capable of simultaneously melting all the 20 samples under the same conditions, and quench them simultaneously as well. Before running the experiment with all samples, two things had to be decided. From previous experiments it was unclear whether 6 hours or 24 hours holding time were necessary for the samples to achieve equilibrium. It was also necessary to find out if it was achievable to melt them at 1873 K without evaporating boron. The samples were packed as well as possible into Pt-20%Rh foil, but it was not determined if evaporation ofB_2O_3 would become relevant even after the sintering reactions, as the sublimation temperature of pure B_2O_3 is 1723 K [35]. Because of this test experiments were run on sample "PD1" and "PD2", as those were the only samples with excess material. First the 6 hour experiment at 1873 K were done, but the Pt-20%Rh wire used to hold the crucible snapped some time during the experiment. The 24 hour test experiment at 1873 K was then conducted, and after ICP-MS analysis at KU Leuven it was seen that the boron content was vastly reduced. To not destroy the only set of samples, and because of the limited time at KU Leuven, the proper experiment was done at 1673 K. This is below the sublimation temperature of B_2O_3, and was suggested by Kai Tang from SINTEF Materials and Chemistry as an option for providing some thermodynamic data for the system. This could in turn be modeled to 1873 K, which would hopefully provide some optimization to the calculated phase diagram.

The purpose of the experiment was to study the effect given by B_2O_3 to the Master Slag, as it would be of high interest to use this element in an eventual recycling process containing industrial mining waste, doped with Nd from Nd-Fe-B magnets from WEEE. It was also deemed valuable experience to conduct phase diagram experiments directly, when working with these kind of slag systems.

6.5 General Experimental Discussion

The work in the present study was of a very experimental nature, with clear goals and real world benefits. The downside of such a focus on the experimental work is when equipment and procedures fail to live up to expectations. The only capable vacuum induction furnace present at NTNU, Trondheim is a very old furnace produced by Elatec Technology Corp., with more parts replaced than original. At the beginning of the project work, the furnace malfunctioned and needed repairs. The electrical wiring, the cooling water system, the pump and several valves needed hundred of hours of

maintenance before it was deemed ready for use by the technical engineers. This meant that the experimental work was delayed by a long time, as well as resulting a significant experimental demand from different projects, creating even more delays. When several time consuming experiments failed, the experimental plan had to be postponed for a future project. There is a lot of potential in the production of Master Slag, but it will require more work to obtain the necessary significant results needed for such a process.

The positive consequence of this was that the author gained important knowledge of the engineering and maintenance of a vacuum induction furnace.

Chapter 7

Conclusion

The present study has explored the production of a Master Slag as a step in the process of recovering REEs from apatite-containing iron mine tailings, *i.e.* from a waste material from the mining industry. The Apatite Concentrate studied in the present study was from LKAB, Kiruna, Sweden. Through a pyrometallurgical procedure, it has been shown that a Master Slag created from Apatite Concentrate doped with Nd_2O_3 and SiO_2, can contain phases with up to 48% Nd by weight.

The Master Slag produced in the present work is based on the relative composition of $Nd_2O_3-SiO_2-CaO$ at 10%-42.5%-47.5% by weight, respectively. It also contains a wide variety of contaminating species, since it originates from a complex raw material. The Master Slag was characterized by SEM-EDS and XRD, which detected three main phase regions with the phases differed mainly by their high, medium and low Nd-content. In the high-Nd region the preliminary analysis suggests that $Ca_2Nd_3(SiO_4)_3F$, $Ca_2Nd_3(SiO_4)_2(PO_4)O$ and $Ca_2Nd_7(PO_4)(SiO_4)_5O_2$ dominate the area, with an concentration of 20-48% Nd by weight in the different samples taken. It should, however, be mentioned that further qualitative and quantitative analysis must be performed, before it can be asserted definitively. Obtaining a solid set of data on the specific compounds in the Nd-rich region should be a priority for the possibility of developing a recovery process for REEs from iron based tailings.

The procedure developed in the present work for the production of Master Slag has been subject to change, and should be further refined if possible.

The removal of phosphorus is a crucial step, which through ICP-MS analysis were determined to achieve reduction of the phosphorus content by up to 99.7%. Through this process the possibilities of extracting P_2O_5 and CaC_2 should be investigated. This could be considered for providing the recovery procedure with a stronger economic motivation in the future. The doped content of Nd in the slag could also potentially be optimized. The present study used a concentration of 10% Nd_2O_3 by weight as a fairly arbitrary amount. The goal was to have a reasonably low concentration while still providing enough material for successful chemical characterization, leaving optimization for future research.

The impact of initial concentration of Nd_2O_3 on the final Nd content in the Nd-rich phase in the Master Slag could be a reasonable theme for a future project. Due to the nature of the raw materials, extrapolating this procedure to a pilot scale project would be a way to address some of the experimental complications experienced, which could be part of a future project, following the work presented in this study. At the same time it could also be useful to investigate possible equilibriation temperatures, as well as its effect on the final composition in a larger scale operation. While the samples taken during processing in the present study indicates that the samples taken at temperatures on the lower end of the scale, *i.e.* between 1773 K and 1873 K, gave higher Nd concentration in the Nd-rich phase, the lack of data to compare and validate makes this impossible to conclude with certainty. However, lower temperature will also affect the casting process, which will have a influence on *e.g.* a larger scale procedure. The chemical behavior needs to be tailored to fit the procedure developed, in a way that provides a balance between theory and feasibility. Regardless, the investigation into adequate equipment and verification of procedure is imperative for the potential continuation of this project.

The potential of doping apatite containing mining waste with Nd-heavy electronic waste is a very interesting process. In theory, it could utilize one high REE-concentration waste to extract more REEs from a source with scarce REE content, but of huge volume. A recycling process of REEs is at mercy of the economic variations in the market, and combining two measures is interesting in the search for a new potential source of REEs.

Due to the B-content of Nd-magnets in electronic scrap, the investigation into the $Nd_2O_3-SiO_2-B_2O_3$ is also of interest to the Master Slag production. Although the results of the phase diagram experiment performed in the

present work did not yield immediate results, experimental knowledge for the Master Slag production was gained, and further research is encouraged. If there is a possibility of boron influencing the enriching of Nd, this could lead to interesting paths for the Master Slag Production in the future. The evaluated results will address the concerns for the method of equilibriation of the slag samples at 1673 K, while also aid the optimization of the equilibriation time needed to produce relevant data for phase diagram optimization.

Bibliography

[1] C. Gupta and N. Krishnamurthy, *Extractive Metallurgy of Rare Earths*. CRC Press, 1992.

[2] European Commission, "Report on Critical Raw Materials for the EU, Report of the Ad hoc Working Group on Defining Critical Raw Materials," no. May, p. 41, 2014.

[3] J. Lifton, "Lithium, Graphite, Cobalt, Neodymium, Praseodymium, Terbium, and Dysprosium poised to Skyrocket." `http://investorintel.com/technology-metals-intel/peak-platinum-demand/`. Accessed: 2016-11-17.

[4] R. J. Weber and D. J. Reisman, "Rare Earth Elements : A Review of Production , Processing , Recycling, and Associated Environmental Issues," *United States Environmental Protection Agency*, no. December, p. 135, 2012.

[5] C. Zhanheng, "Global rare earth resources and scenarios of future rare earth industry," *Journal of Rare Earths*, vol. 29, pp. 1–6, 2011.

[6] X. Huang, G. Zhang, A. Pan, C. F., and C. Zheng, "Protecting the environment and public health from rare earth mining," *Earth's Future*, vol. 4, pp. 182–190, 2016.

[7] B. Palsson, O. Martinsson, C. Wanhainen, and A. Fredriksson, "Unlocking Rare Earth Elements From European Apatite Iron Ores," *ERES2014: 1st European Rare Earth Resources Conference*, pp. 211–220, 2014.

[8] T. Sun, M. W. Kennedy, G. Tranell, and R. E. Aune, "Apatite Concentrate , a Potential New Source of Rare Earth Elements," *Rare Metal Technology*, pp. 145–156, 2015.

[9] F. A. E. Rodahl, "Procedure for Master Slag Production based on the Synthetic System of Nd_2O_3, SiO_2 and CaO," 2016. Specialization Project Report.

[10] G. B. Haxel, J. B. Hedrick, and G. J. Orris, "Rare Earth Elements—Critical Resources for High Technology." `https://pubs.usgs.gov/fs/2002/fs087-02/`. Accessed: 2017-5-25.

[11] T. Dutta, K.-H. Kim, M. Uchimiya, E. E. Kwon, B.-H. Jeon, A. Deep, and S.-T. Yun, "Global demand for rare earth resources and strategies for green mining," *Environmental Research*, vol. 150, pp. 182–190, 2016.

[12] J. Gambogi, "US Geological Survey: Rare Earths Statistics and Information." `https://minerals.usgs.gov/minerals/pubs/commodity/rare_earths/`. Accessed: 2017-5-18.

[13] J. Perkowski, "In China, Illegal Rare Earth Mines Face Crackdown." `https://www.forbes.com/sites/jackperkowski/2012/06/21/behind-chinas-rare-earth-controversy/#8948314074c9`, June, 2012. Accessed: 2017-05-15.

[14] K. Bradsher, "In China, Illegal Rare Earth Mines Face Crackdown." `http://www.nytimes.com/2010/12/30/business/global/30smuggle.html`, December, 2010. Accessed: 2017-05-15.

[15] S. Massari and M. Ruberti, "Rare earth elements as critical raw materials: Focus on international markets and future strategies," *Resources Policy*, vol. 38, pp. 36–43, 2013.

[16] C. C. Pavel, R. Lacal-Arántegui, A. Marmier, D. Schüler, E. Tzimas, M. Buchert, W. Jenseit, and D. Blagoeva, "Substitution strategies for reducing use of rare earths in wind turbines," *Resources Policy*, vol. 52, pp. 349–357, 2017.

[17] Asian Metal. `http://www.asianmetal.com/RareEarthsPrice/RareEarths.html`. Accessed: 2017-05-16.

[18] Ø. Lie, "Her vil de bore 1000 meter dypt for å finne sjeldne metaller og thorium." `https://www.tu.no/artikler/vil-bore-1000-meter-dypt-pa-fensfeltet/277546`. (Norwegian), Accessed: 2017-07-07.

[19] A. Kumari, R. Panda, J. Kumar, J. Kumar, and J. Lee, "Process development to recover rare earth metals from monazite mineral: A review," *Minerals Engineering*, vol. 72, pp. 102–115, 2015.

[20] K. Binnemans, P. Jones, K. Van Acker, B. Blanpain, and D. Mishra, B.and Apelian, "Rare-Earth Economics: The Balance Problem," *JOM*, vol. 65, pp. 36–43, Number 7, 2013.

[21] P. Falconnet, "The Economics of Rare Earths," *Journal of the Less-Common Metals*, vol. 111, pp. 9–15, 2017.

[22] M. McCorkle, "Critical Materials Institute Rare-Earth Recycling Invention Licensed to U.S Rare Earths." `https://www.ornl.gov/news/critical-materials-institute-rare-earth-recycling-invention-licensed-` August, 2015. Accessed: 2016-12-03.

[23] V. Volcovici, "Apple's Robot Rips Apart iPhones for Recycling." `http://www.businessinsider.com/r-apples-robot-rips-apart-iphones-for-recycling-2016-3?r=US&IR=T&IR=T`, March, 2016. Accessed: 2016-12-03.

[24] K. Binnemans, P. Jones, B. Blanpain, T. Gerven, Y. Yang, A. Walton, and M. Buchert, "Recycling of Rare Earths: A Critical Review," *Journal of Cleaner Production*, vol. 51, pp. 1–22, 2013.

[25] N. Curtis, "Rare earths, we can touch them everyday." In: Lynas Presentation at the JP Morgan Australia Corporate Access Days. New York, 27–28 September 2010.

[26] A. Kumar, M. Holuszkoa, and D. Espinosa, "E-waste: An overview on generation, collection, legislation and recycling practices," *Conservation and Recycling*, vol. 122, pp. 32–42, 2017.

[27] C. Bounds, "The recycle of sintered magnet swarf," *Metals and Materials Waste Reduction, Recovery and Remediation*, pp. 173–186, 1994.

[28] J. Lyman and G. Palmer, "Scrap treatment method for rare earth transition metal alloys," 1992. US Patent 5,129,945.

[29] T. Saito, H. Sato, S. Ozawa, J. Yu, and T. Motegi, "The extraction of Nd from waste NdFeB alloys by the glass slag method," *Journal of Alloys and Compounds*, vol. 353, pp. 189–193, 2003.

[30] G. Adachi, K. Shinozaki, Y. Hirashima, and K. Machida, "Rare earth separation using chemical vapor transport with $LnCl_3-AlCl_3$ gas phase complexes," *Journal of the Less Common Metals*, vol. 169, no. 1, pp. L1–L4, 1991.

[31] M. Itoh, K. Miura, and K. Machida, "Novel rare earth recovery process on NdFeB magnet scrap by selective chlorination using NH_4Cl," *Journal of Alloys and Compounds*, vol. 477, pp. 484–487, 2009.

[32] M. W. Kennedy, "Private communications," 2016–2017.

[33] W. Jackson and G. Christiansen, "International Strategic Minerals Inventory Summary Report: Rare Earth Oxides," *U.S. Geological Survey Circular 930-N*, 1993.

[34] P. Henderson, *Rare Earth Element Geochemistry*, vol. 2. Elsevier, 2013.

[35] T. Sun, "Private communications," 2016–2017.

[36] H. Diskowski and T. Hofmann, "Phosphorus," in *Ullmann's Encyclopedia of Industrial Chemistry*, pp. 725–746, Weinheim: Wiley-VCH Verlag GmbH & Co, KGaA, 2012.

[37] H. Bock and H. Müller, "Gas-phase reactions. 44. the $P_4 + 2\,P_2$ equilibrium visualized," *The American Chemical Society*, vol. 23, pp. 4365–4368, 1985.

[38] B. Langhammer, "Calcium carbide," in *Ullmann's Encyclopedia of Industrial Chemistry*, pp. 497–509, Weinheim: Wiley-VCH Verlag GmbH & Co, KGaA, 2012.

[39] J. Campbell, "Le châtelier's principle, temperature effects, and entropy," *Journal of Chemical Education*, vol. 62, p. 231, 1985.

[40] H. Callen, *Thermodynamics and an Introduction to Thermostatistics*. John Wiley and Sons, second ed., 1985.

[41] P. Atkins and J. Paula, *Physical Chemistry*. W. H. Freeman and Company, eighth ed., 2006.

[42] G. Eriksson, P. Wu, M. Blander, and A. Pelton, "Critical evaluation and optimization of the thermodynamic properties and phase diagrams of the $MnO-SiO_2$ and $CaO-SiO_2$ systems ," *Canadian Metallurgical Quarterly*, vol. 33, pp. 13–21, 1994.

[43] N. Toropov and N. Fedorov, "Constitution diagrams of Calcium Orthosilicate-Neodymium Orthosilicate and Calcium Orthosilicate-Lanthanum Orthosilicate," *Izv. Akad. Nauk SSSR, Neorgan. Materialy,*, vol. 1, no. 4, 1965.

[44] R. Miller and D. Rase, "Phase Equilibrium in the System Nd_2O_3–SiO_2," *Journal of the American Ceramic Society*, vol. 47, no. 12, pp. 653–653, 1964.

[45] T. Le, K. Tang, S. Arnout, A. Malfliet, B. Blanpain, and M. Guo, "Thermodynamic Assessment of the Nd_2O_3-CaO-SiO_2 Ternary System," *Calphad*, pp. 1–6, 2016.

[46] L. Jakobsson, G. Tranell, and I. Jung, "Experimental Investigation and Thermodynamic Modeling of the B_2O_3–FeO–Fe_2O_3–Nd_2O_3 System for Recycling of NdFeB Magnet Scrap," *Metallurgical and Materials Transactions B*, vol. 48, pp. 60–72, 2017.

[47] E. Levin, R. Roth, and J. Martin, "Polymorphism of ABO_3 type rare earth borates," *Am. Mineralogist*, vol. 46, 1961.

[48] E. Levin, "V - Liquid Immiscibility in Oxide Systems ," in *Phase Diagrams: Materials Science and Engineering* (A. M. Alper, ed.), pp. 179 – 181, Academic Press, 1970.

[49] S. Decterov, V. Swamy, and I. Jung, "Thermodynamic modeling of the B_2O_3–SiO_2 and B_2O_3–Al_2O_3 systems," *International Journal of Materials Research*, vol. 98, no. 10, pp. 987–994, 2007.

[50] V. Swamy, I. Jung, and S. Decterov, "Thermodynamic modeling of the Al_2O_3–B_2O_3–SiO_2 system," *Journal of Non-Crystalline Solids*, vol. 355, no. 34, pp. 1679–1686, 2009.

[51] T. Le, A. Malfliet, B. Blanpain, and G. Muxing, "Phase Relations of the CaO–SiO_2–Nd_2O_3 System and the Implication for Rare Earths Recycling," *Metallurgical and materials transactions*, vol. 47b, pp. 1736–1744, 2016.

[52] C. Jantzen and F. Glasser, "Stabilization of Nuclear Waste Constituents in Portland Cement," *American Ceramic Society Bulletin*, vol. 58, no. 4, pp. 459–466, 1979.

[53] J. Fahey, W. Weber, and F. Rotella, "An X-ray and neutron powder diffraction study of the $Ca_{2+x}Nd_{8-x}(SiO_4)_6O_{2-0.5x}$ system," *Journal of Solid State Chemistry*, vol. 60, pp. 145–158, 1985.

[54] H. Lukas, S. Fries, and B. Sundman, *Computational Thermodynamics - The Calphad Method*. 2007.

[55] A. Pelton, S. Decterov, G. Eriksson, C. Robelin, and Y. Dessureault, "The Modified Quasichemical Model - I—Binary Solutions," *Metallurgical And Materials Transactions B*, vol. 31B, pp. 651–659, 2000.

[56] C. Jellum, "Graphic designer." Trondheim, Norway, Summer 2017.

[57] "Soil quality - dissolution for the determination of total element content - — part 2: Dissolution by alkaline fusion," Standard, International Organization for Standardization, Geneva, CH, aug 2002. ISO 14869-2:2002(E).

[58] A. Roine, "HSC Chemistry - 7.1." `http://www.outotec.com/products/digital-solutions/hsc-chemistry/`. Version 7.1,.

[59] Y. Ji, J. Liang, S. Xie, and X. Wu, "Phase relations in the system $BaO-Nd_2O_3-B_2O_3$ ($B_2O_3 \geq$ 50 mol%) and crystal growth of $NdBaB_9O_{16}$," *Journal of Crystal Growth*, vol. 137, pp. 521–527, 1994.

Appendix A

Equipment and Chemicals

Chemicals:

- Nd_2O_3 (99.9% powder, CAS: 1313-97-9, Sinoreagent© LOI: 2.93%).
- SiO_2 (99.99% 0.2-0.7 mm powder, CAS: 7631-86-9, Umicore© LOI: 0%)
- CaO (Honeywell, 99.9% powder, CAS: 1305-78-8, Sigma-Aldrich).
- B_2O_3 (99.98% powder, CAS: 1303-86-2, Alfa Aesar© LOI: 4.13%).
- Apatite Concentrate (LKAB).

Equipment:

- Big graphite crucible I (outer crucible).
  - Height: 150 mm ± 1 mm.
  - Outer diameter: 76 mm ± 1 mm.
  - Inner diameter: 53 mm ± 1 mm.
  - Inner depth: 65 mm ± 1 mm.
  - Note: Used with graphite inner crucible.
  - Manufactured by Svenska Tanso AB.
- Big graphite crucible II (outer crucible).
  - Height: 150 mm ± 1 mm.
  - Outer diameter: 76 mm ± 1 mm.
  - Inner diameter: 42 mm ± 1 mm.
  - Inner depth: 70 mm ± 1 mm.
  - Note: Used with molybdenum inner crucible.
  - Manufactured by Svenska Tanso AB.
- Big graphite crucible III (outer crucible).

  - Height: 150 mm ± 1 mm.
  - Outer diameter: 85 mm ± 1 mm.
  - Inner diameter: 70 mm ± 1 mm.
  - Inner depth: 130 mm ± 1 mm.
  - Note: Used with no inner crucible.
  - Manufactured by Svenska Tanso AB.

- Small graphite crucible (inner crucible):
  - Height: 65 mm ± 0.5 mm.
  - Outer diameter: 53 mm ± 0.5 mm.
  - Inner diameter: 32 mm ± 0.5 mm.
  - Inner depth: 50 mm ± 0.5 mm.
  - Manufactured by Svenska Tanso AB.

- Molybdenum crucible (inner crucible):
  - Height: 70 mm ± 0.5 mm.
  - Outer diameter: 42 mm ± 0.2 mm.
  - Inner diameter: 40 mm ± 0.2 mm.
  - Inner depth: 66 mm ± 0.5 mm.
  - Purity: 99.95% Mo
  - Manufactured by Shaanxi Yuheng Tungsten & Molybdenum Co.Ltd (YHTMC).

- Graphite wool:
  - Soft graphite felt
  - Grade: SF-10
  - Thickness: 13 mm ± 1 mm.
  - Note: Insulation material.
  - Delivered by Svenska Tanso AB.

- Mica:
  - Sheet-structured silicate-based material.
  - Thickness: 2 mm ± 0.1 mm.

  - Note: Insulation material.
  - Produced by Capital Refractories.
- Molybdenum wire.
  - Diameter: 1 mm ± 0.1 mm.
- Thermocouple.
  - Type C, 95%W/5%Re–74%W/26%Re.
- Argon 5.0, produced by AGA AS.
- Platinum-Rhodium foil.
  - Pt-20%Rh foil
- Al_2O_3 Crucible.
  - Height: 70 mm ± 0.5 mm.
  - Outer diameter: 42 mm ± 0.2 mm.
  - Inner diameter: 40 mm ± 0.2 mm.
  - Inner depth: 66 mm ± 0.5 mm.
  - Purity: 99.95% Al_2O_3
- Safety Equipment
  - 3M 7000 series gas mask.
  - 3M 6057 triple filter.
  - Dräger Tube: Phosphine 0.1/c.
  - Nitrile Gloves
  - Dust mask

Induction furnace:

- Vacuum induction furnace.
- Max power 7.5 kW.
- Produced by Elatec Technology corp.

Calcining furnace:

- Muffle furnace.
- Max power 2 kW.
- Produced by Nabertherm, Germany.
- Max temperature: 1823K.

Ring mill:

- Tungsten carbide grinding tools.
- Max power 1500 W.
- Produced by Retsch, Germany.
- Model RS 200.

X-Ray Diffractometer

- XRD were recorded on a Bruker D8 Advance fitted with a Lynxeye XE detector, operating with Cu Kα radiation accelerated at 40 kV and 40mA.
- The data were recorded from 15° 2Θ to 75° 2Θ using a step size of 0.013° and a counting time of 0.38s per step. A variable divergence slit opening was used exposing 6 mm of the sample through the recordings.

Appendix B

Tables

Table A1 – Compositions of samples for phase diagram experiment for the Nd_2O_3–SiO_2–B_2O_3 system.

Sample	Compositions					
	Mole ratio			Weight %		
	Nd_2O_3	B_2O_3	SiO_2	Nd_2O_3	B_2O_3	SiO_2
PD1	0.224	0.700	0.076	58.6	37.9	3.5
PD2	0.150	0.700	0.150	46.6	45.0	8.3
PD3	0.076	0.700	0.224	29.1	55.5	15.3
PD4	0.375	0.500	0.125	74.9	20.7	4.5
PD5	0.250	0.500	0.250	62.8	26.0	11.2
PD6	0.125	0.500	0.375	42.3	35.0	22.7
PD7	0.600	0.200	0.200	88.6	6.1	5.3
PD8	0.400	0.200	0.400	78.0	8.1	13.9
PD9	0.200	0.200	0.600	57.4	11.9	30.7
PD10	0.580	0.100	0.320	88.2	3.1	8.7
PD11	0.300	0.100	0.600	70.1	4.8	25.0
PD12	0.060	0.070	0.870	26.1	6.3	67.6
PD13	0.700	0.060	0.240	92.7	1.6	5.7
PD14	0.600	0.050	0.350	89.2	1.5	9.3
PD15	0.150	0.050	0.800	49.5	3.4	47.1
PD16	0.270	0.030	0.700	67.3	1.5	31.2
PD17	0.730	0.025	0.245	93.7	0.7	5.6
PD18	0.250	0.025	0.725	65.0	1.3	33.7
PD19	0.490	0.020	0.490	84.2	0.7	15.0
PD20	0.230	0.010	0.760	62.5	0.6	36.9

Table A2 – Temperature data for phosphorus removal experiments conducted during this thesis. These temperature-time plots can be seen in Figure C.1-C.4.

Time [min]	De-P#1 [K]	De-P#2 [K]	De-P#3 [K]	De-P#4 [K]
1	299	300	300	302
5	504	592	518	571
10	1049	1142	1025	883
15	1289	1390	1291	1133
20	1422	1527	1418	1285
25	1558	1647	1603	1520
30	1639	1715	1699	1659
35	1682	1750	1754	1738
40	1720	1841	1783	1771
45	1765	1883	1803	1804
50	1787	1907	1920	1924
55	1798	1955	1996	1987
60	1804	1980	2022	2018
65	1911	1986	2003	2004
70	1935	2032	1974	2003
75	1905	2037	2064	2038
80	1911	2063	2067	2081
85	1914	2088	2100	2094
90	1914	2100	2121	2082
95	1914	2066	2114	2080
100	1914	2080	2200	2078
105	1915	2083	2065	2077
110	1916	2088	2039	2077
115	1916	2091	2097	2077
120	1916	2093	2077	2077
125	1916	2094	2084	2078
130	1916	2094	2083	2078
135	1917	2095	-	2078
140	1917	2096	-	2078
145	1917	-	-	-

Table A3 – Temperature data for synthetic slag melting experiments with 5% and 20% Nd_2O_3, conducted during this thesis. These temperature-time plots can be seen in Figure C.5-C.7.

Time [min]	Synth-5-1 [K]	Synth-20-1 [K]	Synth-20-2 [K]
1	328	332	323
5	551	548	538
10	751	736	730
15	899	912	867
20	1078	1069	1061
25	1225	1190	1210
30	1331	1280	1314
35	1400	1359	1397
40	1448	1431	1443
45	1540	1545	1520
50	1607	1625	1570
55	1654	1675	1604
60	1716	1697	1660
65	1757	1709	1692
70	1781	1755	1724
75	1830	1787	1743
80	1860	1806	1754
85	1878	1815	1759
90	1889	1846	1762
95	1904	1864	1776
100	1910	1874	1786
105	1908	1880	1791
110	1908	1884	1807
115	1911	1886	1838
120	1910	1887	1847
125	1909	1887	1856
130	1909	1897	1862
135	1908	1907	1875
140	1908	1912	1881
145	-	1915	1885
150	-	1917	1887
155	-	1917	1889
160	-	1918	1889

Table A4 – Temperature data for synthetic slag melting experiments with 10% Nd_2O_3, conducted during this thesis. These temperature-time plots can be seen in Figure C.8-C.12.

Time [min]	Synth-1-1 [K]	Synth-1-2 [K]	Synth-1-3* [K]	Synth-2-1 [K]	Synth-2-2* [K]
1	328	333	333	311	314
5	573	512	553	491	539
10	781	708	727	712	777
15	931	885	856	856	944
20	1088	1045	1037	1051	1093
25	1207	1156	1186	1222	1242
30	1289	1238	1279	1328	1334
35	1407	1353	1373	1428	1411
40	1469	1451	1447	1498	1464
45	1537	1513	1498	1605	1519
50	1575	1545	1527	1675	1560
55	1600	1602	1551	1719	1585
60	1634	1637	1597	1744	1647
65	1653	1669	1625	1759	1687
70	1715	1725	1682	1825	1742
75	1753	1758	1718	1867	1776
80	1774	1774	1739	1891	1802
85	1783	1783	1751	1904	1814
90	1792	1792	1759	1901	1821
95	1810	1833	1773	1901	1826
100	1835	1865	1779	1921	1839
105	1848	1879	1835	1932	1860
110	1872	1885	1889	1940	1883
115	1883	1890	1916	1943	1905
120	1890	1892	1932	1944	1917
125	1896	1893	1944	1943	1923
130	1900	1893	1953	1943	1925
135	1902	1893	1963	1943	1926
140	1903	1893	1970	1943	1926
145	1902	1894	1978	1943	1927
150	1902	1895	1977	1943	1926
155	1902	1895	1977	-	1927
160	1901	1895	-	-	1926
165	1901	-	-	-	1925
170	1901	-	-	-	1925

*At the last recorded temperature, the Sampling procedure from Section 4.2 was begun. Temperatures were recorded for individual samples, not continuously.

Table A5 – Temperature data for Master Slag Melting and Sampling experiments, conducted during this thesis. These temperature-time plots can be seen in Figure C.13, C.14 and C.15.

Time [min]	MS-1 [K]	MS-2 [K]	MS-3* [K]
1	317	316	313
5	523	540	508
10	750	759	700
15	905	912	838
20	1075	1072	1004
25	1210	1191	1148
30	1307	1283	1243
35	1397	1362	1345
40	1463	1431	1409
45	1521	1510	1488
50	1565	1566	1538
55	1602	1594	1574
60	1645	1646	1622
65	1666	1680	1651
70	1703	1734	1696
75	1735	1768	1727
80	1753	1782	1772
85	1763	1814	1799
90	1769	1833	1831
95	1794	1857	1850
100	1816	1872	1857
105	1830	1883	1858
110	1850	1891	1862
115	1862	1895	1867
120	1870	1896	1873
125	1880	1897	1880
130	1888	1896	1886
135	1893	1896	-
140	1897	1896	-
145	1898	1896	-
150	1899	1896	-
155	1900	1897	-
160	1901	1897	-
165	1901	-	-
170	1901	-	-

*At the last recorded temperature, the Sampling procedure from Section 4.2 was begun. Temperatures were recorded for individual samples taken, not continuously.

Appendix C

Figures

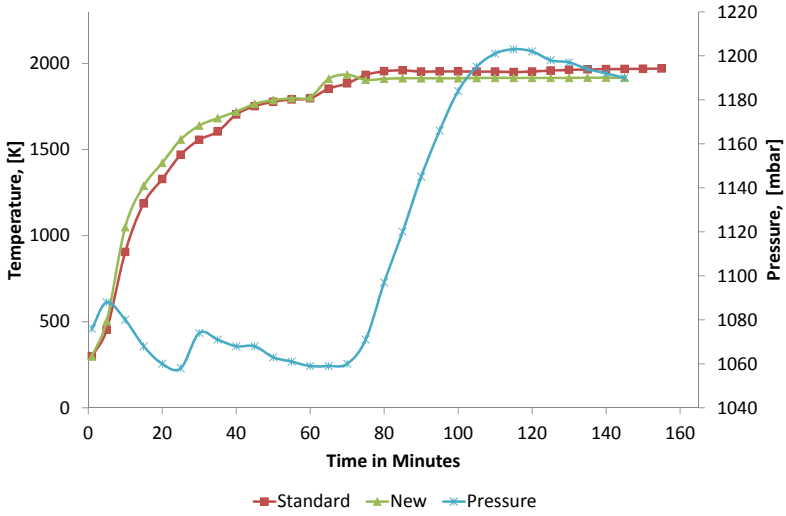

Figure C.1 – Temperature and pressure plots of sample "De-P#1".

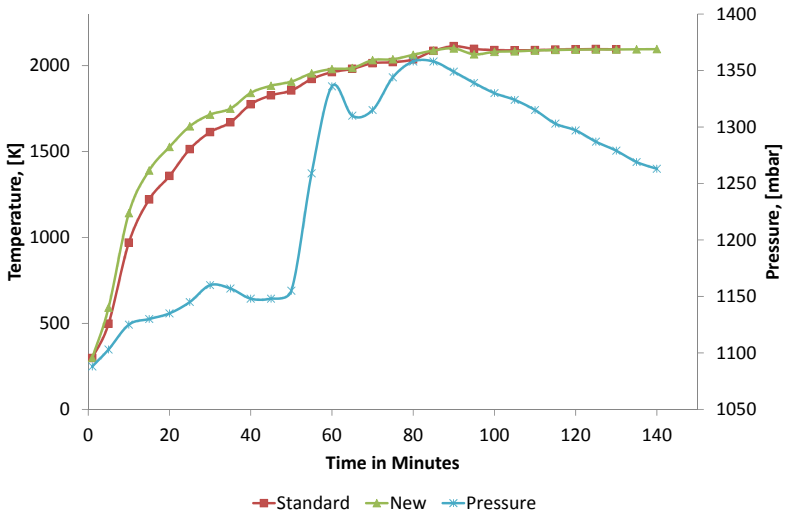

Figure C.2 – Temperature and pressure plots of sample "De-P#2".

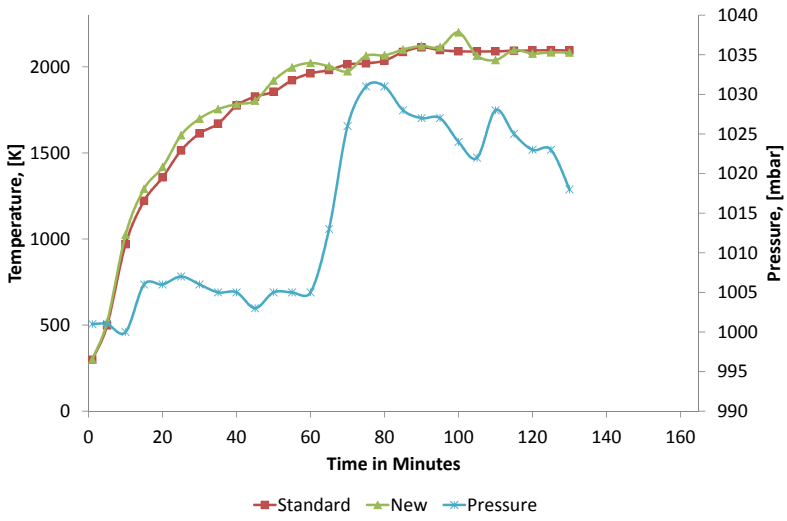

Figure C.3 – Temperature and pressure plots of sample "De-P#3".

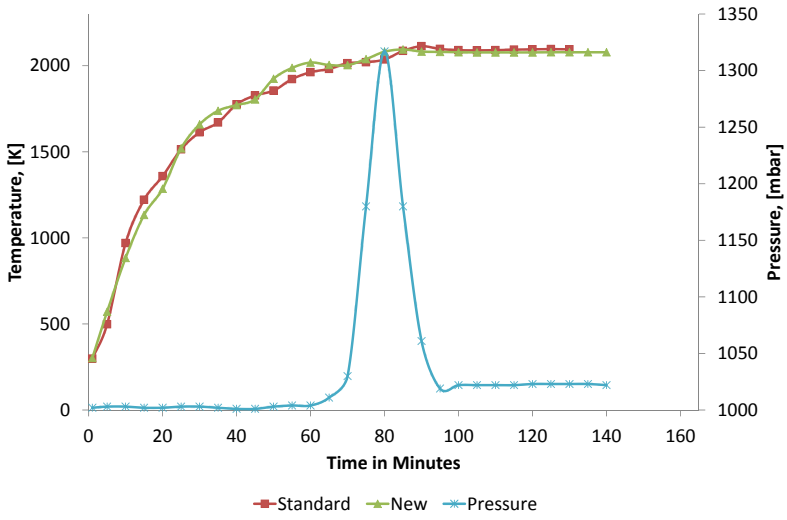

Figure C.4 – Temperature and pressure plots of sample "De-P#4".

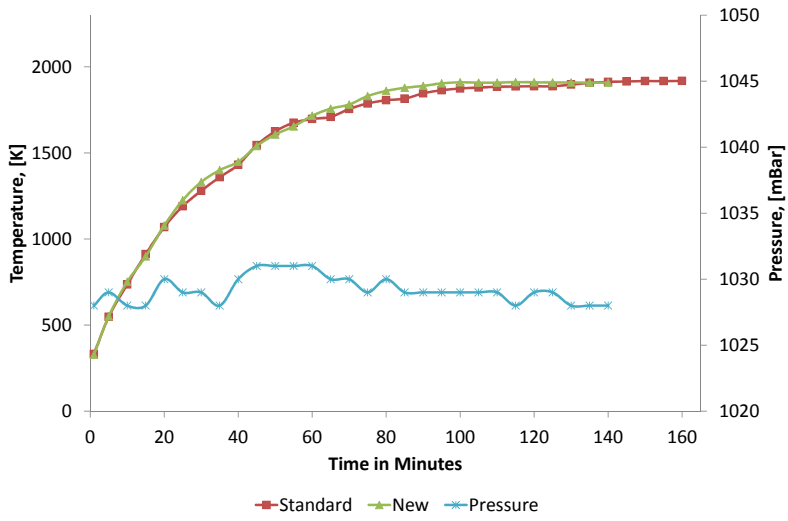

Figure C.5 – Temperature and pressure plots of sample "Synth-5-1".

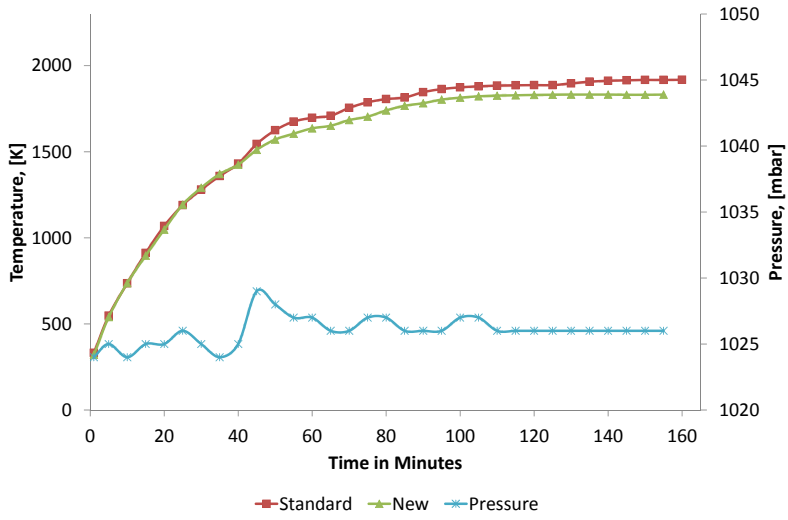

Figure C.6 – Temperature and pressure plots of sample "Synth-20-1".

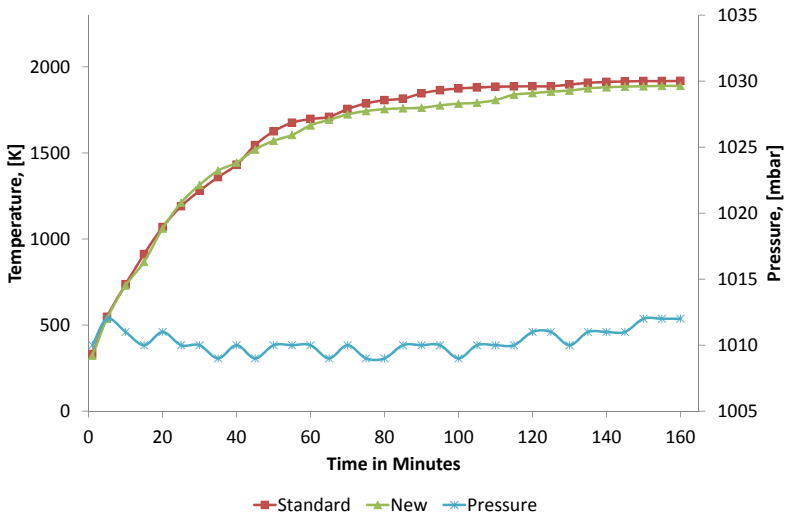

Figure C.7 – Temperature and pressure plots of sample "Synth-20-2".

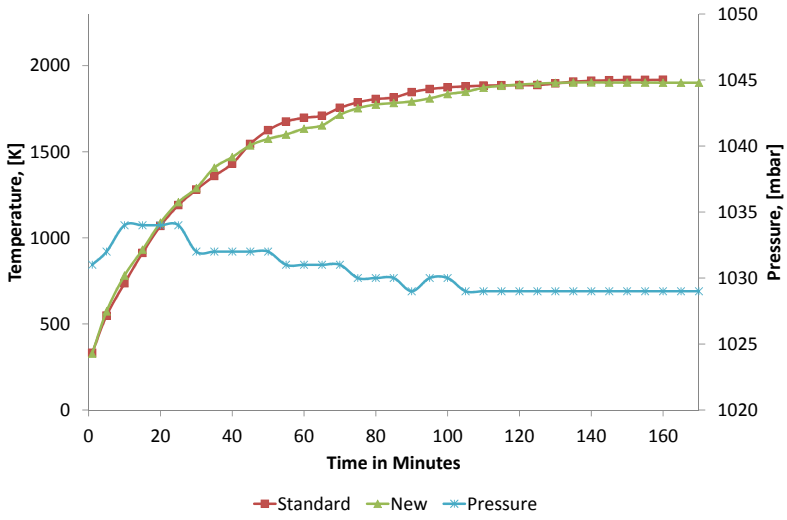

Figure C.8 – Temperature and pressure plots of sample "Synth-10-1-1".

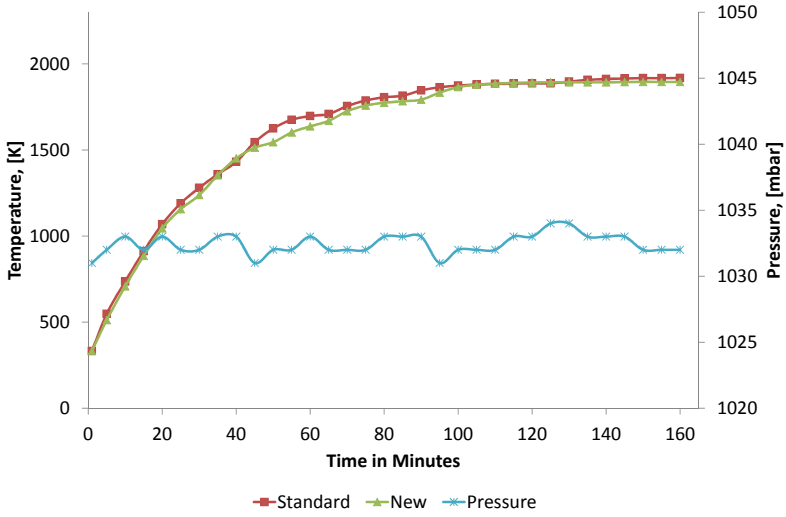

Figure C.9 – Temperature and pressure plots of sample "Synth-10-1-2".

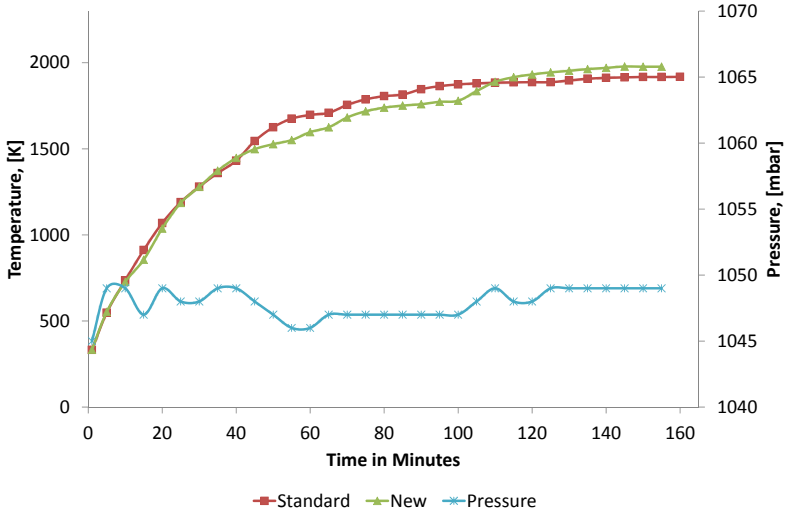

Figure C.10 – Temperature and pressure plots of sample "Synth-10-1-3". Sampling procedure was started after last recorded temperature.

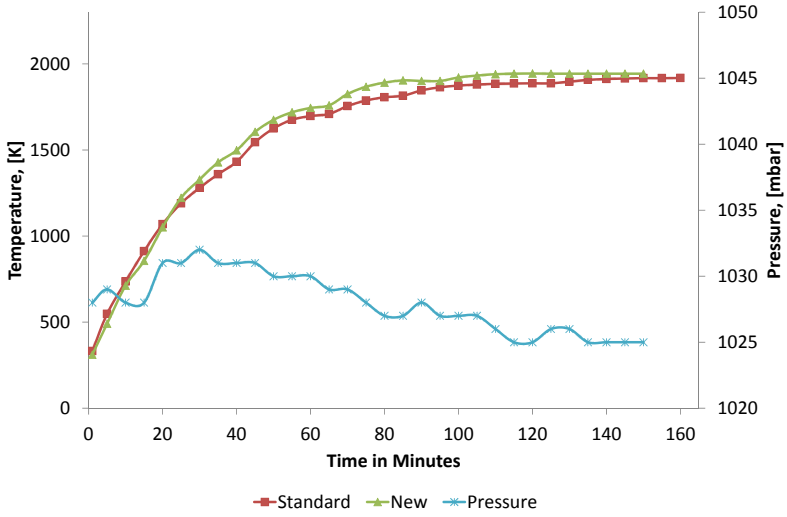

Figure C.11 – Temperature and pressure plots of sample "Synth-10-2-1".

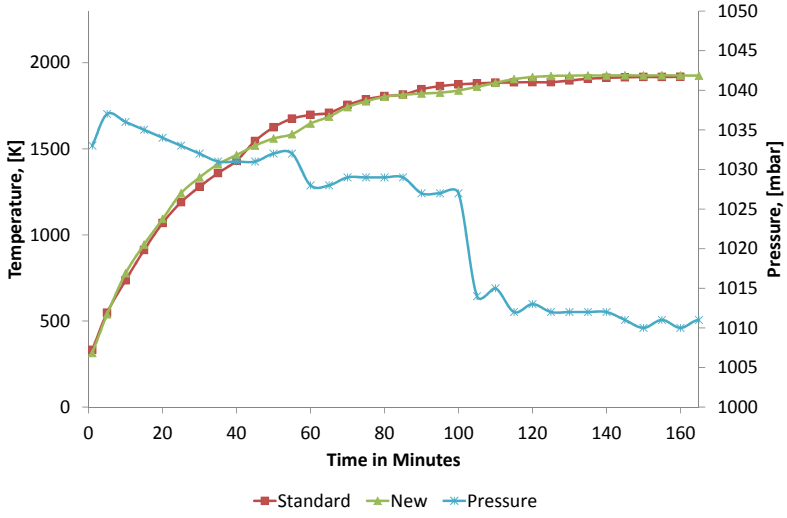

Figure C.12 – Temperature and pressure plots of sample "Synth-10-2-2". Sampling procedure was started after last recorded temperature.

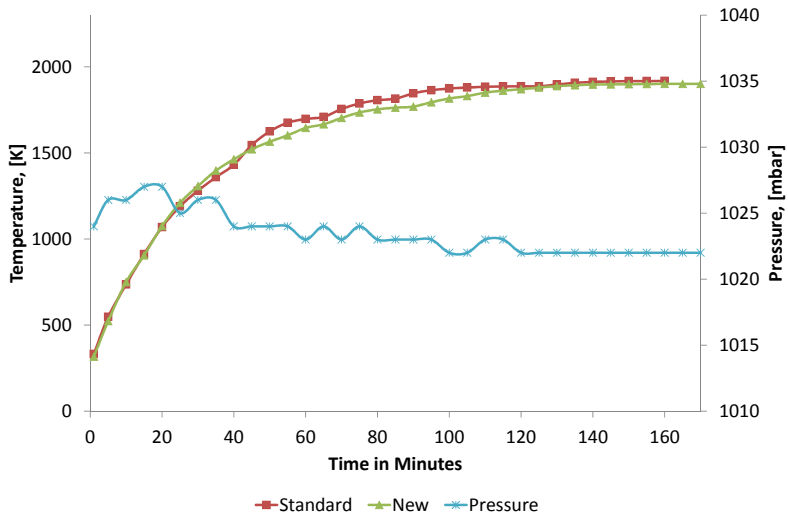

Figure C.13 – Temperature and pressure plots of sample "MS-1-1".

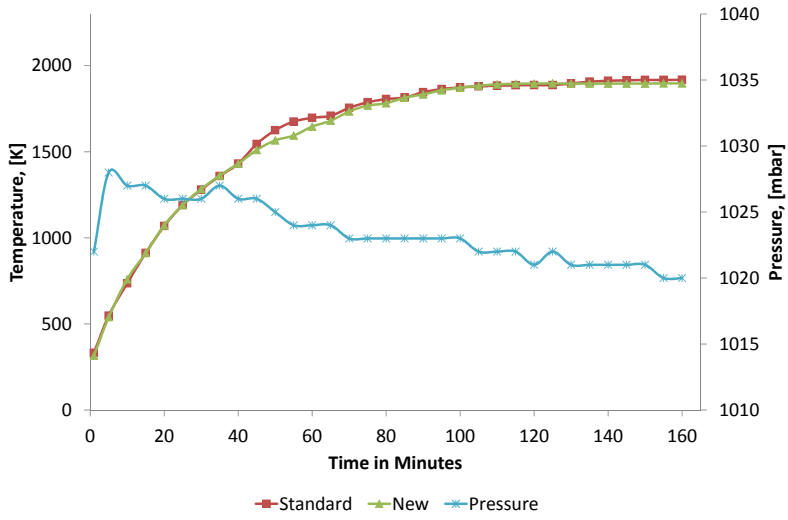

Figure C.14 – Temperature and pressure plots of sample "MS-1-2".

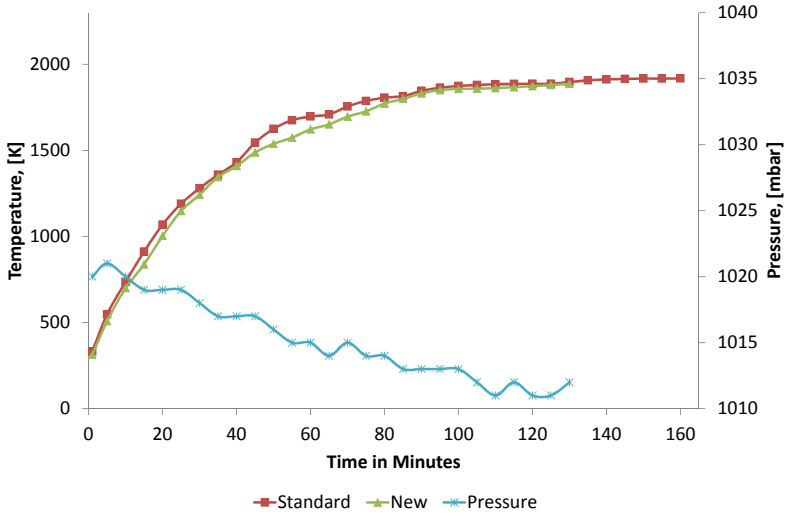

Figure C.15 – Temperature and pressure plots of sample "MS-1-3". Sampling procedure was started after last recorded temperature.

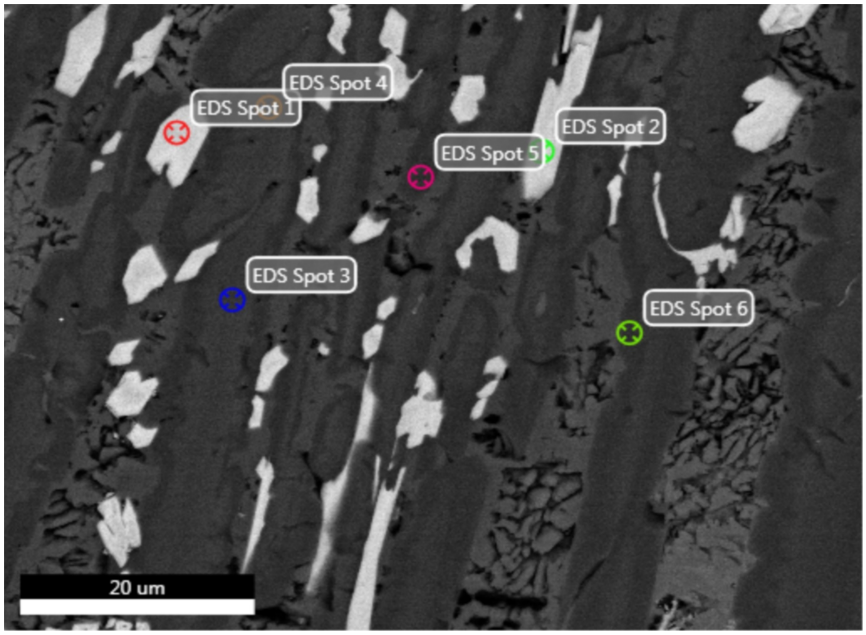

Figure C.16 – SEM picture with EDS spots marked for "Sample 10". Composition shown in Table 5.9 and Table 5.10. Area from Figure C.17.

Figure C.17 – SEM image for "Sample 10". Specifications detailed on image.

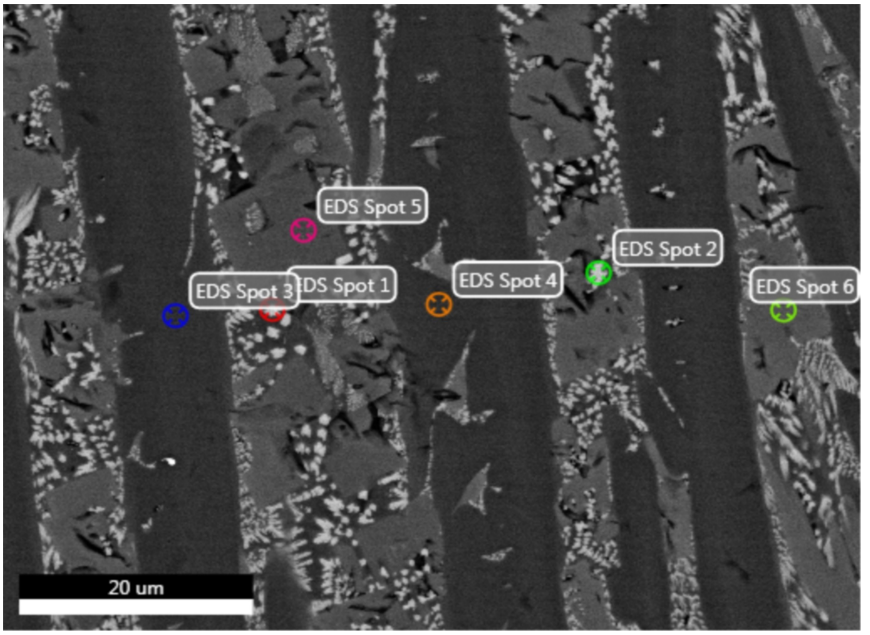

Figure C.18 – SEM picture with EDS spots marked for "Sample 9". Composition shown in Table 5.9 and Table 5.10.Area from Figure C.19.

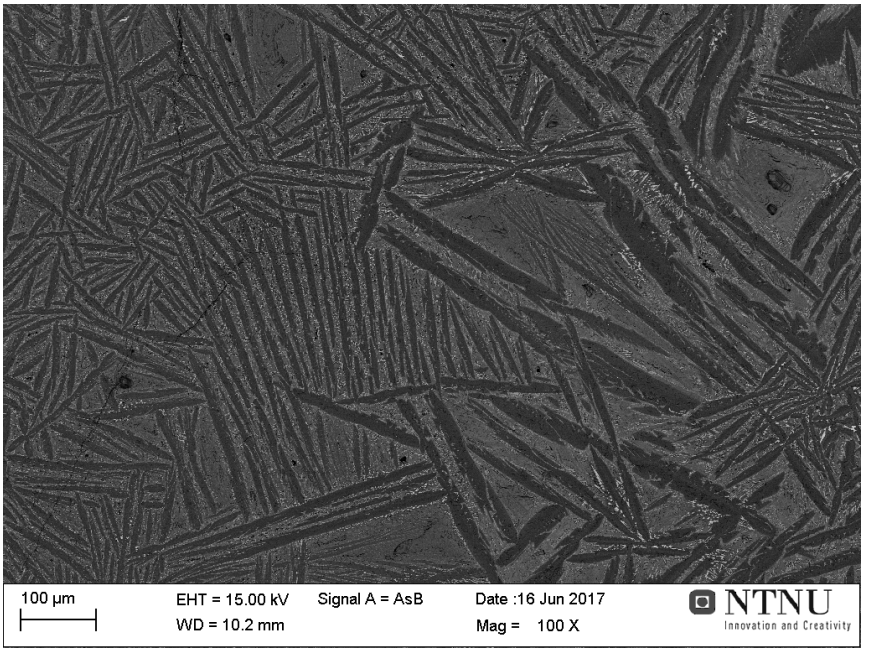

Figure C.19 – SEM image for "Sample 9". Specifications detailed on image.

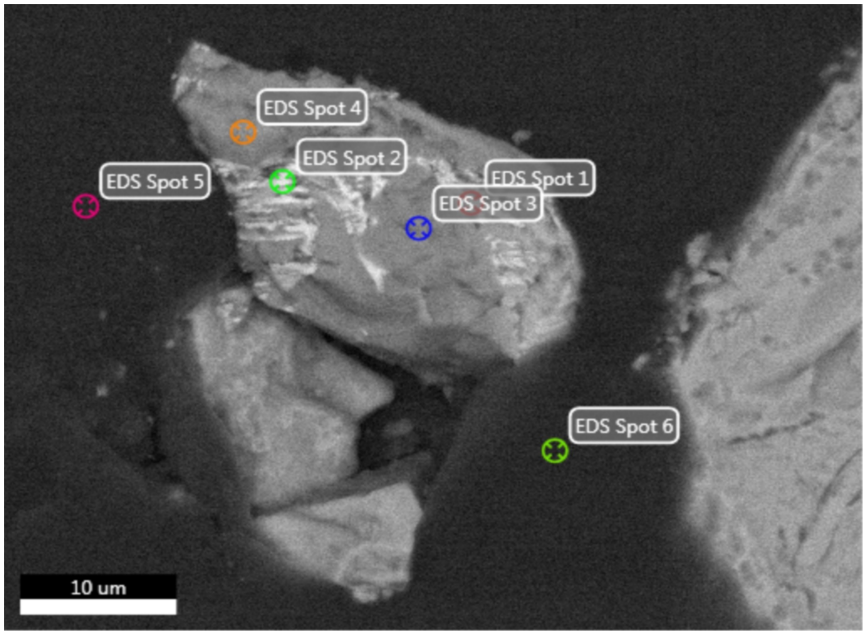

Figure C.20 – SEM picture with EDS spots marked for "Sample 8". Composition shown in Table 5.9 and Table 5.10.Area from Figure C.21.

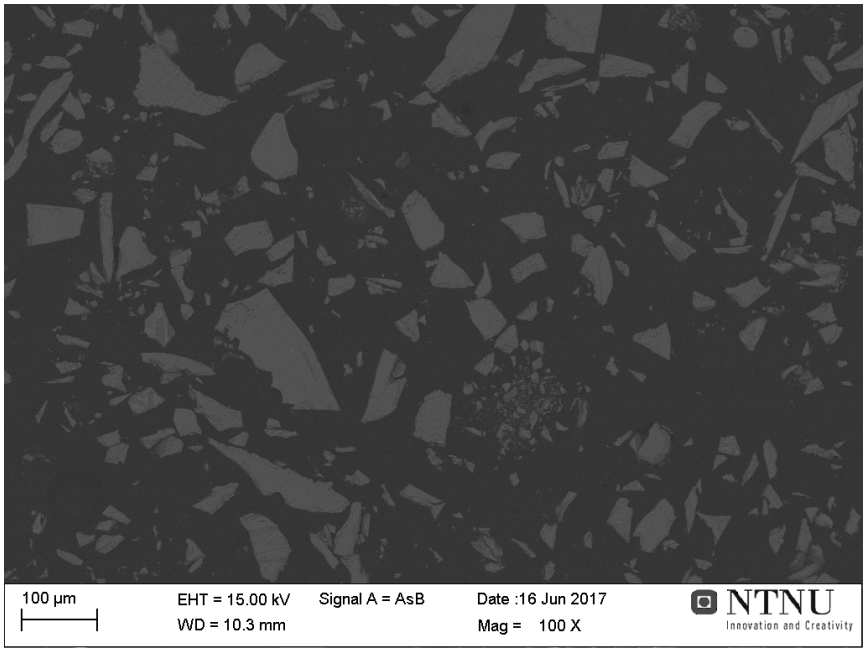

Figure C.21 – SEM image for "Sample 8". Specifications detailed on image.

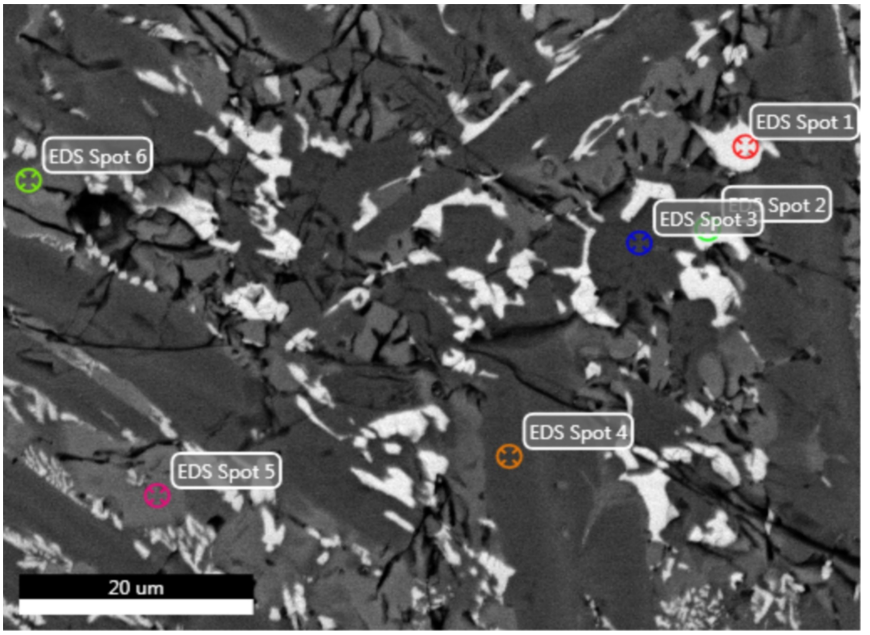

Figure C.22 – SEM picture with EDS spots marked for "Sample 7". Composition shown in Table 5.9 and Table 5.10.Area from Figure C.23.

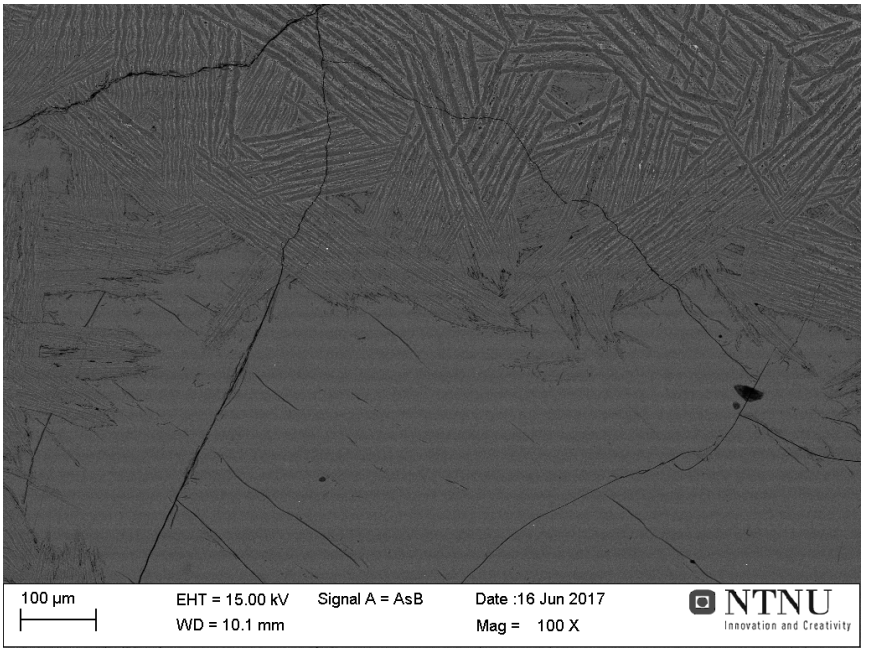

Figure C.23 – SEM image for "Sample 7". Specifications detailed on image.

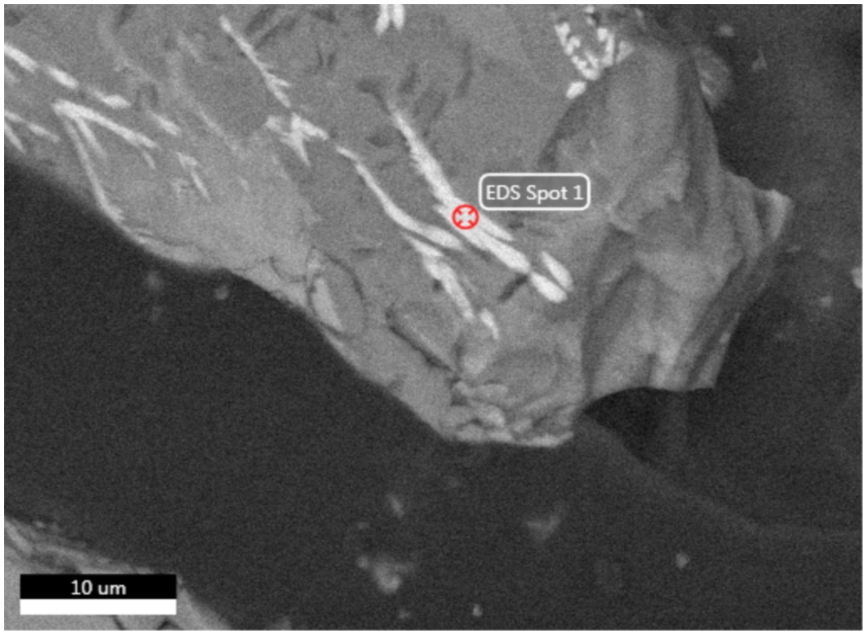

Figure C.24 – SEM picture with EDS spots marked for "Sample 6". Composition shown in Table 5.9 and Table 5.10.Area from Figure C.25.

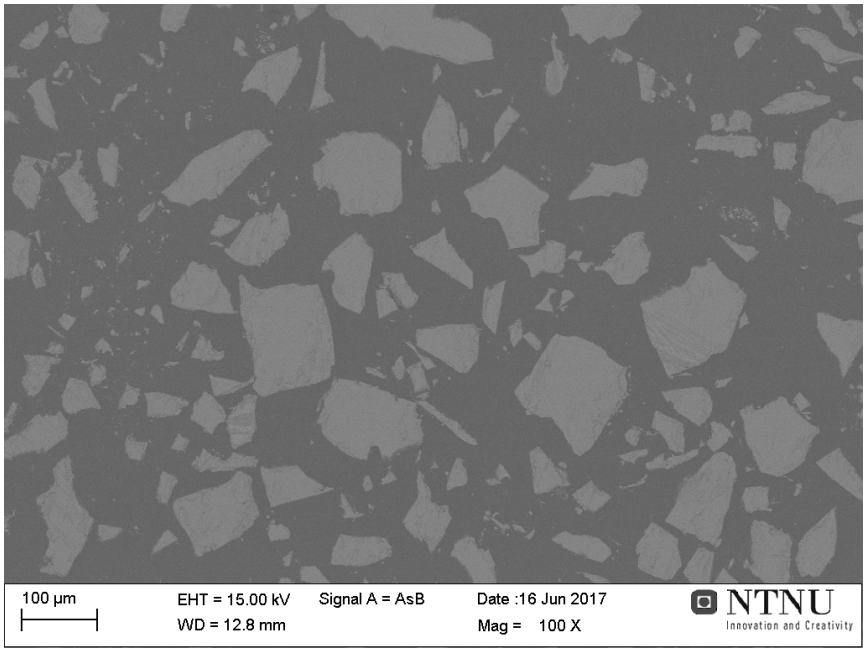

Figure C.25 – SEM image for "Sample 6". Specifications detailed on image.

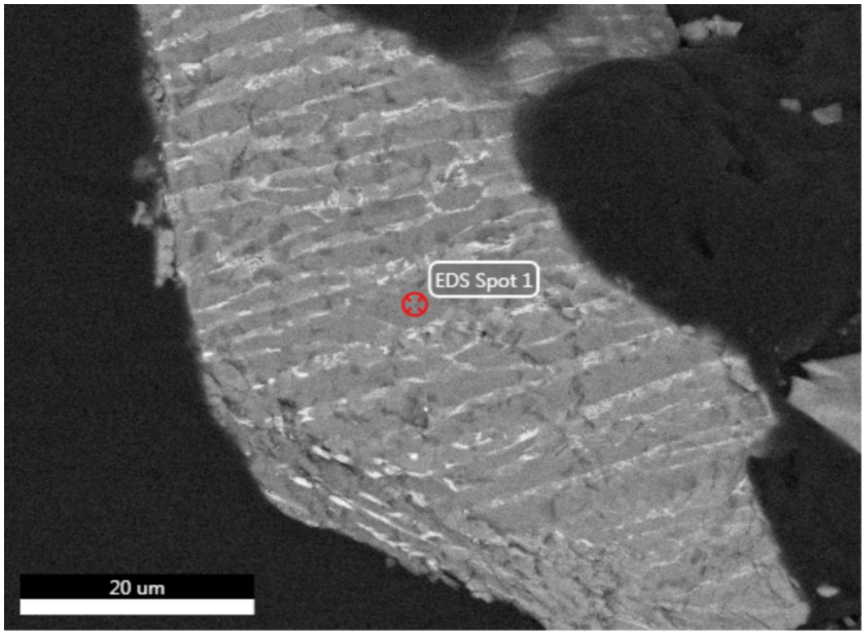

Figure C.26 – SEM picture with EDS spots marked for "Sample 5". Composition shown in Table 5.9 and Table 5.10.Area from Figure C.27.

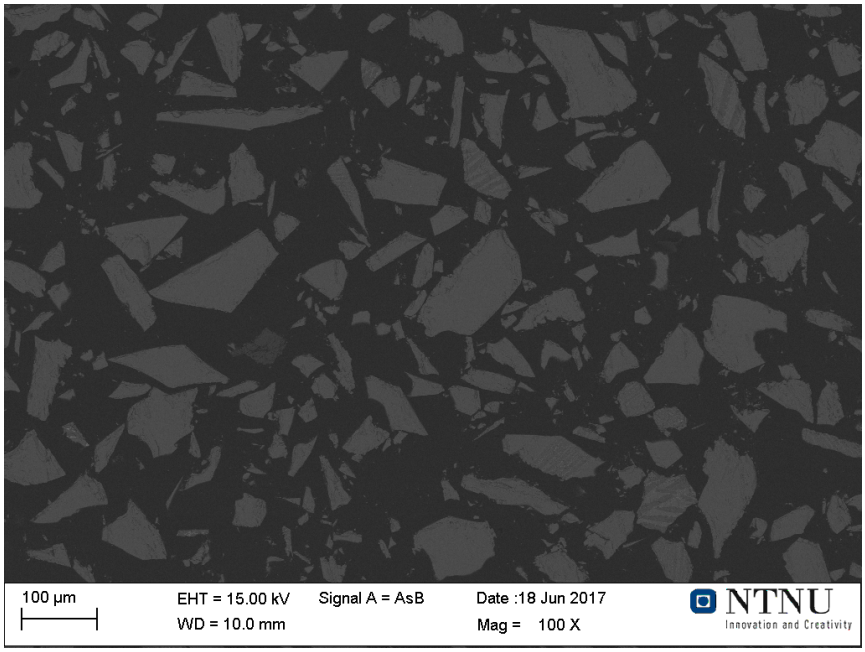

Figure C.27 – SEM image for "Sample 5". Specifications detailed on image.

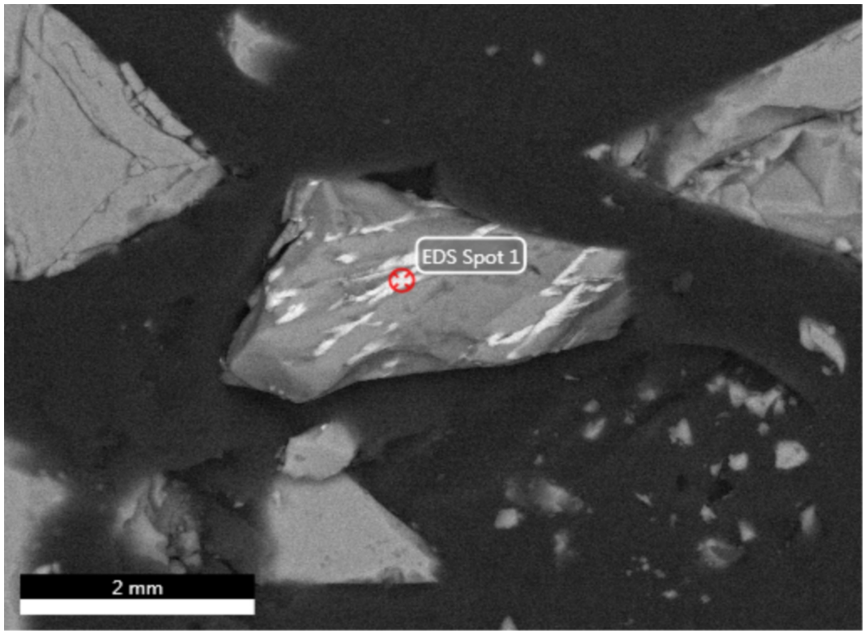

Figure C.28 – SEM picture with EDS spots marked for "Sample 4". Composition shown in Table 5.9 and Table 5.10.Area from Figure C.29.

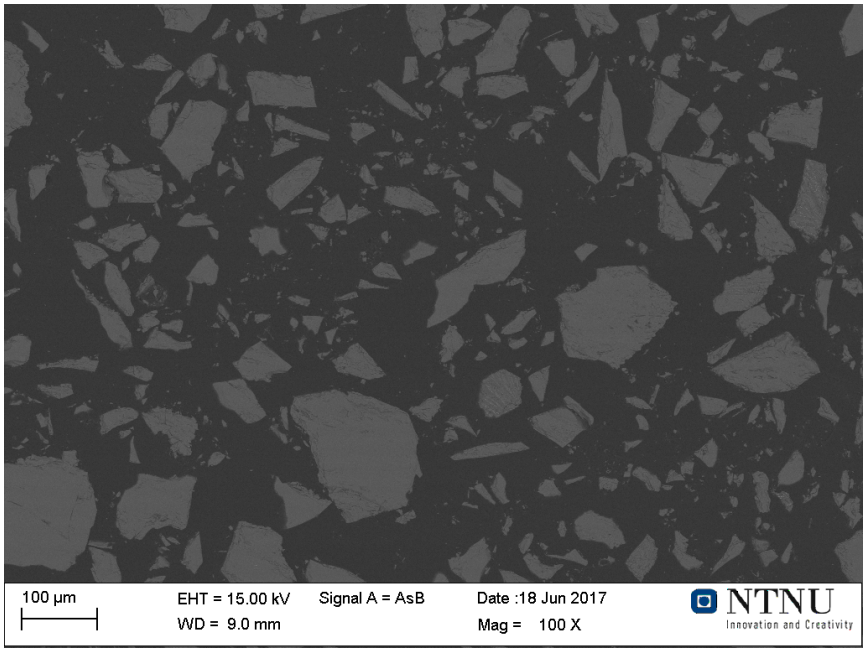

Figure C.29 – SEM image for "Sample 4". Specifications detailed on image.

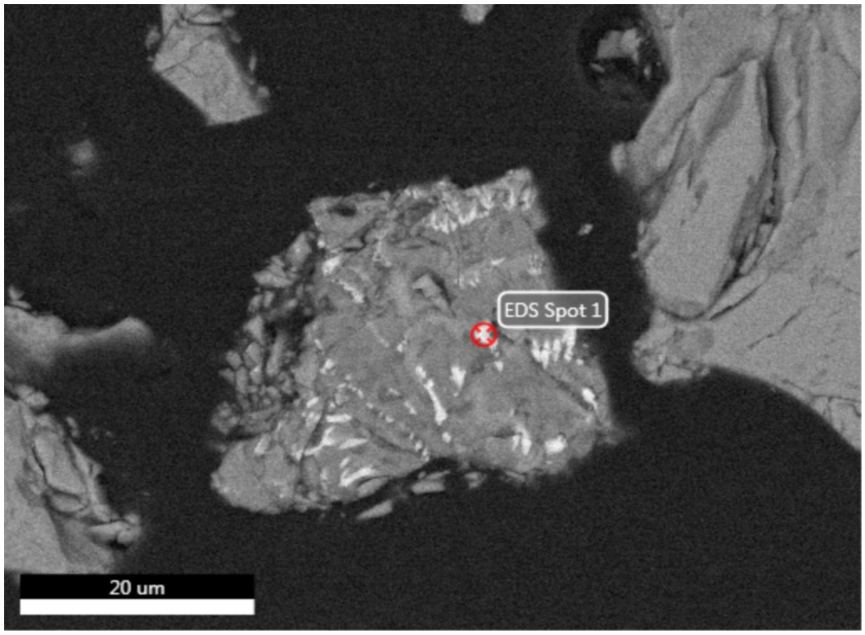

Figure C.30 – SEM picture with EDS spots marked for "Sample 3". Composition shown in Table 5.9 and Table 5.10.Area from Figure C.31.

Figure C.31 – SEM image for "Sample 3". Specifications detailed on image.

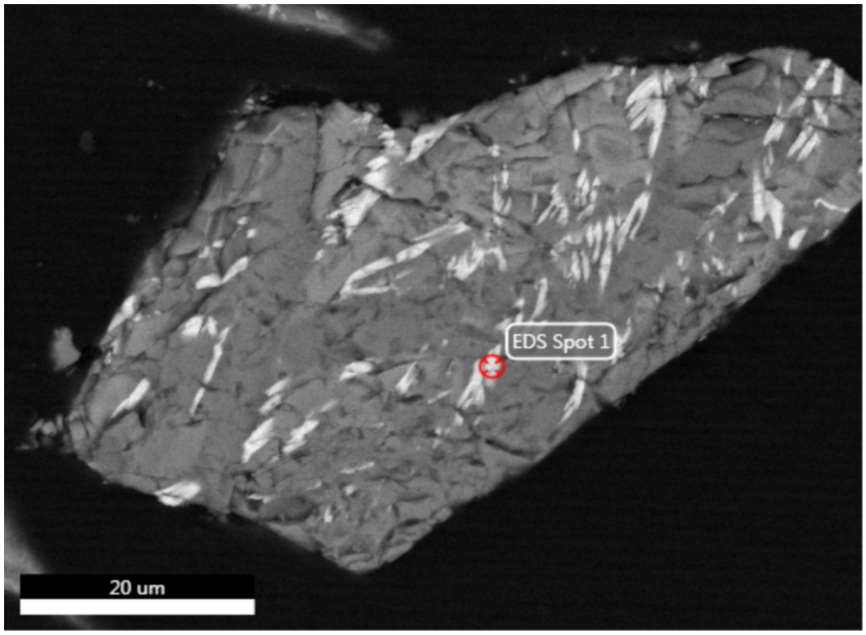

Figure C.32 – SEM picture with EDS spots marked for "Sample 2". Composition shown in Table 5.9 and Table 5.10.Area from Figure C.33.

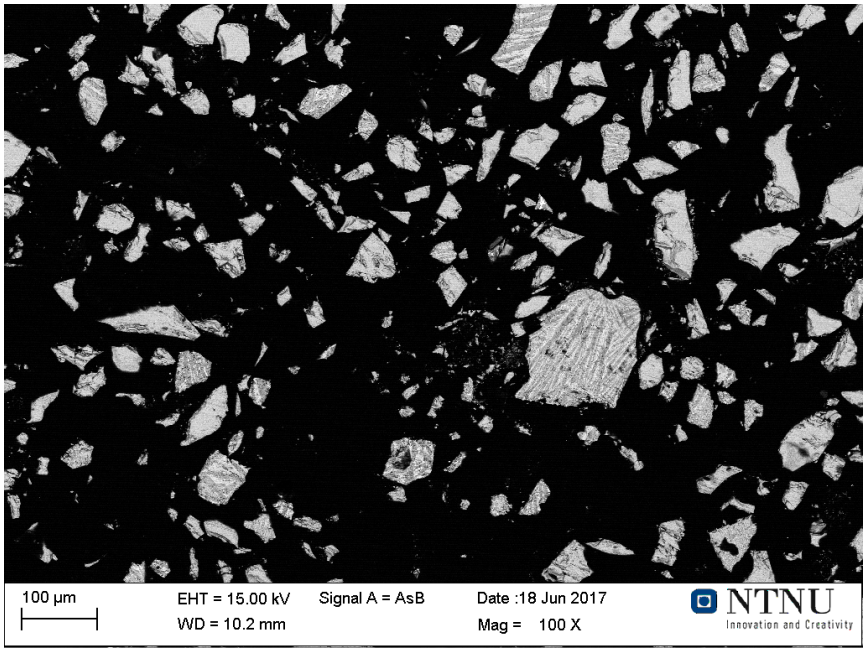

Figure C.33 – SEM image for "Sample 2". Specifications detailed on image.